INVESTIGATION OF CO-CHANNEL INTERFERENCE, CHANNEL DISPERSION, AND MULTI-USER DIVERSITY IN MIMO-BASED CELLULAR SYSTEMS

By

RAHUL N. PUPALA

A Dissertation submitted to the

Graduate School—New Brunswick

Rutgers, The State University of New Jersey

in partial fulfillment of the requirements

for the degree of

Doctor of Philosophy

Graduate Program in Electrical and Computer Engineering

Written under the direction of

Prof. David G. Daut and Prof. Larry J. Greenstein

and approved by

____

____

____

____

____

New Brunswick, New Jersey

May, 2008

ABSTRACT OF THE DISSERTATION

Investigation of Co-Channel Interference, Channel Dispersion, and Multi-User Diversity in MIMO-Based Cellular Systems

by Rahul N. Pupala

Dissertation Directors: Prof. David G. Daut and Prof. Larry J. Greenstein

In recent years, Multiple-Input/Multiple-Output (MIMO) systems employing multiple antennas at both ends of the wireless link have been shown to deliver high spectral efficiencies with reasonable constellation sizes. A MIMO link is a special case of a Multi-Element Antenna (MEA) link, wherein one or both ends use a multi-element array. Recently proposed 4G cellular systems are being evaluated that combine MIMO with Orthogonal Frequency Division Multiplexing (MIMO-OFDM) for use at the radio layer, while WiMAX 802.16e is considering MIMO with Orthogonal Frequency Division Multiple Access (MIMO-OFDMA) for use on the downlink. Multi-User Diversity (MuD) has also been shown to have important consequences in the ever-increasing demand for higher spectral efficiency. A detailed study of MIMO, MIMO-OFDM, and MuD is of utmost importance to understand how to maximize the performance gains that can be realized from these promising technologies.

This thesis is broadly divisible into three parts. Part I investigates aspects of co-channel interference (CCI) as they relate to MIMO channels. First, the throughputs attainable by interference-limited cellular systems that employ MEA links are computed. The emphasis in this study is on the system-level perspective. That is, determining the distribution of performance over a coverage area, e.g., the cumulative distributive function (CDF) of throughput (TP) over the randomness of user location and shadow fading, as well as and taking into account the CCI produced by co-channel links in other cells. Using a general-purpose simulation platform developed in this work, throughput statistics are obtained over several channel conditions and

system-level design choices. In this study, particular interest is in understanding the gains that accrue as a result of using excess receive antennas, and the effects of limiting the constellation sizes to present-day implementations.

Using the simulation platform, an evaluation of alternative Transmit Diversity, and Spatial Multiplexing systems has been carried out. The study incorporates costs/overhead incurred by using a finite alphabet, limited channel coding, and imperfect channel estimation. Next, a noise-like model for co-channel interference is postulated in the context of MIMO/MEA channels. The validity of the noise-like model is demonstrated. The model is then used to derive an analytical solution for throughput in CCI-limited MIMO systems. The analysis is shown to be accurate and to permit extensive investigation without the need for lengthy simulations.

In Part II, the effects of both frequency selectivity and correlation among transmit-receive antenna path gains on a single-carrier MIMO link are addressed. Degradations in system-level throughput statistics are evident when these distortions are assumed to be present in addition to CCI. This study includes the frequency-selective MIMO link when it uses non-dispersive cancellation of cross-stream interference at the receiver. We extend this analysis to MIMO-OFDM, and include the impact of dispersive effects which is the often ignored in such systems.

In Part III, the benefit of adding MuD to the MEA link is quantified. The three important schedulers considered in the MuD implementation are: Maximal Throughput (MAX), Proportional Fair (PF), and Equal Grade of Service (EGoS). Again, performance evaluation is at the system-level, and over several important system design parameters, in particular, excess receive antennas and finite constellation sizes. The main interest is to determine the tradeoff involved in the number of receive antennas on the mobile device versus the number of users needed in order to obtain a particular throughput.

Studying the many tradeoffs discussed above will enable design engineers to make well-founded decisions in crafting link techniques; and will aid system engineers in estimating attainable throughputs for particular designs. The results presented will be to the benefit of operators and customers alike as MIMO, MIMO-OFDM, and MuD technologies are put into service in support of new applications.

Acknowledgements

This is the hardest part of the thesis. Words cannot possibly express in the exact measure what I wish to convey, but here is an approximation...

I would like to express my deepest sense of gratitude to Professor Larry J. Greenstein. As an advisor, he offers students an infrastructure that makes the Ph.D. very easy. For many aspects of my training, he was my single point source. A sampling of the help I received includes: instruction in Wireless Communications and Signal Processing, and the various engineering judgments that are made by the industry; refining my understanding of the background material; formulating Ph.D. thesis problem(s); hearing out absurd ideas; accurately interpreting my garbled words/sign language/body language; regular weekly in-person advising (and tons of email); attending my summer intern talk at Bell Labs (2006); recording my progress over the years; reading/correcting my journal submissions meticulously several times; teaching me English grammar; offering words of encouragement when I was stressed or frustrated; and, helping in the job search. It is easy to concur with what Dr. Andrea Goldsmith and Dr. Dragan Samardzija told me — “you are extremely fortunate to have him as your advisor”.

That was a windfall in itself, and then some... I have *two* advisors. Professor David G. Daut also helped me in extremely many ways. In addition to technical advising, research study, coursework, patience, and reading/correcting my journal submissions meticulously several times, he also helped in student immigration and administrative matters. His flexibility in letting the student choose his own topic, and then rendering invaluable assistance in developing the thesis is very important in the Ph.D. training process. His balanced and steady demeanor creates an atmosphere which is very important for minimizing stress and frustration which inevitably arises in the graduate study program.

I am also fortunate to have studied several courses under extremely qualified professors. Many thanks to Professors Narayan B. Mandayam, Predrag Spasojevic, Roy D. Yates, Christopher Rose, Sophocles J. Orfanidis, and Narindra Puri. Their courses are rigorous and challenging, and an important component of a successful graduate study program. Many thanks are due also to: the ECE Graduate Director Professor Zoran Gajic, the CS Chairman Professor

Eric Allender, Professor Richard P. Martin (my MS graduate advisor from Computer Science days), Professor Dipankar Raychaudhuri, Professor Ivan Marsic, and Ivan Seskar for all the unconditional help and advice I received during my school days.

My summer internship at Bell Labs/Alcatel-Lucent Technologies under the guidance of Dr. Qi Bi and Dr. Yifei Yuan was a pleasant and fun learning experience. A part of this thesis was completed during my internship days at the Whippany office. My sincerest thanks to them for giving me that rare opportunity.

A big part of my Ph.D. learning experience has been interaction and collaboration with fellow students at WINLAB, CS, and other departments at Rutgers. In particular my discussions with Chandrasekaran (Chandru) Raman, Joydeep (Joy) Acharya, Sanjit Kaul, Hithesh Nama, Jasvinder (Jassi) Singh, Soumya (Shomu) Das, Dr. Dragan Samardzija, Sambuddha Roy, Sasi Goteti, Taliver Heath, Chris Peery, Haris Kremo, Sudhir Pattar, Goran Ivkovic, Manjeet Deshmukh, Lalitha Sankaranarayanan, Kemal Karakayali, Omer Ileri, Sachin Ganu, Ozge Kaya, and Suhas Mathur. Thanks also to Douglas Castor from InterDigital Communications Corp. for his help and support. Thanks to Dr. Anant Damle and Dr. Snehal Patel, and to my friend Deepak Nihalani for his many trips to the USA and his support. Thanks also to my younger brother Rajendra Pupala... mostly for staying away and letting me study!

Finally, the great support staff at WINLAB, ECE, CS, and the Graduate School including Kevin Wine, Noreen DeCarlo, Melissa Gelfman, Elaine Connors, Barbara Klimkiewicz, Lynn Ruggiero, Dianne Coslit, John Scafidi, Angela Xa, Alexandria Bachmann, Valentine Rolfe, Maryann Holtsclaw, and Carol Schickner have all helped in making my long stay at Rutgers very comfortable.

Highland Park, New Jersey.
2^{nd} February, 2008.

Dedication

To my uncle and my aunt Vijay and Madhu Pupala.

To my parents Nandkumar and Shakuntala Pupala.

To all my teachers.

Table of Contents

List of Figures

List of Abbreviations

AoA	angle-of-arrival
AoD	angle-of-departure
AS	angular spread
AWGN	additive white Gaussian noise
BER	bir error rate
BPSK	binary phase shift keying
BS	base station
CCI	co-channel interference
CDF	cumulative distribution function
CLT	central limit theorem
COST	Cooperative for Scientific and Technical Research
CQI	channel quality index
CSI	channel state information
dB	decibel measure (of signal or interference power)
DFT	discrete Fourier transform
Div	transmit diversity
EDoF	excess degrees of freedom
EGoS	equal grade of service scheduler
IDFT	inverse discrete Fourier transform
ISI	inter-symbol interference
LOS	line-of-sight
MAC	medium access control layer
MAX	max carrier-to-interference (SINR or SIR) scheduler
MEA	multi-element antenna array
MIMO	multiple-input/multiple-output
MIMO-OFDM	multiple-input/multiple-output OFDM

MISO	multiple-input/single-output
ML	maximum likelihood
MMSE	minimum mean-square error filter (or equalizer)
MRC	maximum ratio combining
MS	mobile station
MSE	mean square error
MuD	multi-user (network) diversity
NLOS	non-line-of-sight
OFDM	orthogonal frequency division multiplexing
OSIC	ordered successive interference canceller
OSIC-MMSE	ordered successive interference cancellation MMSE
PAS	power angular spectrum
pdf	probability density function
PF	proportional fair scheduler
PHY	physical layer (or radio layer)
PSD	power spectral density
QAM	quadrature amplitude modulation
QoS	quality-of-service
QPSK	quadrature phase shift keying
RMS	root mean-square (of the quantity in consideration)
RR	round robin scheduler
SCQI	sum channel quality index (over the transmit sub-streams)
SD	selection diversity
SER	symbol error rate
SIC	successive interference canceller (or cancellation)
SIMO	single-input/multiple-output
SINR	signal-to-interference-plus-noise ratio
SIR	signal-to-interference ratio
SISO	single-input/single-output
SM	spatial multiplexing

SNR	signal-to-noise ratio
SU	single-user system
SVD	singular valued decomposition
TP	cell-wide mean throughput (in bps/Hz)
VBLAST	vertical Bell-Labs layered space-time architecture
WiMAX	worldwide interoperability for microwave access
WLAN	wireless local area network
WSS-US	wide-sense-stationary uncorrelated-scattering
XSI	cross-stream interference
ZF	zero forcing filter (or canceller, or equalizer)

Chapter 1

Thesis Roadmap

In this chapter, a brief tour of the many research problems considered in this study is presented. The particular format that has been adopted is to first state all problems explicitly and definitively. Next, the reasons why the components of this study are timely and important are discussed. Subsequent chapters offer a brief background and survey of current literature that exists, as well as presenting the research contributions of this work. Each problem is discussed in a separate chapter and a research agenda for ongoing and future work is also offered in the concluding chapter. Acronyms are spelt fully when used for the first time, and a complete list can be found in the beginning of this thesis. Definitions, and brief explanations are sometimes presented in footnotes to maintain continuity of the material and repeated in the Appendix for quick reference. An extensive reference list offers links to additional in-depth material for the interested reader.

1.1 Problem Statements

Problem 1 *: Evaluation of Co-Channel Interference Limited SISO/MEA Systems*

Multiple-input/multiple-output (MIMO) links have been demonstrated to offer significant spectral efficiencies, far beyond the capabilities of existing traditional single-input/single-output (SISO) links. The main reason for the telecommunications industry's interest in MIMO links is their ability to offer high data throughputs with reasonable constellation sizes using the spatial dimension, thereby obviating the need for additional bandwidth. In this study, we consider the more general class of techniques involving a multi-element antenna array (MEA) at one or both ends of the link (MIMO being the latter case). We quantify cell-wide mean throughputs in an interference-limited SISO/MEA cellular system along various system-level design dimensions, including: size of the transmit/receive MEAs[1]; frequency-reuse factor; antenna

[1]MIMO/MEA links are assumed to have n transmitters and m receivers. They are referred to here as MIMO (n, m), or MEA (n, m), or simply (n, m).

pattern (omni-directional or sectorized); degree of error protection (Shannon coding, no coding or intermediate coding strategies); allowable constellation size; Rician K-factor; and transmit- or receive-adaptation.

The main observations of this study are that the *actual* potential of MEA systems is obtained by taking into consideration (i) average user experience (for example, cell-wide mean throughputs); and, (ii) limited signal constellation sizes which are prevalent in practical present day systems. Studies which ignore these concerns (e.g., by investigating MIMO in the high SINR regime) often lead to very optimistic results and conclusions. Moreover, transmit-adaptation systems are better equipped to combat channel distortions and cross-stream interference (XSI), while receive-adaptation systems (with excess degrees of freedom) are better co-channel interference (CCI) suppressors. One particular intention of this research was to conduct investigations over a rich number of practical dimensions, laying the foundation for Problems 2, 3 and consequently Problem 4.

Problem 2 *: Evaluation of Practical MIMO/MEA Systems with Resource Overheads*[2]

The advent of applications that need higher throughputs, motivates wireless service providers and cellular operators to embrace newer technologies that can meet these demands. Multiple-input/multiple-output (MIMO) systems have shown promise in their ability to deliver high throughput per bandwidth with reasonable constellation sizes. Adding antennas at the base station (BS) is practical due to reasons of size and cost amortization over many users. However, adding antennas at the mobile station (MS), which does not have similar advantages, needs to be carefully evaluated. We therefore consider the more general class of techniques involving a multiple-element antenna (MEA) at one or both ends of the link (MIMO corresponding to the case of multiple antennas at both ends of the MEA link).

From a commercial standpoint, one needs to address the following questions: (i) What is the benefit of a second antenna at the BS or the MS relative to the single-input/single-output (SISO) case? (ii) What is the added value of a second antenna at both ends? (iii) If a second antenna is indeed used at both ends, is spatial multiplexing (SM) or diversity (Div) the preferred mode

---

[2]This was a Summer internship assignment (2006) at Bell-Labs/Alcatel-Lucent Technologies - Whippany, NJ. The work is in collaboration with Yifei Yuan and Qi Bi.

of operation to use? Using (n, m) to denote a link with n BS transmit elements and m MS receive elements, we compare the downlink throughput performance of the SISO link with that of four MEA configurations: $(1, 2)$, $(2, 1)$, $(2, 2)$ with Div, and $(2, 2)$ with SM. Results obtained indicate that, in the context of adaptive modulation with practical limits on constellation size, $(1, 2)$ is the preferred configuration. We also show this finding to be robust assumptions used in the study.

While our previous studies were concerned only with spatial multiplexing systems, this study also considers transmit diversity systems. Moreover, costs/overhead incurred from finite alphabet, imperfect channel coding, channel estimation are taken into account. Lastly, the software platform from Problem 1 was modified to simulate the standardized 3GPP2 environment.

Problem 3 : Investigating the validity of the Noise Model for Co-Channel Intererence for MIMO/MEA Links

In the past a noise model has been used (in place of an exact treatment) for co-channel interference (CCI) in order to simplify the performance analysis of communication systems. In this model, the thermal noise floor, and the total multipath-averaged CCI power, are lumped into a single interference-plus-noise term. The Central Limit Theorem (CLT) is invoked to justify a Gaussian distribution for the interference-plus-noise term. Accuracy of the noise model has been studied, but only in the context of SISO channels. For MIMO/MEA research, no effort has been undertaken to question the validity of the noise model, or to arrive at a new model.

In this study, we examine the validity of the noise model for CCI for SISO and MEA links. Using system simulations, we identify key conditions under which it continues to remain accurate, and those under which it becomes inaccurate. Specifically, it is shown via simulations that the noise-model can be used for MIMO channels when (a) Transmit Adaptation is used, regardless of whether or not excess degrees of freedom exist[3]; (b) Receive Adaptation is used, and excess degrees of freedom[4] are few or none. The noise model is inaccurate otherwise. This

[3]Degrees of Freedom: the number of decomposable parallel SISO channels that can be created after array processing. It equals the rank of the channel gain matrix $\mathbf{H}$ and is upper-bounded by $\min(n, m)$.

[4]Excess Degrees of Freedom: the excess number of receive elements over transmit elements, i.e., $m - n$. When the receive array has at least as many antenna elements as the transmit array, we can receive all of the transmitted streams at the receiver after array processing.

is an important finding. In the past the noise model was accurate largely because it was used for simplifying the analysis of SISO channels, which have no excess degrees of freedom.

Using results from previous research, an algorithm has been developed for evaluating throughputs of Receive Adaptation systems when excess degrees of freedom exist. Finally, we discuss how the noise model can lead to an all-analytical solution for cell-wide mean throughput (Problem 4), thereby replacing the need for lengthy simulations (Problem 1).

Problem 4 : Analysis of Co-Channel Interference Limited MIMO-Based Cellular Systems

Computation of cell-wide mean throughputs in cellular systems using multiple-input/multiple-output (MIMO) links is a topic of interest to researchers, cellular operators and equipment manufacturers. The validity of the noise model (in the MIMO context) for the co-channel interference (CCI) has been previously confirmed by the author, wherein multipath-averaged CCI powers are added to the thermal noise power, that results in an overall interference-plus-noise floor. This approximation simplifies throughput computation with only a minor loss of accuracy, while allowing the cell-wide mean throughput per user to be derived analytically. The key to the analysis is (i) the invocation of the noise model for CCI, and (ii) the demonstration that the overall CCI power has a distribution that is log-normal for any user distance from the base station (BS). This enables us to use a previously developed analysis for the single-cell (noise-only) systems, and apply it to interference-limited MIMO systems in order to analyze per user cell-wide mean throughput. The analytical method is presented and its accuracy is demonstrated.

Problem 5 : Evaluation of Single-Carrier MIMO Systems with Channel Dispersion and Path-Correlation Impairment

Computation of *cell-wide mean throughputs* of multi-element antenna (MEA)-based cellular systems is of interest to researchers and commercial companies, primarily to discover the actual extent of gains that may be realized by such systems. In a previous work, we quantified cell-wide mean throughputs for the multi-cell case (noise plus co-channel interference (CCI)). We have also examined the validity of a simple noise model for CCI in the context of MEA links; and we have demonstrated how the noise model enables an assessment of the multi-cell case using analysis instead of simulation. Previous studies have considered rather idealized channel behavior, notably in assuming flat fading (no channel dispersion) and i.i.d. path gains (no correlations). These assumptions are relaxed in this study. We derive cell-wide throughputs for a wide range of system-level design parameters, in single- and multi-cell scenarios, using realistic models for channel dispersion, path-correlation, and CCI.

This study also includes the frequency-selective MIMO link when it uses *non-dispersive*, as well as exact cancellation of cross-stream interference (XSI) at the receiver. It is concluded that channel dispersion is a significant adversary: (i) MIMO-OFDM systems must use a sufficient number of sub-carriers to maintain flat-fading in each tone (Problem 6) ; and, (ii) non-dispersive cancellation is impractical even at very low levels of dispersion.

Finally, we also investigate the interplay between device size, number of antennas, path-correlation (as dictated by the particular terrain profile via its AoA/AoD statistics), and carrier frequency. The study reveals this interplay to be a very important consideration.

Problem 6 : Multi-Carrier Wideband MIMO (MIMO-OFDM) Systems

Most early investigations relating to MIMO capacity/throughputs assume a flat-fading model (no channel dispersion). A more recent body of research proposes Orthogonal Frequency Division Multiplexing (OFDM) to “flatten” the dispersive channel in order to improve the design and performance of the MIMO link. Consequently, MIMO-OFDM throughput analysis continues to use the flat channel assumption, ignoring the effect of channel dispersion arising from inter-symbol interference (ISI), and cross-stream interference (XSI). It behooves us to study MIMO-OFDM systems which do not make the flat-fading channel assumption.

Frequency-selective MIMO channels were previously analyzed (Problem 5), and evaluated on a cell-wide mean throughput metric. In the study, the effect of channel dispersion (frequency selectivity) leading to ISI and XSI was quantified under a wide range of system-level parameters. The observations were that: (i) for an ideal canceller with MMSE equalizer, the loss in throughput by way of ISI is small, and that most of this performance loss occurs at very small levels of dispersion; (ii) channel dispersion is a significant adversary because it smears XSI in the time domain which is hard to mitigate without using a cross-dispersive canceller.

In MIMO-OFDM systems each tone may be considered to be a MIMO channel which will not be perfectly flat. OFDM will be able to minimize ISI by using an appropriate value for guard time and incorporating a cyclic prefix. Moreover, XSI can also be removed completely by careful system design. Nevertheless, it is instructive to study the effects of ISI and XSI, since perfect removal of either ISI or XSI may be difficult for a variety of practical reasons including synchronization and imperfect channel estimation. By investigating the effects due to ISI and XSI for the two cases of optimal removal and no removal at all, we will be able to bracket the throughput performance of all MIMO-OFDM systems.

This study quantifies the effects of channel dispersion including XSI and guard time (to mitigate ISI), on the throughputs of MIMO-OFDM systems. Moreover, this quantification is made for several values of number of tones, and over several values of channel rms delay spread.

Problem 7 : Evaluation of Multi-User Diversity Systems

We quantify cell-wide mean throughputs of single-input/single-output (SISO), and multiple-input/ multiple-output (MIMO)-based cellular systems, which employ multi-user diversity (MuD). This study considers several practical and useful system-level design dimensions, including: number of transmit/receive antennas; antenna-pattern (omni-directional or sectorized); degree of error-protection (Shannon coding, no coding or intermediate coding strategies); allowable constellation size; Rician κ-factor; number of users, and scheduling algorithm (Greedy or Maximum Throughput (MAX), Proportional Fair (PF), and Equal Grade of Service (EGoS)) in single-cell (noise-limited) and multi-cell (CCI-limited) environments.

The chief observation is that, although the various dimensions are important considerations for SISO and MEA systems, the potential benefits need to be weighed in the context of limited signal constellations that are prevalent in present day practical systems. For limited signal constellation sizes, EGoS seemed a reasonable choice for the single-cell case, and PF seemed to be a reasonable choice in the context of multi-cell scenarios when delay tolerance was allowed.

We also provide a comparison between single-user systems having excess receive antennas (SU-EDoF), and multi-user diversity systems with no excess receive antennas (MuD-wo-EDoF). Both strategies improve signal quality. Since economic costs of RF chains, mobile size and form factor limit the number of antennas a mobile receiver can have, multi-user diversity can be a more practical option.

Here, among scheduler choices, it is clear that EGoS is not a viable candidate; that PF has limitations in the number of excess receive antennas it can compete against in SU-EDoF based systems; and, that MAX is the best option in terms of cell-wide throughput. In general, MuD with only a few scheduled users, has comparable throughputs as single-user receivers with excess receive antennas. By quantifying the average throughput gains that accrue from using multi-user SISO- and MIMO-based cellular systems, this study serves the needs of system operators in assessing these promising technologies within a practical context.

1.2 Why this Thesis is Important

1. *The study is extremely practical, timely, and useful.*

   - The study is applicable to cellular operators, and equipment manufacturers, who ultimately are interested in knowing the average impact of MEA links (cell-wide mean throughput over location, shadowing and multipath).
   - The study is timely, as new technologies such as MIMO, MIMO-OFDM, and MuD, are currently being evaluated by researchers both in academia and industry.

2. *The study is rich in the number of design dimensions considered.*

   - Size of the Transmit/Receive MEAs (with and without excess degrees of freedom)
   - Frequency-Reuse Factor
   - Antenna Pattern (omni-directional, or sectorized)
   - Degree of Error Protection (Shannon Coding, No Coding, or Intermediate Coding Strategies)
   - Allowable Constellation Size
   - Rician K-Factor
   - Transmit- and Receive-Adaptation
   - Diversity, and Spatial Multiplexing Systems
   - Number of Users

- Scheduling Algorithm (Greedy or Maximum Throughput (MAX), Proportional Fair (PF), and Equal Grade of Service (EGoS))
- Narrowband (Flat Fading) and Wideband (Frequency Selective) Channels
- Channels having i.i.d. and Correlated Path Gains
- Exact- and Non-Dispersive Cancellation (for wideband channels)
- Carrier Frequency
- Single-Cell (noise-limited) and Multi-Cell (CCI-limited) Environments.

3. *The study serves to guide future research investigations into newer ways of modeling CCI for MEA links.*

    - This study specifically considers some important applicable situations [(a) transmitter vs. receiver adaptation, and (b) availability (or lack) of excess degrees of freedom], and also an algorithm for analyzing the impact of CCI. This effort should, in our opinion, stimulate future detailed investigations.

4. *The study underscores the true potential of practical MEA links.*

    - In contrast to link-level studies which are extremely theoretical, highly optimistic in practice, and usually applicable only to high signal-to-noise-plus-interference (SINR) scenarios, this study reveals the actual benefit realized by MEA systems for the average user (over all SINRs).
    - This study also considers the impact of limited constellation sizes (equivalently, the maximum achievable C/I ratio). Important repercussions of this limitation are emphasized. Since systems must ultimately be built, this issue must be addressed. Most other studies fail to consider this important aspect.

Part I

Co-Channel Interference

Chapter 2

Evaluation of Co-Channel Interference Limited SISO/MEA Systems

2.1 Introduction

Communication using multiple-input/multiple-output (MIMO) links has been recognized as one of the most significant breakthroughs in modern digital communications. It has been shown for the case of independent Rayleigh-faded path gains that link capacity increases linearly with the minimum number of transmit-receive antenna elements (corresponding to the maximum number of de-coupled channels that can be created by the link) [4]. For practical signal constellations, this enables throughputs per bandwidth that traditional single-input/single-output (SISO) links cannot achieve. MIMO systems utilize the space dimension for delivering these higher throughputs.

A multi-element antenna (MEA) link employs a multi-element antenna array at one or both ends. When only one end of the link uses an MEA, diversity can be achieved [5–7]; this improves quality and thus enables higher throughput via larger signal constellations. When *both* ends use an MEA, as is the case in MIMO, it is possible to enhance throughput via either diversity (Div), as above; spatial multiplexing (SM), whereby the receiver can de-couple multiple parallel streams sent by the transmitter [4, 8–10]; or a combination of both [11, 12]. Communication using MEA/MIMO links is a fairly mature field at this time [13, 14].

The laboratory implementation of the well-known vertical Bell-Labs layered space-time architecture (VBLAST) demonstrated the feasibility of the MIMO concept, delivering spectral efficiencies of 20–40 bps/Hz under indoor conditions [9]. Not surprisingly, MIMO's potential is being tapped for commercial wireless products and networks such as wireless local area networks (WLANS), third-generation (3G) cellular networks, WiMAX, and future Internet-intensive wireless networks (including 4G networks).

Previous Research: Every cellular network has the usual assortment of link impairment conditions; co-channel interference (CCI) from other cells, multipath fading and thermal noise.

Studies have shown that CCI, more than thermal noise, serves to limit the cell-wide average throughputs that can be achieved in practical cellular systems [15, Ch. 3], [16, Ch. 3], [17, Chs. 5, 7].

CCI investigations have taken either impact-oriented (i.e., performance studies) or mitigation-oriented approaches. The latter attempt to reduce CCI via frequency-reuse, sectorization, micro-cells, and cell-splitting [15, 16]. More recent mitigation approaches include interference avoidance, arising from multi-user diversity [18–20]; and total interference suppression, made possible by base station coordination ("generalized beam forming") [21–23].

This study is concerned with performance of SISO and MEA systems. In this regard, it is noted that most MEA/MIMO performance studies take a *link-level perspective*, with the focus only on the particular link between the transmitter and the receiver (corresponding to a particular user) [4–14]. Performance measures such as bit error rate (BER) or throughput (TP) are determined with signal-to-noise ratio (SNR) treated as a parameter and with external factors such as CCI either being ignored, or indirectly treated using the signal-to-interference-plus-noise ratio (SINR) in place of the SNR.

Some work has been reported, however, that takes a *system-level perspective*. This means, for example, determining the *distribution* of performance over a coverage area, e.g., the cumulative distributive function (CDF) of TP over the randomness of user location and shadow fading, which jointly specify the SNR value. Furthermore, it also means taking into account the CCI produced by co-channel users in other cells. We note, in this regard, the body of work by Catreux who studied the single-cell case (noise only) and the multi-cell case (noise and CCI) for a wide range of system and propagation parameters [1, 2, 24]. For the noise-only case, results for the cell-averaged TP were initially obtained via simulations. Then a purely analytical method was developed and shown to be accurate [24]. For the noise-plus-CCI case, extensive results were obtained via simulation only [1]. The work reported here extends Catreux's work in several respects, including steps towards an entirely analytical approach to dealing with CCI.

Contribution of this study: Here, we extend in particular the work of [1, 2]. First, we quantify the attainable system-level throughputs of interference-limited SISO and MEA cellular systems along various design dimensions, i.e., size of the transmit/receive MEAs; frequency-reuse factor; antenna pattern (omni-directional or sectorized); degree of error protection (Shannon coding, no coding or intermediate coding strategies); allowable constellation size; Rician K-factor and transmit vs. receive-adaptation. We use the cell-wide mean throughput per user as the primary metric. In a cell with many users, this closely approximates the average performance any user can expect [1, 2, 24]. The treatment of reuse factor, and of transmit- vs. receive-adaptation, extends the work reported in [1]. This study is rich in the number of design dimensions considered, thereby creating a foundation for: (i) underscoring the true potential of practical MEA links; and, (ii) validating the use of the noise model for CCI (Chapter 4).

2.2 The Narrowband SISO/MEA Simulation Platform

A system-level simulation platform has been developed for computing the throughputs of SISO and MEA cellular systems. The platform discussed in this chapter is intended for *narrowband* or flat channels. Both kinds of MIMO/MEA systems, i.e., Spatial Multiplexing, and Transmit Diversity systems, have been simulated. Moreover, both Transmit- as well as Receive-Adaptation Systems have been considered. The test-bed is sufficiently general so as to allow for the detailed investigation of the several key system-level parameters, such as:

- Size of the transmit/receive MEAs (with, and without excess degrees of freedom)
- Frequency-reuse factor
- Antenna pattern (omni-directional, or sectorized)
- Degree of error protection (Shannon coding, no coding, or intermediate coding strategies)
- Allowable constellation size
- Rician K-factor
- Single-cell (noise-limited) and Multi-cell (CCI-limited) environments.

2.2.1 SISO/MEA System Model

In the cellular data environment considered in this study, a given cell, consisting of a serving base station (BS) and a set of mobile stations (MS), is surrounded by one contiguous tier of six

Table 2.1: PARAMETER VALUES USED IN THE SYSTEM SIMULATIONS.

Cell Geometry	Hexagonal Array with side $R = 1000$ m
Carrier Frequency	$f_c = 2$ GHz
System Bandwidth	$W = 5$ MHz
Path Loss Exponent	$\Gamma = 3.7$
Shadow Fading	Lognormal, with Standard Deviation $\sigma = 8$ dB
Multipath Fading	Rician, with K-factor = 0 (Rayleigh) or 10
Antenna Pattern	Omnidirectional or Uniform over $120°$
Thermal Noise Density	$N_0 = -174$ dBm/Hz
Mobile Station's Noise Figure	$N_F = 8$ dB
Transmit Power	$P_T = 5$ W
Median Cell-Boundary SNR	$\rho = 20$ dB

cells. While the platform is quite general with respect to system and channel parameters, most numerical results were obtained using the parameters detailed in Table 2.1.

The complex baseband channel gain between the jth transmit antenna of a given base station and the ith receive antenna of a given user-terminal is modeled by

$$h_{ij} = \sqrt{A\left(\frac{d_0}{d}\right)^{\Gamma} s}\left[\sqrt{\frac{K}{K+1}}e^{j\phi} + \sqrt{\frac{1}{K+1}}z_{ij}\right] \tag{2.1}$$

where,

- d is the link length, Γ is the path loss exponent, and A is the median of the path gain at reference distance d_0 ($d_0 = 100$ m in the simulations).
- K is the Rician K-factor. Co-channel base stations, being relatively far, use $K = 0$.
- $s = 10^{S/10}$ is a log-normal shadow fading variable, where S is a zero-mean Gaussian random variable with standard deviation σ dB.
- $\phi = 2\pi d/\lambda$ is the phase shift of a line-of-sight (LOS) plane wave from the transmitter to the receiver. We assume that for a given transmit-receive pair, all link-paths have the

same length.

- z_{ij} represents the phasor sum of scattering components for the (i, j) path which are assumed to be zero-mean, unit-variance, i.i.d. complex Gaussian random variables.

We assume a base station height of $h = 30$ m above ground. For receivers located close to the ground, the direct path has a length $d = [r^2 + h^2]^{1/2}$, where r is the distance along the ground from the receiver to the base station. This implies that all Transmitter-Receiver (T-R) distances are 30 m or greater. We use a loss exponent of 2.0 (free space loss) for distances close to the base station ($30 - 100$ m), and 3.7 for distances beyond 100 m. We also incorporate shadow fading regardless of the T-R distance. This has been shown to be an empirically reasonable model [25]. For antenna sectoring, perfect beams are assumed instead of shaped antenna patterns.

2.2.2 System Model Assumptions

The assumptions often made in conjunction with MEA systems are also invoked here [4, 8]: (i) narrowband signaling, (ii) quasi-static (block) fading, (iii) long burst interval, and (iv) independently faded complex Gaussian path gains. This permits a mathematical representation for the SISO/MEA cellular system as follows[1]

$$\mathbf{Y} = \mathbf{H}\mathbf{X} + \mathbf{Z} \tag{2.2}$$

where $\mathbf{X} \in \mathbb{C}^{7n}, \mathbf{Y} \in \mathbb{C}^{m}$, are transmit (serving as well as interfering) and receive signals, $\mathbf{H} \in \mathbb{C}^{m \times 7n}$ is the channel gain and $\mathbf{Z} \in \mathbb{C}^{m}$ is thermal noise, that is Gaussian distributed with zero-mean and one-sided power spectral density N_0. Since the noise processes corrupting the different receive antennas are independent, $\mathbf{Z}$ has an autocorrelation matrix $N_0\mathbf{I}$, with $\mathbf{I}$ being the identity matrix.

Only one tier of interferers around the serving BS is assumed here. This assumption is made to simplify the simulations and is slightly optimistic. However, the rapid decay of signal power

[1]With throughput as our metric, we can rank interference-limited Spatial Multiplexing systems having 1 or 3 antennas as $(1, 1) < (3, 1) < (1, 3) < (3, 3)$, i.e., the performance of $(3, 1)$ can be gauged from those for $(1, 1)$ and $(1, 3)$. By extension, configurations with more transmit than receive antennas ($n > m$) can be excluded from the family of Spatial Multiplexing systems, as their performances can be bracketed using results for $m \geq n$. Such systems must necessarily employ Transmit Diversity, and as such are grouped under that family of systems.

with distance makes this assumption reasonable. Moreover, we offset it with the pessimistic assumption that all co-channel interferers are transmitting all the time.

An adaptive transmission algorithm is assumed. The algorithm perfectly adapts the modulation (constellation size) on each transmit antenna according to the instantaneous radio channel and interference conditions. Therefore, it is possible for different transmit antennas, in Spatial Multiplexing systems, to choose different bit rates (constellation sizes); although all transmissions operate at the same symbol rate. We note that, all transmit antennas must transmit at a common rate for diversity systems. The procedure to compute the optimum size of the transmit constellations is given in Section 2.2.4.

Since cell-site (macro) diversity has been shown to have minimal impact on mean throughput calculations [1, 2], it is not used in the simulations. That is, for simplicity, we assume that users communicate with the base station that is the nearest, not necessarily the strongest. Finally, perfect channel estimation, T-R synchronization, and instantaneous feedback are also assumed. These simplifications focus the problem onto the essential issues being investigated.

2.2.3 Array Processing Schemes

Depending on the availability of channel state information (CSI) at the transmitter, it is possible to design two different array processing categories, namely, transmit-adaptation and receive-adaptation. We examine singular valued decomposition (SVD) at the transmitter, and minimum mean-square error (MMSE) reception, as representative examples of these categories. In either case, total transmit power is kept constant regardless of n (the number of transmit antennas). The SVD scheme performs spatial water-filling to optimally allocate power to the individual transmit antennas, while MMSE uses uniform power allocation among transmit antennas.

There are more optimal approaches as well. At the transmit side, there is generalized beam forming (of which SVD is a subset), that uses *global* CSI, meaning that path gains to *each* receiver from all interferers are included. However, the practical difficulty of using global CSI adaptation at the transmitter is too great to consider [21–23]. At the receive side, there are variations of successive interference cancellation (SIC) [1, 2, 24], which also pose practical implementation problems. Thus, the focus here is on the two techniques of SVD transmission and MMSE reception, both of which represent excellent compromises between good performance and practical implementation.

Both, SVD and MMSE, are examples of Spatial Multiplexing systems. In this thesis, we also consider the Alamouti Coding scheme as a representative example of Transmit Diversity systems. Like the MMSE scheme, the Alamouti scheme also allocates equal power to the transmit antennas.

The Singular Valued Decomposition (SVD) Transmit Scheme

With CSI available at the transmitter, it becomes possible to employ transmit filtering to pre-compensate for the known distortions the channel will introduce [4]. This permits the creation of several parallel (decoupled) SISO channels via Eigen-Beamforming. The SVD of the channel gain matrix provides the necessary filtering required at both ends of the link.

We assume that CSI is limited, that is each receiver knows only about paths leading to its antennas. Being a transmit-adaptation system[2], the transmitter cannot meaningfully exploit knowledge of path gains from the interferers. Thermal noise and CCI are thus lumped into a single interference-plus-noise term to simplify analysis, and diagonalization is attempted on paths from the serving BS only. Moreover, like thermal noise, CCI is assumed to have Gaussian statistics. This is a reasonable assumption given the central limit theorem, since there are several interfering BSs, each having several paths to the MS. Thus, we have that

$$\begin{aligned}
\mathbf{Y} &= \mathbf{HX} + \mathbf{Z} \\
&= \mathbf{H_s X_s} + \mathbf{H_{CCI} X_{CCI}} + \mathbf{Z} \\
&= \mathbf{H_s X_s} + \mathbf{Z_I}
\end{aligned}$$

where $\mathbf{Z_I} = \mathbf{H_{CCI} X_{CCI}} + \mathbf{Z}$; $\mathbf{X_s}$ and $\mathbf{X_{CCI}}$ are respectively, the transmit and interfering signals; and $\mathbf{H_s}$ and $\mathbf{H_{CCI}}$ are, respectively, the gain matrices for the serving and interfering BSs.

By the singular value decomposition theorem, it is possible to express any matrix $\mathbf{H_s}$ in the form

$$\mathbf{H_s} = \mathbf{UDV}^{\dagger}$$

[2]Any transmit-adaptation system with limited CSI (in this instance, SVD) cannot attempt generalized beam forming, and hence, is ineffective at suppressing co-channel interferers.

where $\mathbf{U}$, $\mathbf{V}$ are unitary matrices, and $\mathbf{D}$ is a diagonal matrix. Thus, $\mathbf{Y}$ can be rewritten as

$$\mathbf{Y} = \mathbf{U}\mathbf{D}\mathbf{V}^{\dagger}\mathbf{X_s} + \mathbf{Z_I}.$$

Pre-multiplying both sides by $\mathbf{U}^{\dagger}$, yields the filtering needed at the receiver, i.e.,

$$\mathbf{U}^{\dagger}\mathbf{Y} = \mathbf{D}\mathbf{V}^{\dagger}\mathbf{X_s} + \mathbf{U}^{\dagger}\mathbf{Z_I}.$$

Here $\mathbf{V}^{\dagger}$ operating on $\mathbf{X_s}$ has the effect of distorting (rotating) the transmitted signal before it reaches the receiver. For our purposes, we may consider $\mathbf{V}^{\dagger}\mathbf{X_s}$ to be the "transmitted signal" and think of the channel as merely "scaling" the various signals on their way to the receiver (via matrix $\mathbf{D}$). Diagonalization is achieved using transmit-receive filtering as shown below

$$\widetilde{\mathbf{Y}} = \mathbf{U}^{\dagger}\mathbf{Y} \qquad \widetilde{\mathbf{X}} = \mathbf{V}^{\dagger}\mathbf{X_s} \qquad \text{and} \qquad \widetilde{\mathbf{Z}} = \mathbf{U}^{\dagger}\mathbf{Z_I}, \tag{2.3}$$

$$\widetilde{\mathbf{Y}} = \mathbf{D}\widetilde{\mathbf{X}} + \widetilde{\mathbf{Z}}. \tag{2.4}$$

Alternatively, we can use $\mathbf{V}$ as the transmit filter, and transmit the signal $\mathbf{V}\mathbf{X_s}$ in place of $\mathbf{X_s}$ (in this case $\widetilde{\mathbf{X}}$ in (2.4) becomes $\mathbf{X_s}$). Equation (2.4) can be written, for each (de-coupled) SISO channel, as

$$\tilde{y}_j = h_j\tilde{x}_j + \tilde{z}_j \qquad j = 1, 2, \ldots, n. \tag{2.5}$$

The h_j's are the diagonal elements of $\mathbf{D}$ and act as the channel gains for the decoupled SISO channels. The transmit power applied to each antenna is determined from "water-filling" the n ($\leq m$) SISO channels, subject to a total power constraint [4], i.e.,

$$P_j = \left(\nu - \frac{\tilde{\sigma_j}^2}{h_j^2}\right)^+ \qquad \sum_{j=1}^{n} P_j = P \tag{2.6a}$$

$$\tilde{\sigma_j}^2 = \sigma^2 + \sum_{k=n+1}^{7n} CCI_{jk} = N_0 + \sum_{k=n+1}^{7n} CCI_{jk} \tag{2.6b}$$

where CCI_{jk} is the instantaneous power from an interfering antenna k to receive antenna j and the P_j's are the respective transmit powers to be applied. From [26], the post-processing SINR for each SISO channel can then be determined using

$$\gamma_j = \frac{P_j|h_j|^2}{\tilde{\sigma_j}^2}. \tag{2.7}$$

The Minimum Mean Square Error (MMSE) Receiver Scheme

Receive-adaptation has long been used to improve the quality of the wireless link (conventionally, to achieve diversity [17, Ch. 4], [27]). In the context of interference-limited MIMO systems, the array processor needs to provide stream separation, while attempting diversity gain and interference suppression as much as possible. One such array processor is the (linear) minimum mean-square error (MMSE) receiver [17, 27]. Other possible processors are successive-interference-cancellation (SIC), ordered-SIC (OSIC) and OSIC-MMSE [2]. For purposes of this work, employing the simpler MMSE scheme will suffice. The added benefits of OSIC-MMSE are quantified in [2].

To evaluate the MMSE scheme, the analyst takes into account the path gains from all BSs, both serving and interfering, in the channel gain matrix ($\mathbf{H} \in \mathbb{C}^{m \times 7n}$). Received data streams are separated by computing a linear combination of the received signals using a set of weights that achieves the minimum mean square error between the output estimate and the true signal sample. Thus, we have

$$\hat{\mathbf{X}} = \mathbf{W}^H \mathbf{Y}. \tag{2.8}$$

The performance index for a given weight matrix is

$$\zeta(\mathbf{W}^H) \triangleq E\left[\sum_{j=1}^{n} |\epsilon_j|^2\right] = E\left[\sum_{j=1}^{n} |x_j - \hat{x}_j|^2\right] \tag{2.9}$$

where x_j is the jth transmitted signal. The expectation in (2.9) is taken with respect to the noise and the statistics of the data sequences. The weight matrix that yields the minimum mean square error is the desired one. The quantity $\mathbf{W}$ is given as [2]

$$\mathbf{W} = \mathbf{A}^{-\mathbf{1}}\mathbf{H} \tag{2.10a}$$

$$\mathbf{A} = \mathbf{H}\mathbf{H}^H + \frac{\sigma^2}{P/n}\mathbf{I}_{m \times m}. \tag{2.10b}$$

The post-processing SINR on the jth decoded stream can be shown to be [2, 24]

$$\gamma_j = (\mathbf{H})_j^H \mathbf{R}_j^{-1} (\mathbf{H})_j, \;\; j = 1, 2, \ldots, n \tag{2.11}$$

where

$$\mathbf{R}_j = \sum_{l=1,\, l \neq j}^{7n} (\mathbf{H})_l (\mathbf{H})_l^H + \frac{\sigma^2}{P/n}\mathbf{I}_{m \times m} \tag{2.12}$$

and $(\mathbf{H})_j$ is the jth column of $\mathbf{H}$.

Transmit Diversity via Alamouti Coding

The Alamouti scheme is an optimal transmit diversity scheme. It is optimal in the sense that it offers the maximum code rate ($r = 1$) and does not suffer from any loss of performance as compared to an MRC diversity scheme. Specific engineering aspects of this scheme are detailed in [5].

Under the assumption that noise plus co-channel interference (CCI) can be treated as complex Gaussian, the Alamouti scheme on a $(2, m)$ link has the same performance as the $(1, 2m)$ MRC receiver at half the transmit power of the $(2, m)$ MIMO configuration [5]. This enables an easy computation of the signal-to-interference-plus-noise-ratios (SINRs) as follows

$$\gamma_i = \frac{|h_{i0}|^2 (P/2)}{\sigma^2 + \sum_k \mathrm{CCI}_{ik}}, \quad i = 1, 2, \ldots, 2m \tag{2.13}$$

$$\gamma_{\text{alamouti}} = \sum_i \gamma_i, \quad i = 1, 2, \ldots, 2m \tag{2.14}$$

where

- h_{i0} is the instantaneous signal gain from the serving BS to the ith receive antenna.
- P is the total transmitter power.
- CCI_{ik} is the instantaneous power from the kth interfering BS at the ith receive antenna.
- γ_i is the input SINR at the ith branch of the MRC receiver.
- $\gamma_{alamouti}$ is the SINR at the receiver output.

Equation (2.14) is the well-known result that the SINR of an MRC receiver is equal to the sum of SINRs of its individual branches.

2.2.4 Link Throughput Bounds

The *instantaneous* per-user data throughput is the sum of the instantaneous throughputs of the sub-streams. The instantaneous throughput T_j of sub-stream j is determined for the following two extreme cases:

Ideally Coded Signals: The throughput is upper-bounded by the Shannon capacity

$$T_j = \log_2 (1 + \gamma_j) \,. \tag{2.15}$$

Uncoded Signals: Assuming no coding, and error detection in each block, the throughput is

$$T_j(M_j) = (1 - BLER_j) \log_2(M_j) = (1 - BER_j)^L \log_2(M_j) \tag{2.16}$$

where $\log_2(M_j)$ is the number of bits per symbol in stream j, and BLER is the corresponding block error rate for L-bit blocks. In this study $L = 500$ bits, although the results are robust for values of L over a wide practical range [2].

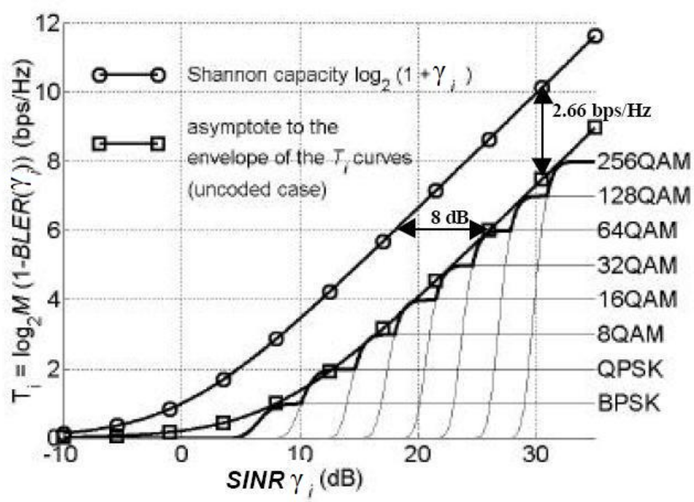

Figure 2.1: Mean throughput for various modulation levels as a function of SINR (from [1,2]).

It is desired to express (2.16) in the form of (2.15) for convenience of calculation. This can be achieved as follows: Under the simplifying assumption of quasi-static block fading, it is possible to regard the channel as *AWGN conditioned on the instantaneous path gains*. For QAM modulation, we can then use for the symbol error rate (SER) the well-known equation [28, Ch. 5] applicable to the Gaussian channel

$$SER = 4Q\left(\sqrt{\frac{3E_s}{(M-1)N_0}}\right) \tag{2.17}$$

where $Q(\cdot)$ is the complementary error function [28, Ch. 2], E_s is the signal energy of the transmitted symbol, M is the constellation size, and N_0 is the noise power spectral density. Then, in (2.16) we can employ the relationship

$$BER = SER / \log_2(M). \tag{2.18}$$

Using the SINR and (2.15)–(2.18), we can plot (i) the uncoded throughputs for a given constellation size M, and (ii) the upper-bound throughput, i.e., the Shannon capacity. Plotting the uncoded throughputs for various constellation sizes, the family of curves shown in Fig. 2.1 is obtained (cf. [1, 2, 24]). The upper-bound throughput is also shown in the figure.

For uncoded signals, it is clear that there exists an optimal constellation for a given SINR. Over the range of SINRs, this optimal 'envelope' curve has a stair-like appearance. An asymptote curve is shown in Fig. 2.1 that closely approximates the stair-like curve. There is a separation of about 8 dB $(10 \log_{10}(6.4))$ between the upper-bound coding curve and the asymptote for the uncoded case. The asymptote curve can thus be accurately approximated by

$$T_j = \max\ T_j(M_j) \approx \log_2 \left(1 + \frac{\gamma_j}{6.4}\right). \tag{2.19}$$

A variety of practical coding strategies can then be modeled by using shifts in SINR less than 8 dB.

2.3 Simulation Methodology

Throughput statistics of SISO/MEA configurations for various design options can be computed as follows:

(1) Randomly place an MS within the cell and generate channel matrix $\mathbf{H}$ as given by (2.1).

(2) Compute post-processing SINR of substream j for SVD ((2.6)-(2.7)) and MMSE ((2.11)-(2.12)).

(3) Compute throughputs for substream j ((2.15), (2.19)).

(4) Compute "MEA throughput" as the sum of the throughputs of the individual substreams.

This computation leads to *instantaneous* throughputs, for given values of MS location (path loss), shadow fading, and instantaneous channel fades from serving and interfering BSs. Averaging over all these leads to the cell-wide mean throughput per user.

For the purpose of averaging, we distribute the MS with uniform randomness at 2500 locations over a given cell/sector. We allow an MS to experience 1000 different shadowing-multipath fades for each location[3]. In this study, both limited and unlimited constellation sizes are considered. For the limited case, modulation levels up to 16-QAM (leading to a symbol rate of up to 4 bits/symbol) are considered. This maximum is practical for present-day cellular implementations[4].

At the beginning of each block-fade interval, the receiver determines array weights via either adaptive search or channel estimation. The receiver then determines the constellation size (M) for each transmit antenna from the substream post-processing SINRs and communicates this information to the transmitter. Adaptive modulators at each transmit antenna then quickly select the corresponding optimal QAM constellation. This entire process (estimation-feedback-adaptation) is assumed to occur before the channel can change appreciably (within the block fade interval).

2.4 Numerical Results

For evaluating the performance of CCI-limited SISO/MEA cellular systems, the platform discussed in Chapter 2 is used. Figures 2.2 and 2.3 show the cell-wide average throughputs that are offered by MMSE and SVD systems for the many dimensions that were considered. Only a representative listing is shown[5], instead of presenting throughputs over all dimensions, so as to keep the presentation useful and concise. Our initial presentation refers to the case of Shannon coding, a reuse factor of 1, a Rician K-factor of zero, omni-directional antennas, and unlimited signal constellation sizes. Deviations from this baseline case are explained subsequently.

Effect of Degrees of Freedom: First we consider the MMSE scheme shown in Fig. 2.2. Neither the SISO $(1, 1)$, nor the MIMO $(3, 3)$ system have excess degrees of freedom. It is clear that, although there is a substantial increase in mean throughput for the MIMO $(3, 3)$ system as compared to the SISO $(1, 1)$ system, the increase cannot be expected to be three-fold despite the

---

[3]The 1000 realizations are sufficient to ensure statistical stability, even under Rayleigh fading.

[4]The state-of-art is 16-QAM for mobile wireless systems, and 64-QAM for fixed wireless systems.

[5]A comprehensive set of data appears in the Tables in Section 2.6

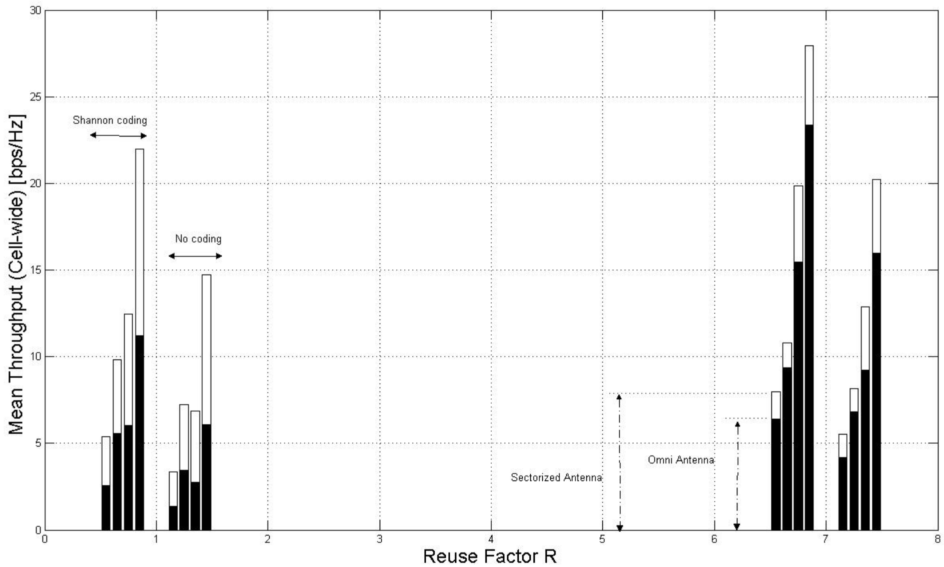

Figure 2.2: Per-link average throughputs of MMSE systems for various design options: (1, 1), (1, 3), (3, 3) and (3, 6) systems with Rician factor $K = 0$, for both Shannon coded and uncoded systems, for Reuse factors 1 and 7. For a Reuse factor $R = 7$, the cell will have $1/7$th the number of channels as compared to the $R = 1$ case. Consequently, system throughputs (cell-wide averages) will use $1/7$th the per-link throughputs.

creation of three parallel de-coupled streams at the receiver. This is because users are typically not in the high SINR regime, and the available degrees of freedom (receive antennas) are used to combat cross-stream interference (XSI), even at the cost of noise enhancement. Also, each transmit antenna in the (3, 3) system now uses only $1/3$ the total transmit power as compared to the SISO system.

By considering the (1, 3) and (3, 6) MEA systems, it can be seen that adding excess degrees of freedom can help better combat fading and CCI. Note however, that SIMO $(1,\, m)$ is still a single stream configuration, although much improved as compared to SISO. Hence, for the most part, MIMO $(n,\, n)$ systems with their multiple streams will fare better, and furthermore, MIMO $(n,\, m)$ with excess degrees of freedom will do even better.

Next, consider the SVD scheme shown in Fig. 2.3. It is observed that MIMO (3, 3) has a greater throughput as compared to the MIMO $(3, 3)$ with MMSE; throughput increase over SISO (1, 1) is closer to a three-fold improvement. On the other hand, the throughput increase brought about by excess degrees of freedom is modest, as evidenced by comparing SISO (1, 1)

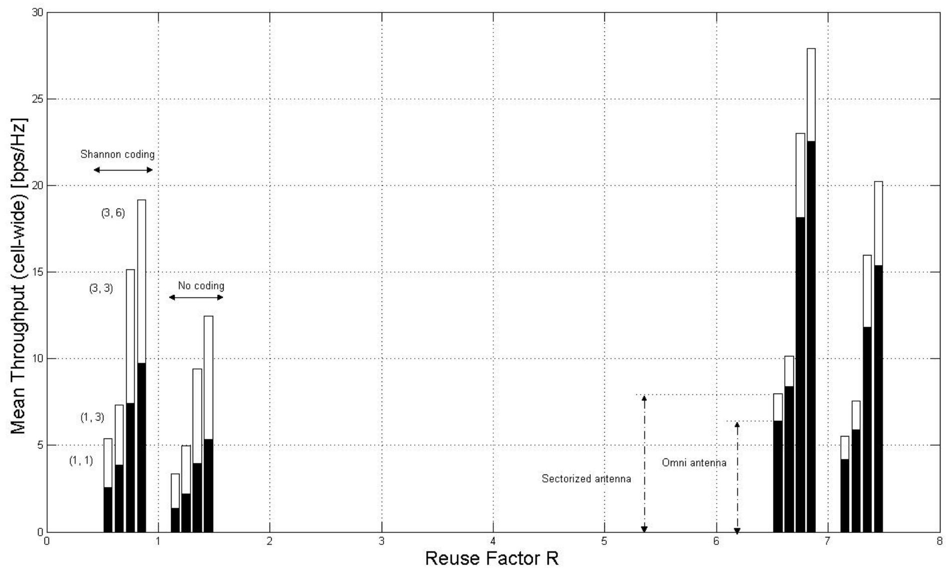

Figure 2.3: Per-link average throughputs of SVD systems for various design options: (1, 1), (1, 3), (3, 3) and (3, 6) systems with Rician factor $K = 0$, for both Shannon coded and uncoded systems, for Reuse factors 1 and 7. For a Reuse factor $R = 7$, the cell will have $1/7$th the number of channels as compared to the $R = 1$ case. Consequently, system throughputs (cell-wide averages) will use $1/7$th the per-link throughputs.

with SIMO (1, 3), or MIMO (3, 3) with MIMO (3, 6). These results show that SVD is better than MMSE at combating XSI, and results in less noise enhancement. On the other hand, since the transmitter has limited CSI and cannot exploit knowledge of path gains from the interferers, it is unable to obtain significant gains when excess degrees of freedom exist.

Effect of Reuse Factor: Increasing the reuse factor to 7 pushes the interfering base stations farther away, and hence, improves per-link throughput. However, system throughput (throughput per bandwidth per cell) reduces, since each cell now has $1/7$ the number of available channels.

Effect of Antenna Sectorization: Using sectorized antennas and a reuse factor of 1 leads to about a two-fold improvement in link throughput over the results for omni-directional antennas. This is consistent with results from conventional systems (using three-sector antennas enables cellular planners to bring down the reuse factor from 12 to 7, which amounts to a similar throughput increase [16, Ch. 3]). At a reuse factor of 7, the link throughput increase due to sectorization is no longer two-fold. The higher reuse factor has already reduced CCI to a point that sectorization can only bring about modest returns. Once again, per-link throughput increases but system throughput per bandwidth decreases.

Effect of Rician K-Factor: In the presence of a strong specular component ($K \sim 10$), the mean throughput of MIMO-MMSE systems decreases by about 30–40%, while that of MIMO-SVD systems decreases by 15%[6], regardless of whether excess degrees of freedom were available or not. This is consistent with our expectation, at least for the case of no excess degrees of freedom. SVD with its transmit-receive processing is better equipped to combat channel fading and XSI as compared to MMSE.

Since the LOS component has much more weightage (in terms of received power) than the NLOS component, throughput improvements for both SVD as well as MMSE systems arising from excess degrees of freedom are limited. Consequently throughput trends for both SVD and MMSE systems for the case when excess degrees of freedom are available, mirror those when excess degrees of freedom do not exist.

For SISO and SIMO systems, throughput of both schemes increases slightly ($\leq 10\%$) at $K = 10$ (see footnote 6). For SIMO systems, the percentage increase is less than for the SISO system. This throughput behavior conforms to previous link-level expectations and proofs [8].

Effect of Limited Constellation Sizes: Whereas unlimited constellation size provides insight to the potentially achievable throughputs the system can offer, it is also necessary to consider values of throughput that practical systems can actually realize. Figure 2.4 offers some illustrative results. Limiting the transmit alphabet size to 16-QAM amounts to capping throughput at $4n$ bps/Hz. The effect is to reduce the potential benefit from excess degrees of freedom, higher reuse factors and antenna sectorization. Compared to the case of unlimited constellation

[6]The channel gain matrix can be regarded as a weighted combination of LOS and NLOS components of ranks 1 and n respectively (see (2.1)). Being a function of the rank, capacity contribution from the NLOS component far exceeds that from the LOS component. A higher K-factor increases the weight of the LOS component, and decreases the weight of the NLOS component, resulting in an overall decrease for $n > 1$.

sizes, we notice a throughput loss of about 50% for both MMSE and SVD schemes for both reuse factors (1 and 7). This observation has important implications for current state-of-the-art systems that can support signal constellations only up to 16-QAM.

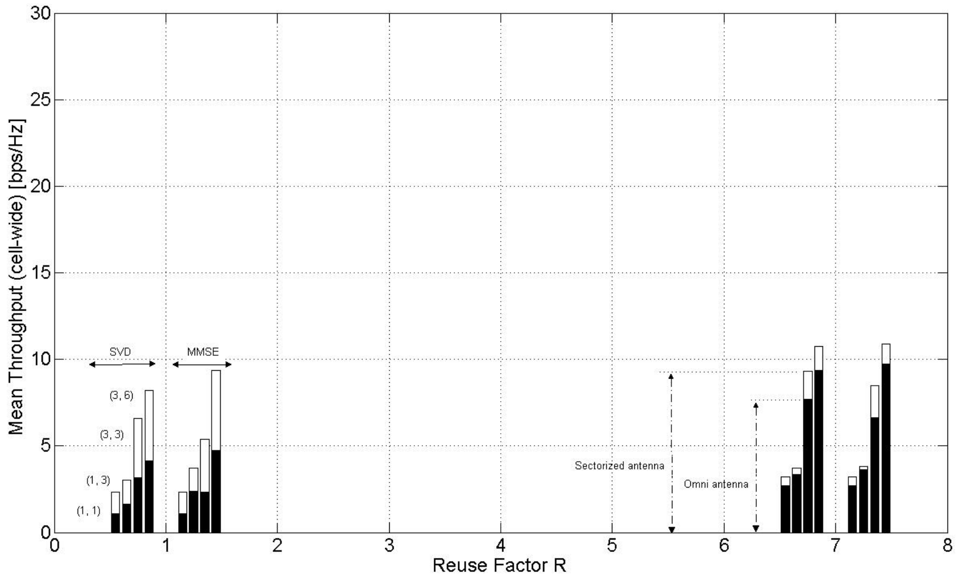

Figure 2.4: Comparison of per-link average throughputs of SVD and MMSE systems for various design options: (1, 1), (1, 3), (3, 3) and (3, 6) systems, Rician factor $K = 0$, with no coding, 16-QAM and for Reuse factors 1 and 7. It is instructive to compare the SVD and MMSE throughputs in this plot (for 16-QAM), with those in Figures 2 and 3 (for unlimited-QAM).

Effect of Coding: The reduction in throughput for transmitting uncoded signals relative to Shannon coded signals is about 40–50% for a reuse factor of 1 and 20–30% for a reuse factor of 7. The amount of reduction decreases with sectorization. Practical coding strategies will perform in the interim range.

SVD vs. MMSE: Both schemes have identical performance for the SISO configuration since it is a degenerate configuration. For configurations that do not have excess degrees of freedom (e.g., MEA (3, 3)), SVD with its stream decoupling performs better. When excess degrees of freedom exist (e.g. MEA (3, 6)), the improvement brought about by SVD is smaller than that for MMSE. MMSE with its receive-adaptation is able to optimally combat interference (via nulling) plus fading (via diversity), and hence, performs better. This result is clear from Figs.

2.2, 2.3 and 2.4.

2.5 Conclusion

We have quantified the mean throughput of MEA systems along many system-level dimensions. An important observation is that the *actual* potential of MEA systems is obtained by taking into consideration (i) average user experience (cell-wide mean throughputs); and (ii) limited signal constellation sizes which are prevalent in practical present day systems. Studies which ignore these concerns, can lead to very optimistic results and conclusions. Another observation is that, although excess degrees of freedom is an important consideration for MEA systems, the potential benefits need to be weighed in the context of limited signal constellations that are prevalent in practical present day systems.

The work reported in this study has ignored the costs arising from channel estimation, synchronization, and finite-delay feedback, among other factors. Practical systems incorporating such realistic considerations have been investigated in [29]. Extensions to this work currently being investigated include dispersive channels and correlations among channel gain matrix elements [30].

2.6 Tabular Results for Co-Channel Interference Study

Per-link cell-wide average throughputs (in units of bps/Hz) of MIMO $(1,1)$ links employing MMSE receivers. An exact model has been used for CCI. The simulation results are over Reuse Factors (R), Rician K-factors, and Antenna-Patterns (Omni-directional or Sectorized).

	R = 1		R = 7	
	K = 0	K = 10	K = 0	K = 10
Omni	2.5827	2.8707	6.4161	7.0239
Sectorized	5.3924	5.9199	7.9572	8.6972

Table 2.2: Infinite-QAM with Shannon coding.

	R = 1		R = 7	
	K = 0	K = 10	K = 0	K = 10
Omni	1.3568	1.5193	4.1902	4.6681
Sectorized	3.3628	3.7484	5.5245	6.1646

Table 2.3: Infinite-QAM with no coding.

	R = 1		R = 7	
	K = 0	K = 10	K = 0	K = 10
Omni	1.0689	1.1889	2.7146	2.9712
Sectorized	2.3218	2.5629	3.2301	3.4870

Table 2.4: 16-QAM with no coding.

Per-link cell-wide average throughputs (in units of bps/Hz) of MIMO $(1, 3)$ links employing MMSE receivers. An exact model has been used for CCI. The simulation results are over Reuse Factors (R), Rician K-factors, and Antenna-Patterns (Omni-directional or Sectorized).

	R = 1		R = 7	
	K = 0	K = 10	K = 0	K = 10
Omni	5.5476	5.6894	9.3825	9.6004
Sectorized	9.8447	10.0873	10.7727	10.8370

Table 2.5: Infinite-QAM with Shannon coding.

	R = 1		R = 7	
	K = 0	K = 10	K = 0	K = 10
Omni	3.4413	3.5437	6.8111	7.0088
Sectorized	7.2472	7.4762	8.1418	8.1979

Table 2.6: Infinite-QAM with no coding.

	R = 1		R = 7	
	K = 0	K = 10	K = 0	K = 10
Omni	2.3929	2.4611	3.6142	3.6827
Sectorized	3.7093	3.7580	3.8330	3.8651

Table 2.7: 16-QAM with no coding.

Per-link cell-wide average throughputs (in units of bps/Hz) of MIMO $(3, 3)$ links employing MMSE receivers. An exact model has been used for CCI. The simulation results are over Reuse Factors (R), Rician K-factors, and Antenna-Patterns (Omni-directional or Sectorized).

	R = 1		R = 7	
	K = 0	K = 10	K = 0	K = 10
Omni	6.0536	3.6245	15.4405	9.8127
Sectorized	12.4518	7.8081	19.8564	13.0161

Table 2.8: Infinite-QAM with Shannon coding.

	R = 1		R = 7	
	K = 0	K = 10	K = 0	K = 10
Omni	2.7526	1.3095	9.2321	4.9344
Sectorized	6.8826	3.5765	12.8915	7.2087

Table 2.9: Infinite-QAM with no coding.

	R = 1		R = 7	
	K = 0	K = 10	K = 0	K = 10
Omni	2.3244	1.1852	6.6512	4.0043
Sectorized	5.3770	3.0625	8.4724	5.6000

Table 2.10: 16-QAM with no coding.

Per-link cell-wide average throughputs (in units of bps/Hz) of MIMO $(3, 6)$ links employing MMSE receivers. An exact model has been used for CCI. The simulation results are over Reuse Factors (R), Rician K-factors, and Antenna-Patterns (Omni-directional or Sectorized).

	R = 1		R = 7	
	K = 0	K = 10	K = 0	K = 10
Omni	11.2184	6.5712	23.3521	15.6724
Sectorized	21.9769	14.5215	27.9538	19.9981

Table 2.11: Infinite-QAM with Shannon coding.

	R = 1		R = 7	
	K = 0	K = 10	K = 0	K = 10
Omni	6.0993	2.9325	15.9538	9.3107
Sectorized	14.7013	8.3358	20.2108	12.9036

Table 2.12: Infinite-QAM with no coding.

	R = 1		R = 7	
	K = 0	K = 10	K = 0	K = 10
Omni	4.7392	2.4953	9.7232	6.8266
Sectorized	9.3484	6.3903	10.9061	8.6843

Table 2.13: 16-QAM with no coding.

Per-link cell-wide average throughputs (in units of bps/Hz) of MIMO $(1, 1)$ links employing SVD receivers. An exact model has been used for CCI. The simulation results are over Reuse Factors (R), Rician K-factors, and Antenna-Patterns (Omni-directional or Sectorized).

	R = 1		R = 7	
	K = 0	K = 10	K = 0	K = 10
Omni	2.5827	2.8707	6.4161	7.0234
Sectorized	5.3924	5.9199	7.9572	8.6972

Table 2.14: Infinite-QAM with Shannon coding.

	R = 1		R = 7	
	K = 0	K = 10	K = 0	K = 10
Omni	1.3568	1.5193	4.1902	4.6681
Sectorized	3.3628	3.7484	5.5245	6.1646

Table 2.15: Infinite-QAM with no coding.

	R = 1		R = 7	
	K = 0	K = 10	K = 0	K = 10
Omni	1.0689	1.1889	2.7146	2.9712
Sectorized	2.3218	2.5629	3.2301	3.4870

Table 2.16: 16-QAM with no coding.

Per-link cell-wide average throughputs (in units of bps/Hz) of MIMO $(1,3)$ links employing SVD receivers. An exact model has been used for CCI. The simulation results are over Reuse Factors (R), Rician K-factors, and Antenna-Patterns (Omni-directional or Sectorized).

	R = 1		R = 7	
	K = 0	K = 10	K = 0	K = 10
Omni	3.8637	4.0271	8.3780	8.5694
Sectorized	7.3378	7.5030	10.1410	10.4115

Table 2.17: Infinite-QAM with Shannon coding.

	R = 1		R = 7	
	K = 0	K = 10	K = 0	K = 10
Omni	2.1936	2.3031	5.8893	6.0566
Sectorized	4.9712	5.1063	7.5389	7.7961

Table 2.18: Infinite-QAM with no coding.

	R = 1		R = 7	
	K = 0	K = 10	K = 0	K = 10
Omni	1.6506	1.7182	3.3581	3.4243
Sectorized	3.0431	3.1124	3.7327	3.7790

Table 2.19: 16-QAM with no coding.

Per-link cell-wide average throughputs (in units of bps/Hz) of MIMO $(3, 3)$ links employing SVD receivers. An exact model has been used for CCI. The simulation results are over Reuse Factors (R), Rician K-factors, and Antenna-Patterns (Omni-directional or Sectorized).

	R = 1		R = 7	
	K = 0	K = 10	K = 0	K = 10
Omni	7.4417	6.2182	18.1434	14.7776
Sectorized	15.1222	12.1579	23.0185	18.9051

Table 2.20: Infinite-QAM with Shannon coding.

	R = 1		R = 7	
	K = 0	K = 10	K = 0	K = 10
Omni	3.9432	3.4295	11.8309	9.5481
Sectorized	9.4009	7.5646	15.9723	12.8322

Table 2.21: Infinite-QAM with no coding.

	R = 1		R = 7	
	K = 0	K = 10	K = 0	K = 10
Omni	3.1651	2.7198	7.7017	6.1965
Sectorized	6.5897	5.2307	9.3198	7.5586

Table 2.22: 16-QAM with no coding.

Per-link cell-wide average throughputs (in units of bps/Hz) of MIMO $(3, 6)$ links employing SVD receivers. An exact model has been used for CCI. The simulation results are over Reuse Factors (R), Rician K-factors, and Antenna-Patterns (Omni-directional or Sectorized).

	R = 1		R = 7	
	K = 0	K = 10	K = 0	K = 10
Omni	9.7512	7.8443	22.5478	18.1592
Sectorized	19.1464	15.1958	27.8813	23.1879

Table 2.23: Infinite-QAM with Shannon coding.

	R = 1		R = 7	
	K = 0	K = 10	K = 0	K = 10
Omni	5.3391	4.4175	15.3582	11.9987
Sectorized	12.4474	9.6476	20.2154	16.2002

Table 2.24: Infinite-QAM with no coding.

	R = 1		R = 7	
	K = 0	K = 10	K = 0	K = 10
Omni	4.1462	3.4319	9.3432	7.4519
Sectorized	8.2101	6.4449	10.7417	9.0524

Table 2.25: 16-QAM with no coding.

Chapter 3

Evaluation of Practical MIMO Systems with Resource Overheads

3.1 Introduction

Multiple-input/multiple-output (MIMO) systems have been recognized as a significant breakthrough in modern digital communications due to their ability to deliver higher spectral efficiencies with reasonable constellation sizes, as compared to single-input/single-output (SISO) systems [4,8,13]. A laboratory implementation of the so-called vertical Bell Labs layered space time architecture (VBLAST) demonstrated the feasibility of the MIMO concept, delivering spectral efficiencies of 20–40 bps/Hz under indoor conditions [9]. Not surprisingly, MIMO's potential is being tapped for commercial wireless products and networks such as wireless local area networks (WLANS), third-generation (3G) cellular networks, WiMAX, and future Internet-intensive wireless networks (including 4G networks).

A multi-element antenna (MEA) link (of which MIMO is a special case) employs a multi-element array at one or both ends. When only one end of the link uses an MEA, diversity can be achieved; this improves quality and enables higher throughput via larger signal constellations. When *both* ends use an MEA, corresponding to the MIMO case, it is possible to enhance throughput via either diversity (Div), as above; spatial multiplexing (SM), whereby the receiver can de-couple multiple parallel streams sent by the transmitter; or a combination of both [11].

This study compares the performance of SISO links and several kinds of MEA links. Application type determines which aspect of performance matters most. For some applications (e.g., data), higher throughput, even if over intermittent connections or over smaller separation distances will be deemed as "good", while other applications (e.g., voice, streaming) may prefer to trade throughput for sustained connections and/or a wider coverage area. It is thus clear that no single performance metric will suffice. Accordingly, we study the following metrics: (i) the mean, over the cell, of the per-link throughput, and (ii) 30th percentile of the link throughput.

Mean throughput provides a measure of the *data volume* an operator can deliver, in that this quantity times the number of channels per cell is a good approximation to the total throughput per cell. The 30th percentile of throughput is a useful measure of *user perception*, in that the vast majority of users (70%) will experience this throughput or more. Hence, each metric has value from one perspective or another.

The essential aim of this study is to decide the merit in modifying a SISO link with added antenna elements at one or both ends. We denote a general downlink configuration by (n, m), where n is the number of base station (BS) transmit elements and m is the number of mobile station (MS) receive elements. Considering present-day technology and economics, we limit our study to the possibility of at most two antenna elements at each end. Thus, we investigate five configurations in all: $(1, 1)$, which is SISO; $(2, 1)$, MISO with transmit diversity; $(1, 2)$, SIMO with minimum-mean-square-error (MMSE) receiver[1]; $(2, 2)$ with Div; and $(2, 2)$ with SM. Computing the performances of these configurations, based on the metrics cited above, the differences can be used to decide whether (and where) addition of antenna elements is justified.

3.2 Simulation Platform

3.2.1 System Model

The platform used in this study is very similar to the one in Chapter 2. The system model, assumptions, and array processing structures are as described therein; some system and propagation parameters have been changed to incorporate aspects of the 3GPP2 environment, as detailed in Table 3.1.

The complex baseband channel gain between the jth transmit antenna and the ith receive antenna is modeled by

$$h_{ij} = \sqrt{A(\theta)}\sqrt{A\left(\frac{d_0}{d}\right)^{\Gamma} s}\left[\sqrt{\frac{K}{K+1}}e^{j\phi} + \sqrt{\frac{1}{K+1}}z_{ij}\right] \tag{3.1}$$

where θ is the (horizontal) azimuth angle between the antenna and the BS-MS link, and $A(\theta)$ is the base station antenna pattern used for each sector, and

$$A(\theta) = -\min\left[12\left(\frac{\theta}{\theta_{\text{3dB}}}\right)^2, A_m\right] \text{dB}, \quad -180 \leq \theta \leq 180. \tag{3.2}$$

[1]For configuration $(1, 2)$, we can employ either the maximal ratio combiner (MRC) or the minimum mean square error (MMSE) receiver structure. Of the two, MMSE is higher performing, as it offers an optimal balance between diversity and co-channel interference suppression, leading to higher throughput. MRC on the other hand offers only a diversity benefit.

Table 3.1: 3GPP2 SIMULATION PARAMETER SUMMARY.

1	Cell Geometry	Regular array of hexagonal cells, with site-to-site distance 2.5 km (i.e., cell radius of 1.4434 km)
2	Number of Cells	1 tier-ring, 3 sector system (21 sectors total)
3	Antenna Horizontal Pattern (sectoring)	70° (–3 dB), with 20 dB front-to-back ratio
4	Antenna Orientation	0° azimuth is North (main lobe). No loss is assumed on the vertical dimension.
5	Propagation Model	$28.6 + 35\log_{10}(d)$ dB, d in meters. Modified Hata Urban Propagation Model @ 1.9 GHz (COST 231). Min. separation of 35 m between MS and BS
6	Shadowing	Lognormal, with Standard Deviation $\sigma = 8.9$ dB
7	Base Station Correlation	0.5
8	Mobile Noise Figure	10 dB
9	Thermal Noise Density	-174 dBm/Hz
10	Carrier Frequency	2 GHz
11	System Bandwidth	5 MHz
12	BS Antenna Gain	15 dB total from 17 dB BS gain; 2 dB cable loss
13	Other Losses	10 dB
14	Fast Fading Model	Rician (see Table 3.2)
15	BS Maximum PA Power	20 W
16	Maximum C/I Achievable (Power Control)	13 dB for typical IS-95 and cdma2000 1x systems and 18 dB for 1xEV-DV and 1xEV-DO systems.

The random shadow fading x_k between a MS and a BS$_k$ (whether serving or interfering) is the weighted sum of a component z common to all cell sites and a component z_k which is independent of z and from one cell site to the next. Both components are Gaussian distributed with zero-mean and standard deviation σ. Thus, $x_k = az + bz_k,\ k = 0 \ldots 6$, where $a^2 + b^2 = 1$. In this study, we assume $a^2 = b^2 = 1/2$, meaning that x_u and x_v, $u \neq v$, are 50% correlated.

Using appropriate parameter values in (3.1), the path-loss portion of the channel gain formula is made to follow the propagation model specified in Table 3.1 (Item 5). The Rician

K-factor typically decreases as the MS moves farther away from the BS. The assumed variation of the K-factor with distance is given in Table 3.2.

Table 3.2: VARIATION OF RICIAN K-FACTOR AS A FUNCTION OF BS-MS SEPARATION DISTANCE (PERCENTAGES SPECIFY THE DISTANCES RELATIVE TO THE CELL RADIUS).

Distance %	0-5	5-15	15-25	25-35	35-45	45-55	55-65	65-75	75-85	85-100
Rician K	10	9	8	7	6	5	4	3	2	0

3.2.2 Link Throughput

For AWGN channels, the *instantaneous* achievable throughput is upper-bounded by the Shannon limit

$$T_j = \log_2(1+\gamma_j) \tag{3.3}$$

where T_j is the sub-channel throughput. The per-user data throughput is $\sum_j T_j$. As was described in Chapter 2, there is a separation of about 8 dB ($= 10\log_{10}(6.4)$) between the upper-bound coding curve and the envelope for the uncoded case (2.19), which is repeated below for convenience

$$T_j = \max\ T_j(M_j) \approx \log_2\left(1+\frac{\gamma_j}{6.4}\right). \tag{3.4}$$

Thus, practical coding strategies can be modeled by using shifts in SINR less than 8 dB.

For practical systems, it is known that link throughput can be approximated by using curves shifted by SINR "offsets" from the Shannon curve [31]. The exact offset used (x dB in equation (3.5) below) depends on the link configuration (SISO, MEA), the receiver structure, etc. We can thus write

$$T_j = \log_2\left(1+\frac{\gamma_j}{10^{x/10}}\right). \tag{3.5}$$

The authors in [31] report that a 3 dB offset from the Shannon curve is needed to take into account finite alphabets and imperfect channel coding (especially when the block size is not very large), as well as overhead. For the SISO configuration, the channel estimation SINR penalty due to the overhead of the pilot signals and from non-ideal demodulation using the noisy channel estimate is about 0.5 dB. This leads to an overall 3.5 dB offset for the SISO configuration.

Table 3.3: OFFSETS FROM THE SHANNON CURVE FOR THE CONFIGURATIONS UNDER CONSIDERATION.

Configuration	$(1, 1)$ SISO	$(2, 1)$ Div	$(1, 2)$ MMSE	$(2, 2)$ Div	$(2, 2)$ SM
Offset (dB)	3.5	4	4	5	6

When two transmit antennas are employed, the transmit power of the pilot has to be split evenly between them; and when two receive antennas are employed, the operating point of each receive antenna is lowered by 3 dB. In either case, the channel estimation penalty gets worse by about 0.5 dB as compared to SISO. When two transmit and two receive antennas are employed, the offset used is 1.5 dB, which is more than the cumulative effect of using either two transmit antennas or two receive antennas. Moreover, in $(2, 2)$ SM, there is an additional 1 dB penalty relatad to channel estimation since the MMSE receiver needs to invert the channel gain matrix as part of the channel estimation procedure. This leads to the offsets from the Shannon curve as given in Table 3.3.

The SINR offsets given in Table 3.3 are used in our computations. To confirm the robustness of these conclusions, we will also consider the case where all offsets are the same.

3.3 Simulation Methodology

We compute throughput statistics of the five configurations, using the steps outlined below:

(1) Distribute MSs in cell.

(2) Generate channel matrix $\mathbf{H}$ as given by (3.1). The size of $\mathbf{H}$ is given by (2.2).

(3) Compute post-processing SINR of substream j [(2.13) and (2.14) for Div, (2.11) and (2.12) for SISO, MMSE and SM].

(4) Compute throughputs for substream j [(3.5) and Table 3.3].

(5) The "MEA throughput" is the sum of the throughputs of the individual substreams.

This computation leads to *instantaneous* throughputs for given values of MS location (path loss), shadow fading, and instantaneous channel fades from serving and interfering BSs. Averaging over all these results in the cell-wide mean throughput per user.

For the purpose of averaging, we distribute the MS with uniform randomness at 1000 locations over a given sector. To accommodate the fact that shadow fading and multipath fading are random, we allow each MS to experience 100 different shadow fades at a given location, and 100 different multipath fades for each location-shadowing combination.

At the beginning of each block-fade interval, pilot signals are transmitted to estimate the receiver array weights. The receiver then determines the constellation size (M) from the substream post-processing SINRs, and communicates this information to the transmitter. Adaptive modulators at each transmit antenna then quickly select the corresponding optimal QAM constellation. The channel remains known throughout since estimation-feedback-adaptation occurs within the block fade interval.

We computed throughputs of all five configurations, $(1, 1)$ SISO; $(2, 1)$; Div; $(1, 2)$ MMSE; $(2, 2)$ Div; $(2, 2)$ SM, both where the SINR offsets are non-uniform, as given by Table 3.3, and where they are all the same. In the latter case, a 6 dB offset had been used.

Trying many possible combinations of offsets for the various configurations is too expensive an undertaking for gauging the sensitivity of our conclusions with respect to the chosen SINR-offsets. The search space is considerably reduced by investigating reasonable offsets that will likely put our conclusions to the test. This is best brought about by using offset values that benefit the $(2, 2)$ configurations or degrade the performance of the others. A uniform 6 dB offset for all configurations is one such example.

3.4 Simulation Results

In this study, only a small, discrete set of constellation sizes are considered. They include BPSK and $4/8/16$-QAM (corresponding, respectively, to symbol rates of $1/2/3/4$ bits/symbol). These sizes are practical for present-day cellular system implementations. We now address the main questions motivating this study:

(i) What is the benefit of a second antenna at the BS or MS relative to the SISO case?

(ii) What is the added value of a second antenna at both ends?

(iii) If a second antenna is indeed used at both ends, thereby creating a MIMO $(2, 2)$ system, which mode of operation is the preferred one: SM or Div?

Table 3.4: MEAN THROUGHPUT OBTAINED (IN UNITS OF $\mathrm{bps/Hz}$) FOR THE VARIOUS CONFIGURATIONS.

System	$(1,1)$ SISO	$(2,1)$ Div	$(1,2)$ MMSE	$(2,2)$ Div	$(2,2)$ SM
Diff. Est. Offsets (bps/Hz)	2.50	2.58	3.17	2.87	3.06
Unif. Est. Offsets (bps/Hz)	2.24	2.37	3.00	2.77	3.06

We shall answer these questions by measuring the performance realized by each configuration with respect to the metrics defined earlier. The results are summarized next.

3.4.1 Metric 1: Mean Throughput

This metric gives the cell-wide average of the link throughput. Throughputs were obtained for the both cases, differential SINR offsets, as well as uniform SINR offsets, as shown in Table 3.4.

From this table, we conclude the following:

- $(1,2)$ MMSE is the best configuration for the case of differential SINR-offsets, and is very close to the best configuration for the case of uniform SINR-offsets. Hence, neither $(2,2)$ configuration is attractive when considering receiver complexity and costs.
- $(2,1)$ Div is only slightly better than $(1,1)$, and is within approximately 0.6 bps/Hz of (1, 2) MMSE.
- $(2,2)$ SM is slightly better than $(2,2)$ Div.
- The performance gap among configurations narrows for the more realistic case of differential offsets as compared to the case of uniform offsets.

3.4.2 Metric 2: 30th Percentile of User Throughputs Cell-Wide

This metric gives the multipath averaged throughput achieved or exceeded on 70% of all links, taken over location and shadow fading state. Again, throughputs were obtained for the both cases, differential SINR offsets, as well as uniform SINR offsets, as shown in Table 3.5. From

Table 3.5: 30th Percentiles of the Multipath-Averaged Throughputs Obtained (in units of bps/Hz) for Various System Configurations.

System	$(1, 1)$ SISO	$(2, 1)$ Div	$(1, 2)$ MMSE	$(2, 2)$ Div	$(2, 2)$ SM
Diff. Est. Offsets (bps/Hz)	0.64	0.66	1.60	0.97	0.52
Unif. Est. Offsets (bps/Hz)	0.43	0.47	1.26	0.83	0.52

this table, we draw conclusions similar to those above except that in this case $(2, 2)$ Div has slightly higher mean throughput than $(2, 2)$ SM.

The $(2, 2)$ SM configuration produces lower multipath-averaged throughputs for its 30th percentile users than $(2, 2)$ Div (Table 3.5), but produces higher mean throughput (Table 3.4). Since both configurations experience the same set of users statistically, it is the receiver structure that results in these differences. The implication is that stream decoupling/cross-stream interference (XSI) in SM works against a set of some users, while enhancing a favored set of users. Div, on the other hand, attempts throughput improvement over all users. These differences will likely become exaggerated for higher-order MEAs.

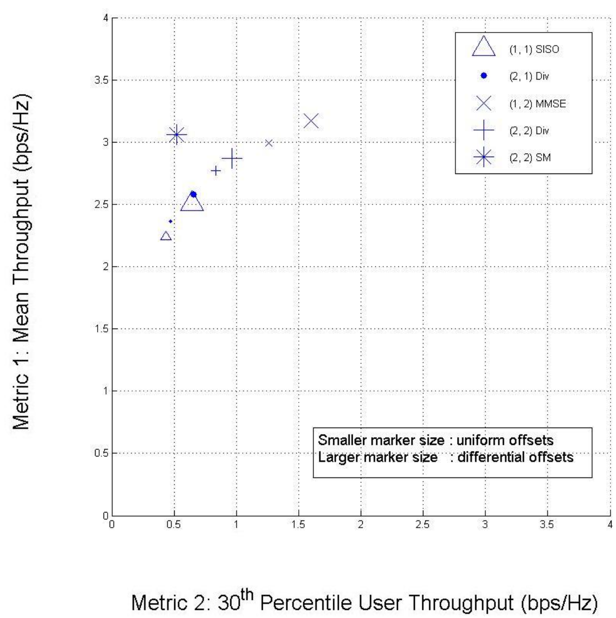

Figure 3.1: Scatter plot of the five system configurations for Metrics 1 and 2. The cases for both uniform (smaller markers) and differential offsets (larger markers) are shown.

Figure 3.1 shows a scatter plot ranking all five configurations for both Metrics 1 and 2. The plot enables us to see two perspectives simultaneously. From both perspectives, and for either offset case, $(1, 2)$ MMSE is more attractive than the others, confirming previous conclusions.

Figure 3.2 shows the mean throughputs realized within 10 concentric rings each of which has an equal user population. Ring 1 consists of the 10% of users closest to the BS. The throughput is averaged over multipath fading, shadowing, and user locations within the ring. Examining Fig. 2, the following observations can be made:

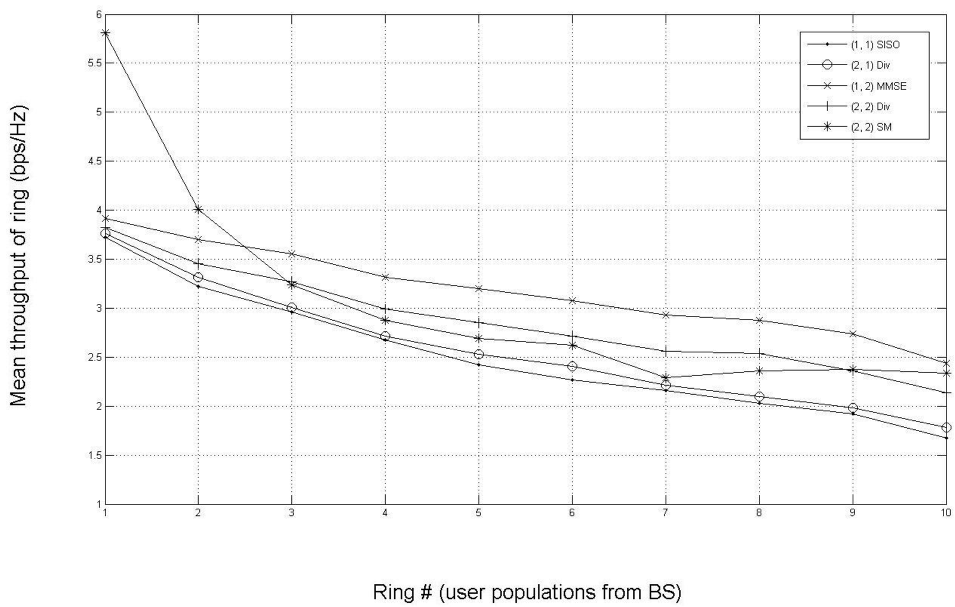

Figure 3.2: Mean throughputs of 10 rings of equal user population with differential SINR offsets.

- For users closest to the BS the $(2, 2)$ SM system offers a high average throughput.
- For other users, all configurations except $(1, 2)$ MMSE provide comparable performance, with $(2, 2)$ SM performing slightly better than $(2, 2)$ Div for ring 10.

Figure 3.3 shows the same plot for the case of uniform SINR-offsets. As expected, the curves diverge since higher-order MEAs benefit from a lower relative offset penalty. However, the divergence is small. Moreover, except for populations closest to the BS, the $(1, 2)$ MMSE system remains the most attractive configuration.

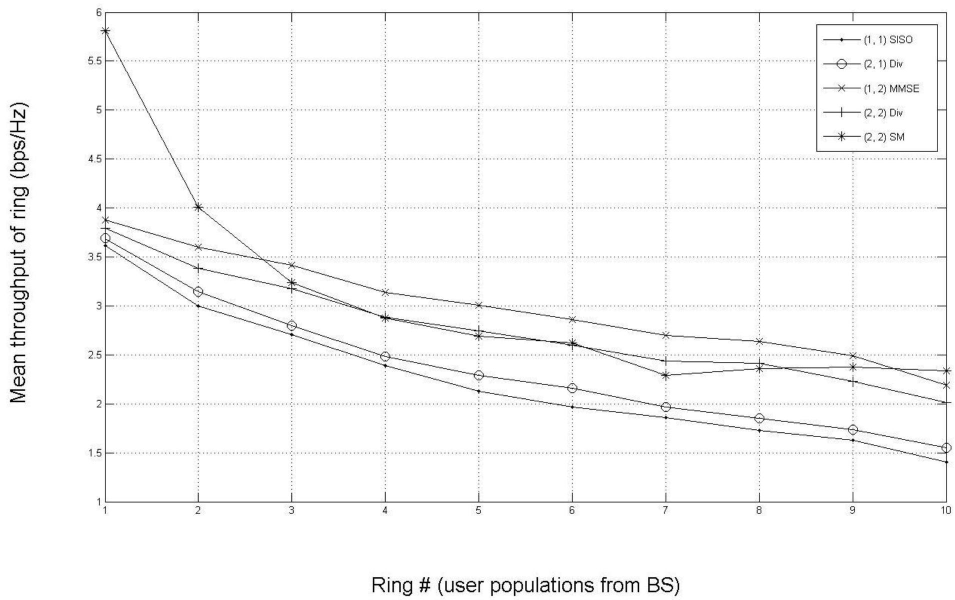

Figure 3.3: Mean throughputs of 10 rings of equal user population with uniform SINR offsets.

We have established that, although both SINR-offset cases result in minor differences in throughputs among the various system configurations, the overall conclusions remain the same. Therefore, the case of uniform SINR-offsets is dropped from further consideration. Instead, we shall choose to use the more realistic case of differential SINR-offsets from this point on.

Figure 3.4 shows another throughput statistic: the distribution of multipath-averaged user throughputs on a cell-wide basis. The following salient points should be noted:

- All configurations, with the exception of the $(2, 2)$ SM system, operate with only one transmit stream, and hence, have a peak rate of 4 bps/Hz. The $(2, 2)$ SM system operates with two streams, thus it can offer up to 8 bps/Hz.

- The $(2, 2)$ SM system merits consideration only for throughput requirements exceeding 4 bps/Hz. In fact, for throughputs less than 4 bps/Hz, it is the worst system configuration.

- In the mid-region, the curves are about parallel to one another. It is for this reason that the value of the percentile chosen (lowest 30th) for Metric 2 is somewhat arbitrary.

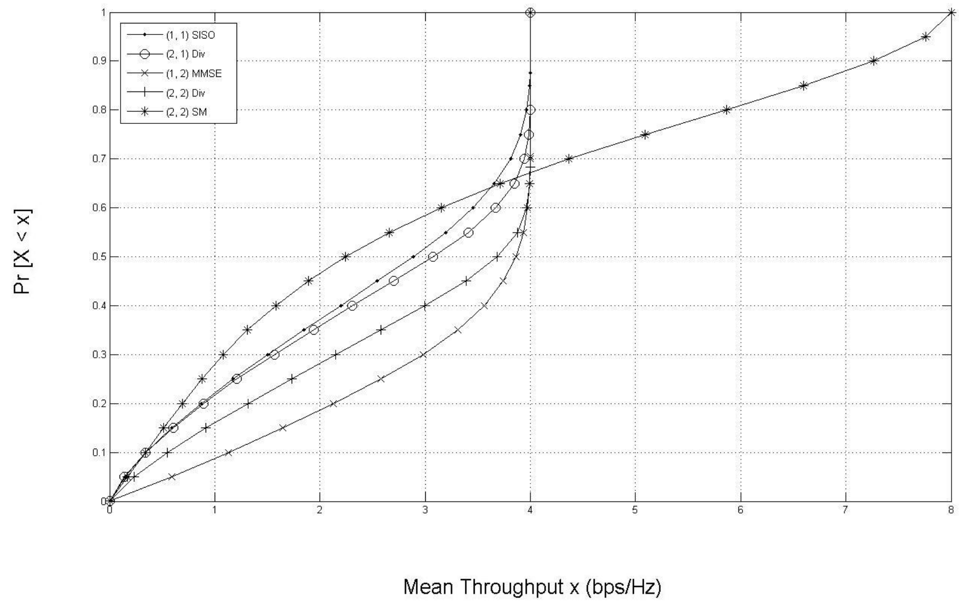

Figure 3.4: Fast-fading-averaged cell-wide distribution of throughput for all five configurations (differential offsets).

3.5 Conclusion

The objective of this study was to quantify and compare the throughput performance of five link configurations involving one or two antenna elements at each end.

The results obtained indicate that, in the context of a limited number of constellation sizes, and for the case of differential SINR-offsets, the $(1, 2)$ MMSE system is the configuration of choice for both metrics considered. The other four configurations are comparable in performance with each other. The main reasons why the $(1, 2)$ MMSE configuration scores best are: relatively low channel estimation penalty, the absence of cross-stream interference at receive antennas, and an excess receive antenna to suppress CCI.

For the case of uniform offsets, the throughput results change by small amounts, but the main conclusions do not change from those noted for differential offsets. This result further reinforces our conclusions and shows them to be robust to assumptions used in the study.

The MMSE receiver assumed here for $(2, 2)$ SM is one example of the many receivers that can decouple the SM streams. The ZF, SIC, OSIC, and OSIC-MMSE receivers are some others. Since changing the particular receiver amounts to changing the SINR offset, for which our conclusions are found to be stable, we claim that the $(1, 2)$ MMSE configuration is the preferred configuration regardless of the particular receiver chosen by the $(2, 2)$ SM configuration to decouple its streams.

Chapter 4

Validity of the Noise Model for CCI for MIMO/MEA Links

4.1 Introduction

When analyzing communication systems, either for BER or throughput performance, a simple Gaussian noise model is typically used for interference in place of an exact treatment. The Gaussian noise model is fairly prevalent, and applicable under a variety of situations [32–34]. In the cellular context, a Gaussian distribution for the total CCI is justified by the application of the central limit theorem due to the many interfering co-channel streams at the BS. The resulting simplification *summarizes* the effect of thermal noise and CCI terms into a single interference-plus-noise term, which also has Gaussian statistics and a total power equal to the sum of the thermal noise and CCI powers. Whereas, the model is accurate for traditional SISO links, its validity has not been examined for the newer MEA/MIMO links where the structure of the CCI signals can be exploited to suppress them. Such an investigation forms an integral part of this study. For the MEA/MIMO channel, the noise model can be extended in like manner, adopting a vector instead of a scalar set of equations that need to be analyzed.

It will seen that the noise model for CCI is less accurate when interference suppression is possible. We have remarked that, transmit-adaptive systems with limited CSI, as well receive-adaptation systems which do not possess excess degrees of freedom, are not effective at CCI suppression. Thus, we find it once again convenient to broadly classify SISO/MEA links according to whether or not they have excess degrees of freedom (defined as the excess number of receive elements over transmit elements). Likewise, communication systems shall also be broadly classified into transmit- or receive-adaptation systems. This will facilitate investigation of the noise model over a variety of situations.

We will also consider how the noise model permits the possibility of a tractable analysis of MIMO systems for the multi-cell (CCI) case, that would obviate the need for extensive system simulations.

4.2 Approach

We proceed by identifying the search space over which the noise model should be examined.

(a) Noise Model for CCI: The system analyst ignores the instantaneous channel fading and signal structure from interfering BSs. Interference contributions from interfering base stations are treated as additional noise. Specifically, the thermal noise floor is augmented with the sum of multipath-averaged CCI values. For the vector channel, due to the averaging over multipath fading, *each* receive antenna experiences the same noise-plus-interference power. Moreover, the independence of fading among all interfering base-to-receiving antenna paths results in mutually independent instantaneous noise-plus-interference values.

(b) Exact Model for CCI: In this model, the analyst uses knowledge of the instantaneous channel fading from all BSs (serving and interfering) for the MMSE receiver, i.e., $\mathbf{H} \in \mathbb{C}^{m \times 7n}$. For the SVD case, the analyst uses the *different* instantaneous values of noise-plus-interference[1] power experienced by each receive antenna.

In arriving at a systematic evaluation of the noise model for MEA systems, some well-known facts have been employed: (i) cross-stream interference (XSI) is potentially stronger than CCI, since the MS is closer to its serving BS than the interferers. Although, due to various combinations of shadow fading and multipath fading values, it is possible for CCI to be larger than XSI at times; (ii) when excess degrees of freedom *do not* exist, the existing degrees of freedom are used by the receiver to combat XSI; and, (iii) when excess degrees of freedom *do* exist, it is not only possible to combat XSI, but CCI as well. Specifically, D excess degrees of freedom can be used to gain diversity or suppress up to D interfering streams [27]. These facts provide an intuitive justification for the simplification algorithm (given in Section 4.5) which is used in conjunction with the noise model.

Thus, we will find it convenient to classify all wireless channels according to: (i) Type of communication system — whether transmit- or receive-adaptation.
(ii) Excess Degrees of Freedom — whether or not they possess excess degrees of freedom[2].

---

[1]Since the SVD cannot suppress co-channel users, we again combine CCI terms with thermal noise, only this time we use instantaneous values.

[2]For receive-adaptation systems, CCI suppression is decided entirely by the availability (or lack) of excess degrees of freedom.

4.3 Simulation Platform and Methodology

Once again, the simulation platform discussed in Chapter 2 is used. The investigation of the noise model for CCI is limited to the case of spatial multiplexing configurations. Transmit diversity configurations have been excluded from consideration. The experiments conducted (that is, the methodology followed) are also very similar to those performed in Chapter 2, with the difference being that analyst now uses a noise model for the CCI. Section 4.5 details the algorithm for evaluating throughputs using the noise model.

4.4 Numerical Results

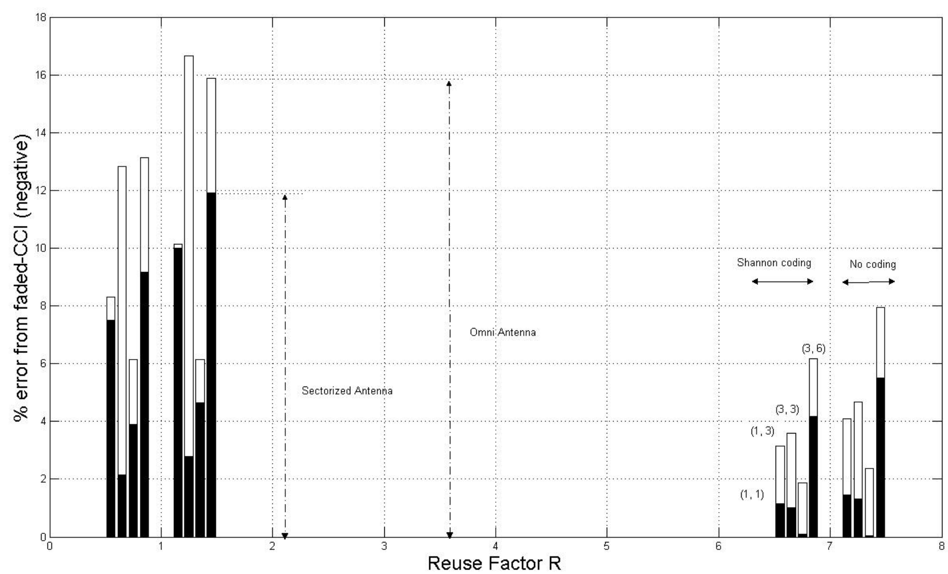

Figure 4.1: Demonstrating the accuracy of the noise-like CCI model (and accompanying algorithm) for various system sizes and design options: (1, 1), (1, 3), (3, 3) and (3, 6) MMSE systems with a Rician factor $K = 0$, for unlimited constellation sizes, for Shannon coded and uncoded cases. (Note change of scale: sectorized antennas now correspond to the lower part of the bar).

Figure 4.1 compares throughputs obtained using the noise and the exact model for the MMSE receiver with those obtained for various MEA configurations and several system design options. Only a representative set of data are shown[3] corresponding to the maximum error

[3] A comprehensive set of system performance data appears in the Tables in Section 4.8.

between the exact and noise models. The error bars in Fig. 4.1, and for other values for the dimensions under consideration, can be obtained by considering the appropriate (and corresponding) entries from the tables in this chapter, as well as the tables presented in Chapter 2.

When excess degrees of freedom are few or nonexistent (configurations (1, 1), (1, 3) and (3, 3)), the model is highly accurate for a reuse factor of 7, and is below 10% for a reuse factor of 1. Accuracy does not vary appreciably for different Rician K-factors or coding schemes, and improves for sectorized antennas and limited constellation sizes. Where several excess degrees of freedom exist, as in (3, 6), the inaccuracy between and two models can be more substantial, but is still no greater than 16%. Moreover, this amount of excess is not used in practical scenarios.

	Transmit-adaptation Systems (e.g. SVD)	Receive-adaptation Systems (e.g. MMSE)
Systems that do not possess Excess Degrees of Freedom	good	good
Systems that possess Excess Degrees of Freedom	good	fair

Figure 4.2: Summarizing the validity of the noise model for co-channel interference for SISO and MEA channels.

For the SVD scheme, the noise-like model is *more* accurate when compared to the MMSE scheme. The percentage error never exceeds 10% over *all* the design options considered, even for systems having excess degrees of freedom. Percentage error improves for higher order MEA systems, higher reuse factors, higher Rician K-factors and antenna patterns. Furthermore, the percentage error does not vary appreciably for intermediate or no coding, and clear trends are not obvious for limited constellation sizes. The noise model is accurate since SVD is ineffective at interference suppression, regardless of the availability (or lack) of excess degrees of freedom.

Figure 4.2 presents a summary of the findings in this study.

4.5 Algorithm for Analyzing CCI Impact

There are two cases to consider.

Case 1 - No excess degrees of freedom ($m = n$):

(1) Obtain channel gain matrix **H** ((2.1)), incorporate paths from the serving BS only.

(2) Compute the kth interferer's multipath averaged power CCI_k, for the given MS position.

(3) Compute interference plus noise power $(N_o + \Sigma CCI_k)$ for the (complex Gaussian) **Z** term.

(4) Compute system throughput (as explained in Section 2.3).

Case 2 - Excess degrees of freedom ($m > n$):

Excess degrees of freedom can be optimally expended toward gaining diversity or CCI suppression or some of both. Effectively, we consider various combinations by "removing" one antenna at a time from the MS and the strongest interferer. For MIMO (n, m), the combinations of diversity gain, CCI suppression are: (m, 0), ($m - 1$, 1) $\ldots$ (n, $m - n$) or fewer if there are insufficient interfering antennas. The process is then as follows:

(1) Evaluate the various combinations using the procedure in Case A. Antenna removal at the MS is done by removing any one row of the **H** matrix. For the interfering BS, it implies reducing the interferer's power by the appropriate fraction.

(2) Select the choice that leads to the maximum throughput.

4.6 An Important Use of the Noise-Like CCI Model

In [2, 24], Catreux developed an analytical method for computing cell-wide mean throughputs for the single-cell (noise-only) case, and showed it to be highly accurate by comparing the analysis with extensive simulation results. She used the multipath averaged SNR at a distance r from the BS, obtained the corresponding link throughput, and then averaged this throughput over shadow fading and path loss. Her approach had been greatly facilitated by the fact that SNR at any distance r is log-normally distributed, since it is directly proportional to the shadow fading term.

We propose adopting a similar strategy for the analysis of interference-limited systems. That is, find the distribution of SIR ($\ll$ SNR) at given distance r, compute and average the throughput over this distribution, and then average over r. Fortunately, SIR is well-approximated as a log-normal random variable at a given r since it is the ratio of a log-normal signal power to a sum of log-normal interference power. Also, the sum of log-normal variables has been shown to be log-normal itself [35,36]. Thus, an approach very similar to that in [24] for the single-cell noise-only case can be used to estimate cell-wide throughput for the multi-cell CCI-limited case. This forms the foundation for the analysis to be presented in the next chapter.

4.7 Conclusion

We have demonstrated that detailed channel modeling of the interferers has very limited value to the analyst, particularly for systems which are ineffective at interference suppression. The key feature of the noise-model for MEA systems is the treatment of interference as an additional Gaussian noise, *and* an algorithm for evaluating those cases when excess degrees of freedom are available. The impact of this contribution, particularly when the excess degrees of freedom are few (e.g., one) or do not exist, is simplified system simulations at the cost of minor inaccuracy. Moreover, by analyzing the multi-cell case in a manner similar to that done for the single-cell case, the analysis of MIMO systems which had been previously difficult, has now been successfully undertaken [37]. Analytical tractability follows from the observation that CCI modeled as noise has a distribution that is log-normal for given user distance from the BS.

The results obtained here are for two specific MIMO techniques, namely SVD transmission and MMSE reception. In the case of more optimal but less practical approaches, such as transmitter beam forming with global CSI or OSIC-MMSE at the receiver, the efficacy of the noise-like CCI model in analyzing performance is less clear. This is a worthwhile topic for further research. What we *can* say is that, just as in SISO systems, the noise-like CCI model works quite well for practical MIMO systems that cannot suppress CCI (for lack of either excess degrees of freedom or sufficient CSI), and works to some extent in those systems that can.

We also note that the systems considered above were spatial multiplexing systems. Transmit diversity systems, send dependent bit-streams over the transmit antennas, i.e., they use only one degree of freedom. Moreover, they do not suppress CCI. We conjecture that the noise model will also serve with reasonable accuracy in such systems.

4.8 Tabular Results for Noise Model Study

Per-link cell-wide average throughputs (in units of bps/Hz) of MIMO $(1, 1)$ links employing MMSE receivers. The noise model has been used for CCI. The simulation results are over Reuse Factors (R), Rician K-factors, and Antenna-Patterns (Omni-directional or Sectorized).

	R = 1		R = 7	
	K = 0	K = 10	K = 0	K = 10
Omni	2.3680	2.6197	6.2144	6.7561
Sectorized	4.9873	5.5218	7.8665	8.5923

Table 4.1: Infinite-QAM with Shannon coding.

	R = 1		R = 7	
	K = 0	K = 10	K = 0	K = 10
Omni	1.2193	1.3462	4.0184	4.4280
Sectorized	3.0263	3.4070	5.4439	6.0673

Table 4.2: Infinite-QAM with no coding.

	R = 1		R = 7	
	K = 0	K = 10	K = 0	K = 10
Omni	0.9682	1.0798	2.6363	2.8859
Sectorized	2.1670	2.4102	3.1983	3.4582

Table 4.3: 16-QAM with no coding.

Per-link cell-wide average throughputs (in units of bps/Hz) of MIMO $(1, 3)$ links employing MMSE receivers. The noise model has been used for CCI. The simulation results are over Reuse Factors (R), Rician K-factors, and Antenna-Patterns (Omni-directional or Sectorized).

	R = 1		R = 7	
	K = 0	K = 10	K = 0	K = 10
Omni	4.8357	5.0377	9.0455	9.1751
Sectorized	9.6328	9.9988	10.6634	10.6820

Table 4.4: Infinite-QAM with Shannon coding.

	R = 1		R = 7	
	K = 0	K = 10	K = 0	K = 10
Omni	2.8680	3.0042	6.4929	6.6048
Sectorized	7.0455	7.3851	8.0355	8.0457

Table 4.5: Infinite-QAM with no coding.

	R = 1		R = 7	
	K = 0	K = 10	K = 0	K = 10
Omni	2.1006	2.2003	3.5479	3.6009
Sectorized	3.6733	3.7640	3.8216	3.8540

Table 4.6: 16-QAM with no coding.

Per-link cell-wide average throughputs (in units of bps/Hz) of MIMO $(3,3)$ links employing MMSE receivers. The noise model has been used for CCI. The simulation results are over Reuse Factors (R), Rician K-factors, and Antenna-Patterns (Omni-directional or Sectorized).

	R = 1		R = 7	
	K = 0	K = 10	K = 0	K = 10
Omni	5.6818	3.3557	15.1495	9.5203
Sectorized	11.9654	7.3331	19.8365	12.7479

Table 4.7: Infinite-QAM with Shannon coding.

	R = 1		R = 7	
	K = 0	K = 10	K = 0	K = 10
Omni	2.5838	1.2135	9.0144	4.7636
Sectorized	6.5633	3.3184	12.8862	7.0023

Table 4.8: Infinite-QAM with no coding.

	R = 1		R = 7	
	K = 0	K = 10	K = 0	K = 10
Omni	2.1823	1.0987	6.5265	3.8522
Sectorized	5.1581	2.8435	8.4559	5.4953

Table 4.9: 16-QAM with no coding.

Per-link cell-wide average throughputs (in units of bps/Hz) of MIMO $(3, 6)$ links employing MMSE receivers. The noise model has been used for CCI. The simulation results are over Reuse Factors (R), Rician K-factors, and Antenna-Patterns (Omni-directional or Sectorized).

	R = 1		R = 7	
	K = 0	K = 10	K = 0	K = 10
Omni	9.7444	5.5756	21.9140	14.5263
Sectorized	19.9610	13.2675	26.7837	18.6486

Table 4.10: Infinite-QAM with Shannon coding.

	R = 1		R = 7	
	K = 0	K = 10	K = 0	K = 10
Omni	5.1315	2.3677	14.6843	8.4054
Sectorized	12.9503	7.4136	19.1004	11.7158

Table 4.11: Infinite-QAM with no coding.

	R = 1		R = 7	
	K = 0	K = 10	K = 0	K = 10
Omni	4.0669	2.0537	9.2291	6.3227
Sectorized	8.6408	5.7745	10.6975	8.2170

Table 4.12: 16-QAM with no coding.

Per-link cell-wide average throughputs (in units of bps/Hz) of MIMO $(1,1)$ links employing SVD receivers. The noise model has been used for CCI. The simulation results are over Reuse Factors (R), Rician K-factors, and Antenna-Patterns (Omni-directional or Sectorized).

	R = 1		R = 7	
	K = 0	K = 10	K = 0	K = 10
Omni	2.3680	2.6197	6.2144	6.7561
Sectorized	4.9873	5.5218	7.8665	8.5923

Table 4.13: Infinite-QAM with Shannon coding.

	R = 1		R = 7	
	K = 0	K = 10	K = 0	K = 10
Omni	1.2193	1.3462	4.0184	4.4280
Sectorized	3.0263	3.4070	5.4439	6.0673

Table 4.14: Infinite-QAM with no coding.

	R = 1		R = 7	
	K = 0	K = 10	K = 0	K = 10
Omni	0.9682	1.0798	2.6363	2.8859
Sectorized	2.1670	2.4102	3.1983	3.4582

Table 4.15: 16-QAM with no coding.

Per-link cell-wide average throughputs (in units of bps/Hz) of MIMO $(1, 3)$ links employing SVD receivers. The noise model has been used for CCI. The simulation results are over Reuse Factors (R), Rician K-factors, and Antenna-Patterns (Omni-directional or Sectorized).

	R = 1		R = 7	
	K = 0	K = 10	K = 0	K = 10
Omni	3.5593	3.6866	8.1855	8.3707
Sectorized	6.8368	7.0978	10.0490	10.1354

Table 4.16: Infinite-QAM with Shannon coding.

	R = 1		R = 7	
	K = 0	K = 10	K = 0	K = 10
Omni	1.9743	2.0490	5.7051	5.8662
Sectorized	4.5127	4.7330	7.4502	7.5245

Table 4.17: Infinite-QAM with no coding.

	R = 1		R = 7	
	K = 0	K = 10	K = 0	K = 10
Omni	1.5038	1.5663	3.3242	3.3902
Sectorized	2.9113	3.0080	3.7180	3.7601

Table 4.18: 16-QAM with no coding.

Per-link cell-wide average throughputs (in units of bps/Hz) of MIMO $(3, 3)$ links employing SVD receivers. The noise model has been used for CCI. The simulation results are over Reuse Factors (R), Rician K-factors, and Antenna-Patterns (Omni-directional or Sectorized).

	R = 1		R = 7	
	K = 0	K = 10	K = 0	K = 10
Omni	7.1621	6.0540	17.9419	14.6046
Sectorized	14.7769	11.9418	22.9066	18.9821

Table 4.19: Infinite-QAM with Shannon coding.

	R = 1		R = 7	
	K = 0	K = 10	K = 0	K = 10
Omni	3.7680	3.3174	11.6505	9.4378
Sectorized	9.1075	7.3941	15.8729	12.9100

Table 4.20: Infinite-QAM with no coding.

	R = 1		R = 7	
	K = 0	K = 10	K = 0	K = 10
Omni	3.0210	2.6509	7.6514	6.1075
Sectorized	6.4698	5.1646	9.2860	7.5666

Table 4.21: 16-QAM with no coding.

Per-link cell-wide average throughputs (in units of bps/Hz) of MIMO $(3, 6)$ links employing SVD receivers. The noise model has been used for CCI. The simulation results are over Reuse Factors (R), Rician K-factors, and Antenna-Patterns (Omni-directional or Sectorized).

	R = 1		R = 7	
	K = 0	K = 10	K = 0	K = 10
Omni	9.5292	7.6345	22.3117	17.9387
Sectorized	18.7143	14.8167	27.7026	23.0228

Table 4.22: Infinite-QAM with Shannon coding.

	R = 1		R = 7	
	K = 0	K = 10	K = 0	K = 10
Omni	5.1784	4.2730	15.1396	11.8147
Sectorized	12.0620	9.3421	20.0428	16.0534

Table 4.23: Infinite-QAM with no coding.

	R = 1		R = 7	
	K = 0	K = 10	K = 0	K = 10
Omni	4.0327	3.3475	9.2793	7.3857
Sectorized	8.0676	6.3229	10.7157	9.0100

Table 4.24: 16-QAM with no coding.

Chapter 5

Analysis of Co-Channel Interference Limited MIMO-Based Cellular Systems

5.1 Introduction

Multiple-input/multiple-output (MIMO) links are an active area of research due to their demonstrated ability to offer significant spectral efficiencies, far beyond the capabilities of existing traditional single-input/single-output (SISO) links [8, 9, 11]. Computation of cell-wide mean throughputs of MIMO-based cellular systems has been of interest to researchers, cellular operators and equipment manufacturers primarily to know the actual extent of gains that MIMO systems can offer.

Previous Research: A significant step in this direction is the work of Catreux, [1, 2, 24], who developed an analytical method for computing cell-wide mean throughputs for the single-cell (noise-only) case [2, 24], and showed it to be accurate by comparing her analysis with extensive simulation results. Catreux's approach is greatly facilitated by the fact that signal-to-noise ratio (SNR) at any distance r from the base station (BS) is log-normally distributed, since it is directly proportional to the shadow-fading term. For the multi-cell (interference) case, Catreux had obtained results via simulations only [1].

Contribution of this study: The contribution of this study is to extend the analysis method of [24] to the co-channel interference (CCI)-limited (multi-cell) case. Our approach rests on two results. One is that the sum of the CCI components from other base stations can be treated as additional Gaussian noise and added to the thermal noise. This result has been validated in Chapter 4 (and in [38]), particularly for the case transmit and receive antennas have the same number of elements. The second result is that the total CCI power at a mobile receiver, for a given distance r from the serving base, is a log-normal variate over the shadow fadings of the CCI components. This result, derived from findings in [35] and [36], is validated here. Moreover, signal-to-interference-ratio (SIR) (which is thus a ratio of two log-normals) continues to be log-normal for given r, and we are able to use Catreux's approach to obtain an analysis for the CCI case. The simulation platform used to assess the analytical predictions is described in Chapter 2 (and in [38]) and is very similar to that used in [1, 2, 24].

5.2 Analysis

Step 1: The Zero-Forcing Assumption. We now use Catreux's analysis [24], appropriately tailored to our situation, which is focused on the CCI-limited case. At the outset, it is to be pointed that her analysis is facilitated by assuming a zero-forcing (ZF) receiver (no cross-stream interference). However, that analysis holds for the minimum mean-square error (MMSE) receiver as well, since SNRs in the noise-only scenario tend to be very high, leading to very similar results for ZF and MMSE receivers. In the interference-limited scenario considered here, signal-to-interference-plus-noise ratios (SINRs) are no longer sufficiently high for this equivalence to hold. Here the ZF assumption is again employed, so that the analysis will somewhat underestimate the throughputs offered by an MMSE receiver.

Step 2: Invoking the Noise model. In Chapter 4 (and in [38]), it was established that using a noise model for the CCI is most accurate for MIMO systems having an equal number of transmit and receive antennas. This is also the most interesting kind of MIMO system, since the physical size limitations discourage the use of excess receive antennas. Consequently, analysis is limited to that particular case, i.e., n elements at each end, which we refer to as MIMO (n, n), or simply (n, n). Following the detailed treatment and arguments presented in Chapter 4 (and in [38]), we will treat CCI as a noise-like process with a Gaussian distribution. Moreover, since we are operating in an interference-limiting environment, henceforth thermal noise is ignored, SINR is replaced by SIR.

System Description Consider a MIMO (n, n) system, with a user (or mobile station, MS) at ground distance r from the BS[1]. For the purposes of this study, a MIMO path gain matrix $\mathbf{H}$ is assumed whose $n \times n$ elements are i.i.d. zero-mean, complex Gaussian random variates over the multipath fading of the channel. Also, the squared magnitude of each instantaneous path gain is proportional to $d^{-\Gamma} s_0 |\zeta|^2$, where Γ is the pathloss exponent; s_0 is the large-scale power fading due to shadowing; and $\zeta \sim \mathbb{CN}\left(0, 1^2\right)$ is the small-scale fading due

[1]The slant distance to the user is thus $d = \sqrt{r^2 + h^2}$, where h is the BS antenna height.

to multipath. The dB value of s_0 (denoted by S_0) is a zero-mean Gaussian random variate with standard deviation σ_0. Likewise, we denote distances from co-channel base stations by $\mathbf{d_{CCI}} = [d_1, \cdots, d_6]^T$ as shown in Fig. 5.1, and shadow fading values on the corresponding MS-CCI$_k$ link by $\mathbf{s_{CCI}} = [s_1, \cdots, s_6]^T$ ($k = 1, 6$, for the six BSs surrounding the cell of interest). The s_k's have the same distribution as s_0, and are assumed to be independent of each other.

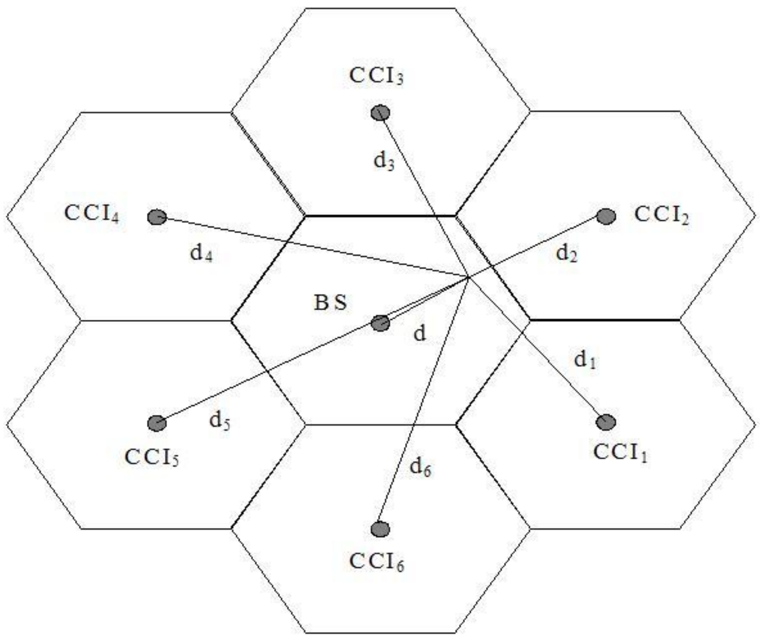

Figure 5.1: Plot of the interference-limited $(1, 1)$ system, showing the serving and co-channel base stations. Regular hexagonal geometry with side $R = 1000$ m is assumed.

Step 3: Calculation of the Instantaneous Per User Throughput. Assuming instantaneous adaptation of the transmissions to the signal fading condition, the instantaneous user throughput $Y(d, s_0, \zeta, \mathbf{d_{CCI}}, \mathbf{s_{CCI}})$ in a given block at a given time is the sum of the throughputs of its n transmit sub-streams [24]. Thus,

$$Y(d, s_0, \zeta, \mathbf{d_{CCI}}, \mathbf{s_{CCI}}) = \sum_{j=1}^{n} b \ln \Big(1 + a\gamma_j (d, s_0, \zeta, \mathbf{d_{CCI}}, \mathbf{s_{CCI}})\Big) \tag{5.1}$$

where $\gamma_j(d, s_0, \zeta, \mathbf{d_{CCI}}, \mathbf{s_{CCI}})$ is the post-processing SIR of substream j for that data block; $b = 1/\ln 2$; and a depends on the coding used. Under the most ideal condition (Shannon limit), $a = 1$; and for the case of no coding, $a = 1/10^{0.8} \sim 1/6.4$.[2] We obtain results for both

[2]It is shown in Section 2.2 (and in [1, 24]) that, for adaptive QAM in every substream, with no coding, the throughput for an instantaneous output SNR (or SIR) of γ is closely approximated by $\log_2\left(1 + \frac{\gamma}{6.4}\right)$.

extremes.

Step 4: Analyzing the (n,n) System in Terms of the $(1,1)$ System. In [24], Catreux shows that the output (post-processing) SNR for a MIMO (n,n) link with a ZF receiver, is statistically identical to $1/n$ times the output SNR for the $(1,1)$ scenario. Under our ZF receiver assumption, we can thus write the output SIR for our MIMO (n,n) system as

$$\gamma_j\left(d, s_0, \zeta, \mathbf{d_{CCI}}, \mathbf{s_{CCI}}\right) = \frac{1}{n} \cdot F\left(d, s_0, \mathbf{d_{CCI}}, \mathbf{s_{CCI}}\right) \cdot |\zeta_j|^2 \tag{5.2}$$

where,

$$F\left(d_0, s_0, \mathbf{d_{CCI}}, \mathbf{s_{CCI}}\right) = \frac{PA\left(\dfrac{d_0}{d}\right)^{\Gamma} s_0}{PA\sum_{k=1}^{6}\left(\dfrac{d_0}{d_k}\right)^{\Gamma} s_k}. \tag{5.3}$$

Here, P is the total transmitter power, $\zeta_j \sim \mathbb{C}\mathcal{N}\left(0, 1^2\right)$, and d_0 is a reference distance (typically 100 m, cf. [25]). It is assumed that s_0 and s_k's are i.i.d. log-normal variates whose dB values have zero-mean and standard deviation σ_0 (8 dB is used in subsequent numerical examples). Also, as seen in Fig. 5.1, the d_k's are uniquely specified by the MS location, which are uniformly distributed over the serving cell. The task now reduces to that of averaging (5.1) over the multipath fadings (ζ), the shadow fadings ($[s_0, \mathbf{s^T_{CCI}}]$), and the MS location($[d, \mathbf{d^T_{CCI}}]$), using (5.2) and (5.3) for the γ's. The result will then yield the cell-wide mean throughput per user, Y.

Step 5: Averaging over Multipath using the Catreux-Greenstein Procedure. At a given user position (as specified by $[d, \mathbf{d_{CCI}}]$), s_0 and $\mathbf{s_{CCI}}$, the function $F\left(d_0, s_0, \mathbf{d_{CCI}}, \mathbf{s_{CCI}}\right)$ is a constant. Thus, $\gamma_j\left(d, s_0, \zeta, \mathbf{d_{CCI}}, \mathbf{s_{CCI}}\right)$ is an exponential variable (since ζ_j is complex Gaussian) with mean

$$\begin{aligned} \gamma_j\left(d, s_0, \mathbf{d_{CCI}}, \mathbf{s_{CCI}}\right) &= E_{\zeta}\left[\gamma_j\left(d, s_0, \zeta, \mathbf{d_{CCI}}, \mathbf{s_{CCI}}\right)\right] \\ &= \frac{1}{n} \cdot F\left(d, s_0, \mathbf{d_{CCI}}, \mathbf{s_{CCI}}\right) \end{aligned} \tag{5.4}$$

where $E_{\zeta}[\cdot]$ denotes expectation over ζ. Using (5.4), and following the procedure in [24], we can write the user spectral efficiency $Y\left(d, s_0, \mathbf{d_{CCI}}, \mathbf{s_{CCI}}\right)$ for a MIMO (n,n) system as

$$\begin{aligned} Y\left(d, s_0, \mathbf{d_{CCI}}, \mathbf{s_{CCI}}\right) &= n\alpha_1 \ln\left(1 + \frac{\beta_1}{a}\gamma_j\left(d, s_0, \mathbf{d_{CCI}}, \mathbf{s_{CCI}}\right)\right) \\ &= \alpha_1 n \ln\left(1 + \frac{\beta_1}{an}F\left(d, s_0, \mathbf{d_{CCI}}, \mathbf{s_{CCI}}\right)\right) \end{aligned} \tag{5.5}$$

where, $\alpha_1 = 1.4$ and $\beta_1 = 0.82$ (cf. [2, 24]).

Step 6: Consolidating $[d, \mathbf{d_{CCI}}]$ *and* $[s_0, \mathbf{s_{CCI}}]$. At a given location, the randomness of F is due to the presence of the s_0 and s_k terms. The numerator and denominator of F are the multipath-averaged signal-power and the total interference-power at ground distance r, respectively. The numerator is log-normal due to the shadowing variable s_0. The denominator, being a sum of independent log-normal variables, can be approximated by a single, and appropriately chosen, "equivalent" log-normal variable. Works by Fenton [35], and Schwartz and Yeh [36] suggest ways of obtaining this equivalent random variable. In our simulations, it was found that the denominator (for any given r) was very nearly log-normal. This result is illustrated in Fig. 5.2 for a representative distance ($r = 200$ m).

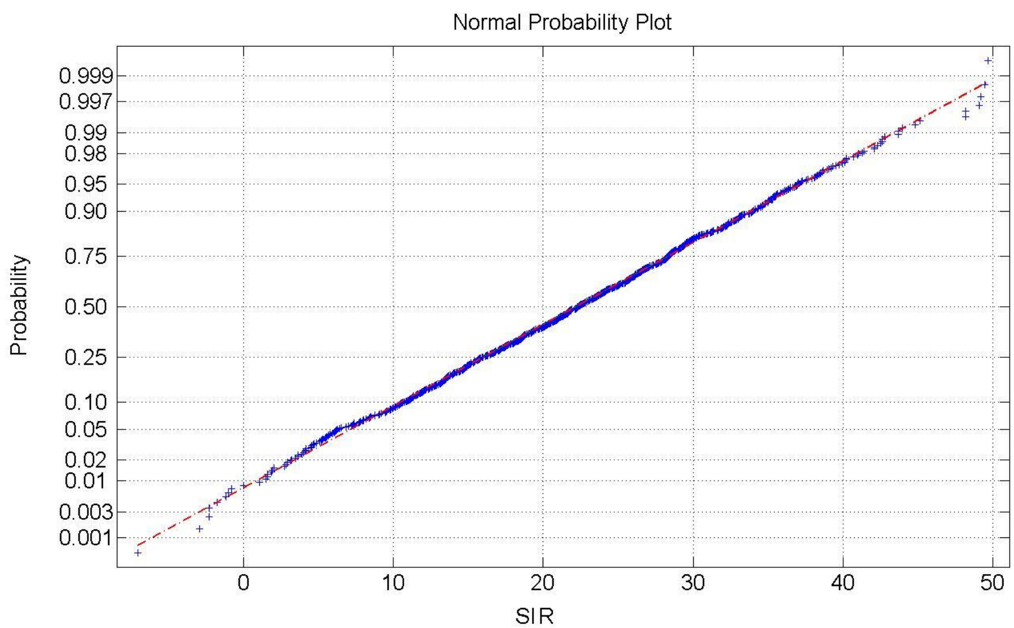

Figure 5.2: Probability (normal) plot of the SIR of the received signal at a distance of 200 m from the BS. The dashed line shows a Gaussian pdf which closely matches that of the dB SIR, confirming that the SIR has a distribution which is log-normal for given r.

By interpreting F as a ratio of two log-normal variables, it can be regarded as also log-normal. Hence, being log-normal, F is specified by μ and σ^2. From (5.3) it is obvious that both μ and σ^2 are functions of the MS location, as specified by the slant distance d and the d_k's. Alternatively, we can use the distance along the ground r and θ to specify MS location, θ being the angle between the transmit antenna horizontal azimuth and the direction of the serving link. From simulations (see Section 5.3 for details), it has been found that the effect of θ on μ, σ^2 and mean spectral efficiency (Y) is extremely mild ($\leq 3\%$). Discarding θ from consideration substantially reduces computation with negligible compromise with respect to accuracy. Figure 5.3 shows how μ and σ^2 vary with r, and also shows the small influence of user azimuth, θ. Consequently, it has been justified that

$$\begin{aligned} F\left(d, s_0, \mathbf{d_{CCI}}, \mathbf{s_{CCI}}\right) &\approx F\left(d, s, \mathbf{d_{CCI}}\right) \\ &\approx F\left(r, s, \theta\right) \\ &\approx F\left(r, s\right) \end{aligned} \tag{5.6}$$

where, we use the "overall" log-normal variable s to denote the randomness of the SIR at given r. From (5.5) and (5.6) it follows that

$$Y\left(d, s_0, \mathbf{d_{CCI}}, \mathbf{s_{CCI}}\right) \approx Y\left(r, s\right). \tag{5.7}$$

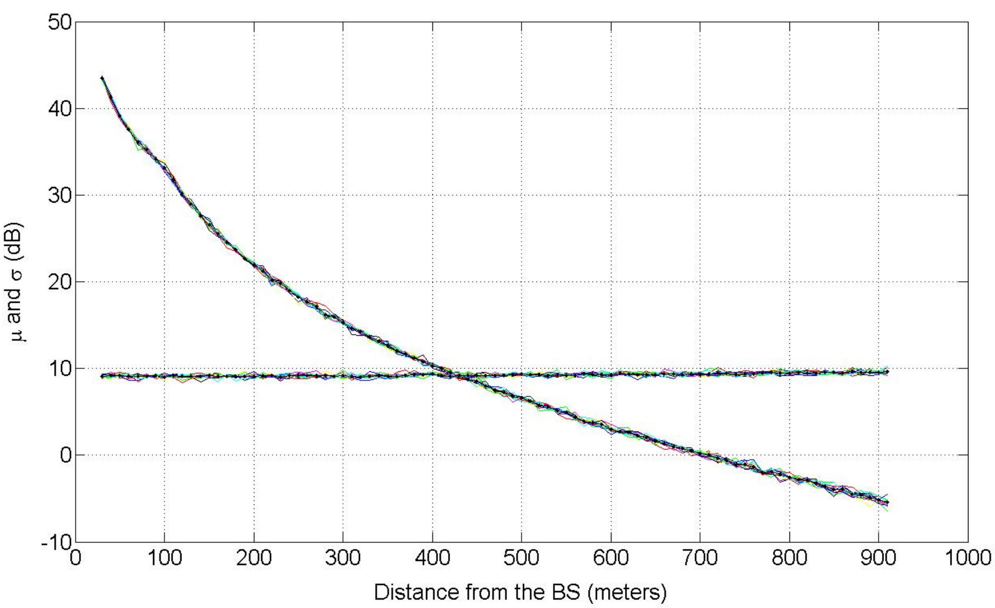

Figure 5.3: Plot of the dB mean (μ) and dB standard deviation (σ) of the received SIR as a function of the BS-MS distance d and azimuth angle θ. A total of 11 curves have been plotted for each, with θ taking values from 0° to 60° in increments of 6°. (Due to symmetry of the cell geometry, it is not necessary to use θ values from 60° to 120°). The near overlap of all the curves demonstrates the very mild dependences on θ. Moreover, the results for $\sigma\left(r\right)$ are sufficiently constant that they can be approximated using a single value.

Step 7: Averaging over Shadow Fading. Integrating over the shadow fading variable, we

Table 5.1: VALUES OF THE POLYNOMIAL COEFFICIENTS USED TO OBTAIN $\mu(r)$ AND $I(\mu')$. THE EXPONENTS ARE TO THE BASE 10. THE TABULATED ENTRIES ARE STRICTLY FOR $\sigma(r) = 9.5$ dB (i.e., CONSTANT OVER ALL r).

Coefficient	Curve: $\mu(r)$	Coefficient	Curve: $I(\mu')$
p_0	$4.8113e1$	q_0	$1.1386e0$
p_1	$-1.8760e{-1}$	q_1	$5.0000e{-1}$
p_2	$3.5506e{-4}$	q_2	$6.6438e{-2}$
p_3	$-3.6323e{-7}$	q_3	$-4.5733e{-9}$
p_4	$1.4167e{-10}$	q_4	$-4.4712e{-4}$
p_5	–	q_5	$4.7705e{-11}$
p_6	–	q_6	$1.6950e{-6}$

obtain the expected throughput for ground distance r, that is

$$\begin{aligned} Y(r) &= \int_S Y(r,s)\, p_S(s)\, ds \\ &= \int_0^\infty \alpha_1 n \ln\left(1 + \frac{\beta_1}{an} F(r,s)\right) p_{F(s)|R}\left(F(s)\,|r\right) dF(s) \end{aligned} \tag{5.8}$$

where we use $p_{F(s)|R}(F(s)\,|r)$ in place of $p_S(s)$ to emphasize the quantity over which averaging is being carried out.

Let $x'(r,s) = 10\log_{10} F(r,s)$, so that, $F(r,s) = e^{cx'(r,s)}$, where $c = (\ln 10)/10$. Then,

$$Y(r) = \int_{-\infty}^{\infty} \alpha_1 n \ln\left(1 + \frac{\beta_1}{an} e^{cx'(r,s)}\right) p_{X'(s)|R}\left(x'(s)\,|r\right) dx'(s) \tag{5.9}$$

where $p_{X'(s)|R}(x'(s)\,|r) \sim \mathbb{C}\mathcal{N}\left(\mu(r), \sigma^2(r)\right)$ for μ, σ in dB.

In order to change to a standard normal pdf, let $x'(s,r) = \mu(r) + \sigma(r)x(s,r)$. Then, temporarily suppressing the dependence of μ and σ on r, we can write

$$\begin{aligned} Y(r) &= \int_{-\infty}^{\infty} \alpha_1 n \ln\left(1 + \frac{\beta_1}{an} e^{c\mu + c\sigma x(r,s)}\right) p_{X(s)|R}\left(x(s)\,|r\right) dx(s) \\ &= \int_{-\infty}^{\infty} \alpha_1 n \ln\left(1 + \frac{\beta_1}{an} e^{c\mu + c\sigma x}\right) \frac{e^{-x^2/2}}{\sqrt{2\pi}} dx \\ &= \alpha_1 n \int_{-\infty}^{\infty} \ln\left(1 + e^{\mu' + c\sigma x}\right) \frac{e^{-x^2/2}}{\sqrt{2\pi}} dx \end{aligned} \tag{5.10}$$

where

$$\mu'(r) = c\mu(r) + \ln\frac{\beta_1}{an} \tag{5.11}$$

$$\mu(r) = \sum_{i=0}^{4} p_i \cdot r^i \qquad 0 \le r \le 910\, m. \tag{5.12}$$

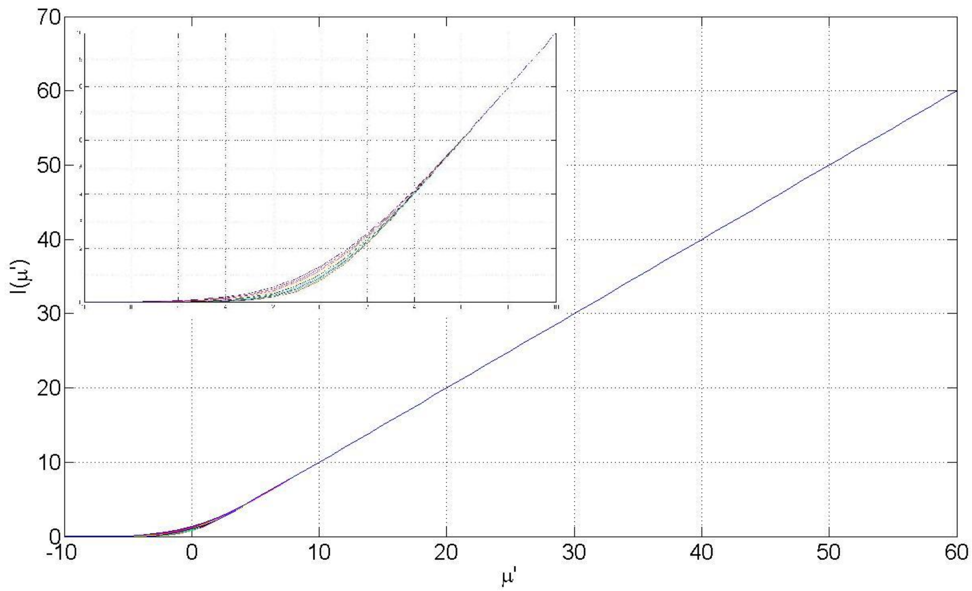

Figure 5.4: Plot of $I(\mu')$ vs. μ', demonstrating the near independence of $I(\mu')$ (and consequently, cell-wide mean throughput) with respect to the exact value of SIR standard deviation σ ($\sigma = 9.5$ dB was used in the analysis, independent of the ground distance r between the BS and the MS). A total of 9 curves have been shown, with σ taking on values from 4 dB to 12 dB in increments of 1 dB. The inset figure shows a magnified view, with μ' ranging from -10 dB to 10 dB.

Step 8: Curve-Fitting. At this point, it is necessary to curve-fit the integral in (5.10). However, rather than construct a function of both μ' and σ, which will be computationally expensive, a simplified approach is desired. From Fig. 5.3, and using many simulations, it was determined that using a constant σ (that is 9.5 dB) does not change the obtained throughput values significantly. Thus, we can curve-fit the integral in $\mu'(r)$ *only*, i.e.,

$$Y(r) = \alpha_1 n \cdot I(\mu') \tag{5.13}$$

Table 5.2: THROUGHPUTS (bps/Hz) FOR VARIOUS MIMO CONFIGURATIONS WITH A PATH LOSS EXPONENT $\Gamma = 3.7$, $\sigma_0 = 8$ dB AND OMNI-DIRECTIONAL BS ANTENNAS.

n	Level of Coding	MMSE Simulation Exact model for CCI	MMSE Simulation Noise model for CCI	ZF Analysis Noise model for CCI
$(1,1)$	uncoded	1.36	1.22	1.27
	coded	2.58	2.37	2.48
$(2,2)$	uncoded	2.10	1.93	1.91
	coded	4.38	4.07	3.92
$(3,3)$	uncoded	2.75	2.58	2.41
	coded	6.06	5.68	5.08

where

$$I\left(\mu'\right) = \begin{cases} \sum_{i=0}^{6} q_i \cdot (\mu')^i & \mu' < 10 \text{ dB} \\ \\ \mu' & \mu' \geq 10 \text{ dB}. \end{cases} \tag{5.14}$$

We have assumed a polynomial model for curve fitting μ' and $I(\mu')$, Table 5.1. Further investigation of Fig. 5.4 demonstrates the near insensitivity of $I(\mu')$ to variations of σ (and consequently σ_0).

Step 9: Averaging over Distance. Next, by averaging $Y(r)$ over r, we obtain an expression for the average cell-wide spectral efficiency. A minor complication is that cells are typically modeled as hexagons, this model was employed in conducting simulations over the cell. Proceeding as in [24], the analysis is facilitated by approximating the conventional hexagon cell with maximum distance D by a circle having an effective radius of D_{ef}. The radius is defined such that the areas of the hexagon and circle are the same. It is easy to show that

$$\frac{D_{ef}}{D} = \sqrt{\frac{3\sqrt{3}}{2\pi}} \approx 0.909. \tag{5.15}$$

Assuming that users are uniformly distributed over a circular cell of radius D_{ef}, the pdf for r is

$$p_R\left(r\right) = \frac{2r}{D_{ef}^2}, \quad 0 \leq r \leq D_{ef}. \tag{5.16}$$

Finally, the cell-wide mean spectral efficiency per user is easily determined by numerically evaluating the finite integral

$$Y = \int_0^{D_{ef}} Y\left(r\right) p_R\left(r\right) dr. \tag{5.17}$$

5.3 Simulation Methodology and Results

The MS were distributed along the 0° azimuth over intervals of $r = 10$ m. A total of 1000 trials were conducted for each location. Each trial involving different values for shadow fading and multipath. The number of trials is large enough to permit sufficient statistical stability even under Rayleigh fading. SIR was confirmed to be nearly log-normal for each r, and $\mu(r)$ and $\sigma(r)$ were computed, resulting in the curves for $\mu(r)$ and $\sigma(r)$ as shown in Fig. 5.3. The trials were repeated for 10 other values of θ, ranging from 6° to 60° in increments of 6°, and the independence of both $\mu(r)$ and $\sigma(r)$ over θ was noted.

Using (5.13)-(5.16), and the values in Table 5.1, we can evaluate (5.17) numerically, to obtain the cell-wide mean spectral efficiency of a MIMO system. Table 5.2 demonstrates the accuracy of the analysis by comparing the analytical results with those obtained using simulation. Only the $(1, 1)$ case with Shannon coding (i.e., Row 2 of Table 5.2) was analyzed, the remaining five cases were obtained directly using appropriate values for n and a, without resorting to simulation. All results are for $D = 1$ km and $h = 30$ m. It is important to note that $\mu(r)$ and $\sigma(r)$ are functions of system-level parameters, including, the path-loss exponent, and the dB value of the standard deviation of shadow fading assumed by the BS-MS (both serving and interfering) links. Similar agreements have been obtained for numerous other cases (i.e., different reuse factors, path loss exponents, limited constellation sizes, etc.).

5.4 Conclusion

In this study, we presented an analysis of interference-limited MIMO systems. Two important concepts used in this work were (i) a noise-like model for CCI, and (ii) a log-normal model for the CCI power. These constructs allowed us to analyze the multi-cell case in a manner similar to that for the single-cell (noise-only) analysis found in [2, 24].

The approach used here does not lead to an explicit single formula which covers all system design parameters. However, throughputs for any particular design option can be computed using the method described above. In all design options, the overall framework remains the same. Cases involving different choices for reuse factor, sectorization, path loss exponent, and level of shadowing can be dealt with by obtaining $\mu(r)$ and $\sigma^2(r)$ for each case via rapid simulations. The analysis can also be generalized to the cases of correlated path gains in the gain matrix $\mathbf{H}$. The method described in this study is straightforward and produces numerical solutions that are accurate, far less time-consuming than pure simulations, and more useful for gaining an intuitive understanding of the impact that the different parameters have on overall system performance.

Part II

Channel Dispersion and Path Correlation

Chapter 6

Evaluation of Single-Carrier MIMO Systems with Channel Dispersion and Path Correlation Impairment

6.1 Introduction

The idea behind incorporating multiple antennas at both ends of the link is to use spatial resources to reduce demand on frequency resources (system bandwidth). This produces higher spectral efficiencies and permits narrower bandwidths. Under narrowband signaling, the channel frequency characteristic can be treated as flat, i.e., the channel is memoryless. As the push for higher bit rates continues, designers are again pressed to stretch frequency or space resources. The mobile device (and consequently the overall wireless link) for reasons of shape and form-factor, cannot have too many antennas. Designers are thus forced to revisit the frequency resource. As signal bandwidth increases, fading becomes frequency selective and intersymbol interference (ISI) comes into play. In addition, a variety of natural environment factors result in correlations among the path gains of the multi-element antenna (MEA)[1] channel. Both elements, channel dispersion and path-correlation, can adversely affect channel capacity, and our aim here is to analyze and quantify these influences.

Previous Research: Research in the area of MEA channels is very extensive, and is considered to be a well-developed body of work at this time [4–14, 39]. Early MEA research analyzed narrowband signaling (flat channels). While much of this literature bears a *link-level*[2] focus, works [1, 2, 24, 29, 38] offer a *system-level*[3] perspective of MEA channel performance. Later research on MEA systems attempted a better understanding of channel-dispersion, and

---

[1]MEA links are assumed to have n transmitters and m receivers. They are referred to here as MEA (n, m) or simply (n, m).

[2]By link-level perspective is implied that performance measures such as bit error rate (BER) or throughput (TP) are determined with signal-to-noise ratio (SNR) treated as a parameter, and external factors such as CCI ignored or indirectly treated using the signal-to-interference-plus-noise ratio (SINR) in place as SNR.

[3]By system-level perspective is implied the distribution of performance over a coverage area, e.g., the cumulative distribution function (CDF) of TP over the randomness of user location and shadow fading, which jointly specify the SNR value; and taking into account the CCI produced by co-channel users in other cells.

path-correlation.

Research in the area of frequency-selective MEA channels, is focused primarily on MEA links with multiple antennas at both ends (i.e., the multiple-input/multiple-output (MIMO) channel). Channel modeling [40], channel estimation [41,42], space-frequency coding [43,44], diversity-multiplexing tradeoff [45], capacity scaling [46], achievable throughputs [47], non-coherent detection [48], and channel-access strategies [49] among other issues are addressed. Orthogonal Frequency Division Multiplexing (OFDM) is typically employed to "flatten" the dispersive channel, thereby improving the design and performance of the MIMO link (see [50–52] for an excellent overview of MIMO-OFDM). MIMO-OFDM throughput analysis [47], thus uses the flat channel assumption, thereby ignoring treatment of ISI.

Research in the area of path-correlation is primarily focused on the channel modeling aspect. Numerous research articles have attempted to characterize the MIMO channel with increasing levels of sophistication. Models have been developed for a variety of situations: indoor-outdoor, macro-micro-pico, time varying/invariant, narrowband-broadband, single/ multiple bounce scattering, keyholes. Various physical channel models (deterministic ray-tracing, geometry/ non-geometry based stochastic), analytical channel models (i.i.d., Kronecker, Weichselberger, finite scatterer, maximum entropy, virtual representation), and standardized channel models (3GPP SCM, COST 259 and 273, IEEE 802.11n) have been developed [53–58]. Again, as in the frequency-selective case, throughput analyses of channels with path-correlation have been developed only for flat channels (either narrowband MIMO, or MIMO-OFDM) [59,60].

Contribution of this study: In much of the literature, the focus is on *link-level* performance. To the best of our knowledge, there is no *system-level* throughput study to date, which truly addresses co-channel interference (CCI), channel-dispersion, and path-correlation in a single setting. Furthermore, no other work to our knowledge, has quantified the impact of ISI as the signal band widens. Here, we address these issues for single-carrier MIMO systems, extending the work in [1,2,24,29,38]. Specifically, we quantify the attainable cell-wide mean throughputs of interference-limited frequency-selective MIMO cellular systems along various design dimensions, i.e., size of the transmit/receive antenna arrays; level of dispersion; receiver adaptivity; antenna pattern (omni-directional or sectorized); degree of error protection (Shannon coding, no coding or intermediate coding strategies); and level of path-correlation. Both the single- and the multi-cell scenarios are considered.

This study also evaluates the frequency-selective MIMO link when *non-dispersive*, as well as *exact* cancellation of cross-stream interference (XSI) are implemented at the receiver. Our aim is to see if the former, which is simpler, can be effective in a dispersive channel.

Moreover, simulations are performed for the two different carrier frequencies of 2 GHz and 5 GHz[4]. Using *fixed* values for the physical lengths of the transmit and receive arrays, but *different* numbers of antennas, and *different* carrier frequencies enables an investigation of the interplay between: path-correlation; number of antennas; the physical sizes of the transmit and receive arrays; and carrier frequency, for the case of frequency-selective channels.

6.2 The Single-Carrier Wideband MIMO Simulation Platform

Both a system-level and a link-level simulation platform have been developed for computing the throughputs of MIMO-based cellular systems. The link-level platform computes link throughputs over the range of values of input signal-to-interference-plus-noise ratio (SINR), multipath fading, degree of channel-dispersion, and path-correlation. The system-level platform produces the distribution of input SINR for the mobile station over the entire cell via path-loss and shadow-fading. Using the output SINR values from link-level lookup table, for the corresponding input SINR values obtained in the system simulations, results in the throughputs of dispersive-MIMO systems.

6.2.1 System-Level Description

In the cellular data environment considered here, a given cell consisting of a serving base station (BS) and a set of mobile stations (MS), is surrounded by one contiguous tier of six cells. The overall platform allows for the detailed investigation of the several system-level dimensions noted earlier. While the platform is quite general with respect to system and channel parameters, most numerical results were obtained using the parameters detailed in Table 6.1.

---

[4]We note that a 5 GHz carrier leads to more rapid path loss than that resulting from the use of a 2 GHz carrier. Accordingly, to ensure fair comparison, transmit power was recalculated so that median cell-boundary SNR remained at 20 dB for both cases.

We assume a base station height of $h = 30$ m above ground. For receivers located close to the ground the direct path has a length $d = [r^2+h^2]^{1/2}$, where r is the distance along the ground from the receiver to the base station. This implies that all transmitter-receiver (T-R) distances are 30 m or greater. A loss exponent of 2.0 (free space loss) is used for distances close to the base station ($30 - 100$ m), and 3.7 is used for distances beyond 100 m. Shadow fading is also applied regardless of the T-R distance. This has been shown to be an empirically reasonable model [25]. The transmitting and receiving antenna arrays are assumed to be uniform linear arrays. For antenna sectoring, perfect beams are assumed instead of shaped antenna patterns.

Table 6.1: PARAMETER VALUES USED IN THE SYSTEM SIMULATIONS.

Cell Geometry	Hexagonal Array with side $R = 1000$ m
Carrier Frequency	$f_c = 2$ GHz and 5 GHz
System Bandwidth	$W = 5$ MHz
Path Loss Exponent	$\Gamma = 3.7$
Shadow Fading	Lognormal, with Standard Deviation $\sigma = 8$ dB
Multipath Fading	Rayleigh (K-factor = 0)
Antenna Pattern	Omnidirectional, or Uniform over 120°
Thermal Noise Density	$N_0 = -174$ dBm/Hz
Mobile Station's Noise Figure	$N_F = 8$ dB
Transmit Power	$P_T = 5$ W for $f_c = 2$ GHz $P_T = 31.25$ W for $f_c = 5$ GHz
Median SNR at cell-boundary	$\rho = 20$ dB
Transmit Antenna Array (BS) Length	$l_{BS} = 3$ m
Receive Antenna Array (MS) Length	$l_{MS} = 0.1$ m
AoD Statistics (at the Base Station)	Laplacian Power Angular Spectrum with Angular Spread $\sigma_{BS} = 15° = \pi/12$
AoA Statistics (at the Mobile Station)	Laplacian Power Angular Spectrum with Angular Spread $\sigma_{MS} = 45° = \pi/4$

Only one tier of interferers around the serving BS is used in the simulations. This assumption is made to simplify the simulations, and is slightly optimistic. However, the rapid decay of signal power with distance makes this assumption reasonable. Moreover, we offset it with the pessimistic assumption that all co-channel interferers are transmitting all the time.

Co-channel interference is treated as an additive noise component. Specifically, the thermal noise floor is augmented with the sum of the multipath-averaged CCI values. This assumption has been demonstrated to be quite reasonable [38], especially in the case $m = n$, as assumed in the simulations.

Since cell-site (macro) diversity has been shown to have minimal impact on mean throughput calculations [1, 2], it is not used in the simulations, i.e., for simplicity, it is assumed that users communicate with the base station that is the nearest and not necessarily the strongest.

For this setup, the input SINR between any BS transmit antenna and any MS receive antenna is

$$SINR = \frac{P_T}{n} \cdot A \left(\frac{d_0}{d}\right)^{\Gamma} s \cdot \frac{1}{(\sum_k CCI_k + N_o)} \tag{6.1}$$

where,

- P_T is the total transmit power, d is the link length, and Γ is the path-loss exponent.
- A is the median of the path gain at reference distance d_0 ($d_0 = 100$ m in the simulations).
- $s = 10^{S/10}$ is a log-normal shadow-fading variable, where S is a zero-mean Gaussian random variable with standard deviation σ dB.
- CCI_k is the multipath-averaged power at the receiver, from co-channel base station k.

6.2.2 Link-Level Description

Figure 6.1 depicts a MIMO channel which models frequency-selective fading in its path gains. For simplicity, we have shown, and used for our presentation a MIMO $(2, 2)$ channel, although the presentation can easily be extended to the general case of MIMO (n, m).

The dispersive-MIMO channel is characterized by a pair of co-dispersive $[H_{11}(f), H_{22}(f)]$ and cross-dispersive $[H_{12}(f), H_{21}(f)]$ channel frequency response functions. For the initial part of this study, all path gains are assumed to follow the same statistics, with no correlation

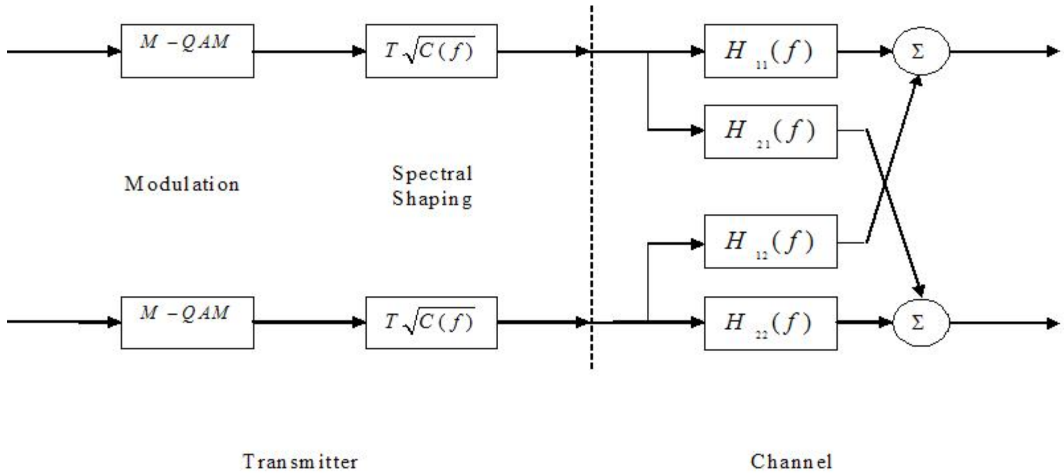

Figure 6.1: The MIMO $(2, 2)$ channel which models channel dispersion. The transmitter uses M-QAM modulation and root-cosine-roll-off spectral shaping. The channel response functions are slowly-varying during periods of multipath activity.

between the different delay taps of any path. This is the widely used uncorrelated-scattering (US) assumption [61]. Moreover, for the initial part of this study, path gains are also i.i.d. The second part of this investigation expands the scope of the study, generalizing the channel model to include the case of correlation among path gains.

The transmitter operates in the Spatial Multiplexing (SM) mode [4, 8–10], using M-ary Quadrature Amplitude Modulation (M-QAM) in its various transmit streams. The end-to-end spectral shaping (excluding channel-dispersion and adaptive filtering) is cosine roll-off, with roll-off factor α; and the shaping is evenly divided between the transmitter and the receiver. The cross-dispersion canceller at the receiver linearly combines the received signals to remove cross-stream interference (XSI). This is followed by fixed-filtering and adaptive-equalization in each stream. Equalization is implemented via the minimum-mean-square-error (MMSE) equalizer [28].

For this study, $\alpha = 0$ (zero roll-off), in which case the spectral shaping is a unit rectangle on the f-interval $[-\frac{1}{2T}, \frac{1}{2T}]$. This simplification is justified by earlier findings that, over the practical range $\alpha \leq 0.5$, the roll-off factor has only a mild effect on the performance results [62]. Cross-stream interference is treated as a noise-like process.

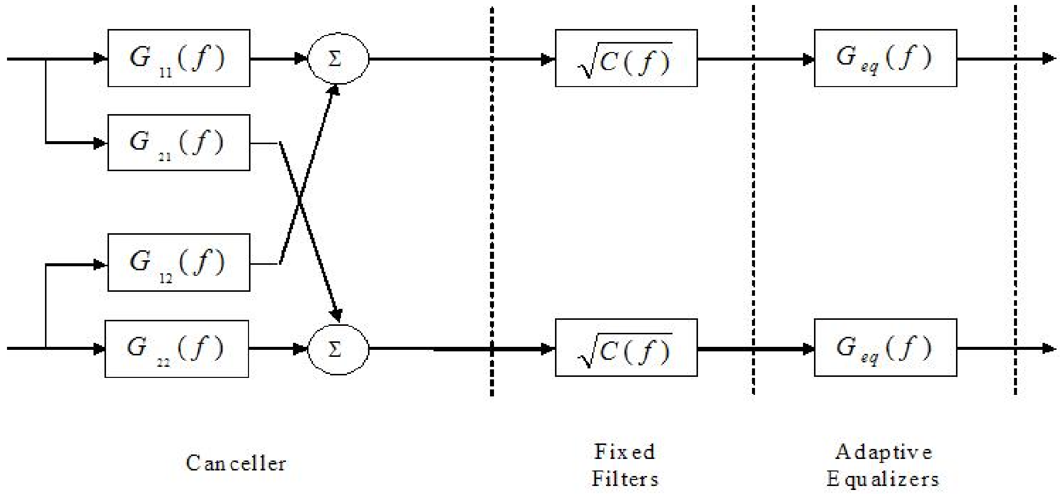

Figure 6.2: The receiver for a MIMO $(2, 2)$ channel which models channel dispersion. The receiver consists of a canceller, a root-cosine-roll-off-filter and an adaptive equalizer. The canceller functions adapt to the instantaneous channel response.

An adaptive transmission algorithm is assumed that perfectly adapts the modulation (constellation size) on each transmit antenna according to the instantaneous radio channel and interference conditions. It is thus possible for different transmit antennas to choose different bit rates (constellation sizes) although all transmissions operate at the same symbol rate. The procedure to compute the optimum size of the transmit constellations appears in Section 6.3.

Finally, perfect channel estimation, T-R synchronization, and instantaneous feedback are assumed. These simplifications focus the problem on the essential issues that are investigated in this study.

Channel Dispersion Modeling

The MIMO channel considered in this study is frequency-selective, but slowly varying. The complex baseband channel impulse response between the jth transmit antenna of a given BS and the ith receive antenna of a given MS is modeled by

$$h_{ij}(t) = \sum_{l=0}^{50} h_{ij}^{l} \delta\left(t - \frac{0.1l}{W}\right) \tag{6.2}$$

where W is the channel bandwidth, and h_{ij}^{l} is the amplitude of the l^{th} tap ($l = 0$ corresponds to the tap (or multipath) with zero delay). Each tap is assumed to be comprised of a number of individual rays, so that the h_{ij}^{l} are complex Gaussian with zero-mean and variance distributed according to an exponential delay profile, i.e.,

$$h_{ij}^{l} \sim \mathbb{CN}\left(0, \sigma_l^2\right), \qquad \sigma_l^2 = \frac{1}{\tau}\exp^{-\theta_l/\tau}, \qquad \theta_l = \frac{0.1l}{W}. \tag{6.3}$$

The h_{ij}^{l} are normalized, so that

$$\sum_l |h_{ij}^{l}|^2 = 1 \tag{6.4}$$

where θ_l is the delay of the l^{th} multipath, and τ is a delay profile parameter. Used in conjunction with the channel bandwidth, τ determines the degree of dispersion present in the channel. Here, $W\tau = 0$ corresponds to the case of a flat channel, while $W\tau$ values ranging from $\frac{1}{16}$ to 2 simulate channels that range from mildly to severely dispersive.

As can be seen, the channel model uses only one cluster for simplicity. More sophisticated models employ $2-6$ overlapping clusters, and combine overlapping taps from the different clusters, so that they model the power delay profile accurately [63]. Moreover, (i) the impulse response is allowed to extend (up to) five signal durations (resulting in a channel having a memory of up to five symbol durations); and (ii) a factor of ten oversampling is employed (resulting in taps which are spaced $\frac{0.1}{W}$ apart) so that only multipaths with negligible power are discarded from consideration, even for the case of $W\tau = 2$ (which is a severely dispersive channel).

In the frequency domain, the channel path from transmit antenna j to receive antenna i is characterized by the Discrete Fourier Transform (DFT) of the channel impulse response

$$H_{ij}\left(f\right) = \sum_{l=0}^{50} h_{ij}^{l} \exp^{-\frac{j2\pi f 0.1l}{W}}. \tag{6.5}$$

Channel Path-Correlation Modeling

Path-correlation is modeled as in [59, 63] using suitable parameter values for power angular spectrum (PAS) shape, angular spread (AS)[5], and array length, for both the transmit and the receive ends. The procedure is detailed below.

Correlated channel gain matrices for the MIMO channel can be generated using

$$\mathbf{H_{corr}}\left(\mathbf{t}\right) = \mathbf{R_{rx}}\left(\mathbf{t}\right)^{1/2}\mathbf{H_{iid}}\left(\mathbf{t}\right)\left(\mathbf{R_{tx}}\left(\mathbf{t}\right)^{1/2}\right)^{T} \tag{6.6}$$

[5]Analogous to the notions of power delay profile and delay spread in the time domain, we have the PAS and AS in the spatial domain. PAS is the power density of the received signal over the range of angle-of-arrival/departure, with rms value AS.

where, $\mathbf{R_{tx}}(\mathbf{t})$ and $\mathbf{R_{rx}}(\mathbf{t})$ for a given tap t, are the transmit and receive correlation matrices, respectively. $\mathbf{H_{iid}}$ ($\mathbf{H_{corr}}$) at a given tap, is a matrix of zero-mean, independent (correlated) complex Gaussian random variables; $\mathbf{H_{iid}}(\mathbf{t}) = [h_{ij}(t)]$.

The transmit and receive correlation matrices are given by

$$\begin{aligned} \mathbf{R_{tx}} &= \left[\rho_{ij}^{tx}\right] \\ \mathbf{R_{rx}} &= \left[\rho_{ij}^{rx}\right] \end{aligned} \tag{6.7}$$

where ρ_{ij}^{tx} (ρ_{ij}^{rx}) is the complex spatial correlation coefficient between the ith and jth transmitting (receiving) antennas, and is independent of the antenna element used at the other end of the link. Both ρ_{ij}^{tx} and ρ_{ij}^{rx}, can be obtained from the appropriate PAS shape, and the AS (i.e., σ_{BS} and σ_{MS} respectively, for computing ρ_{ij}^{tx} and ρ_{ij}^{rx}). We assume that each tap has the same PAS shape and AS value, [64], resulting in the same values of correlation matrices for all taps, i.e., $\mathbf{R_{tx}}(\mathbf{t}) = \mathbf{R_{tx}}$, and $\mathbf{R_{rx}}(\mathbf{t}) = \mathbf{R_{rx}}$ in (6.6).

For the uniform linear array, ρ_{ij}^{tx} is given by

$$\rho_{ij}^{tx} = R_{xx}(D_{ij}) + jR_{xy}(D_{ij}) \tag{6.8}$$

where $D_{ij} = 2\pi d_{ij}/\lambda, d_{ij} = |i-j|\Delta$ and $\Delta = \frac{l_{BS}}{n-1}$. Also, d_{ij} is the distance between the ith and jth antenna elements, and R_{xx} and R_{xy} are the cross-correlation functions between the real parts and between the real and imaginary parts, respectively. Similar expressions can be used for the receive end.

The cross-correlation functions are given by

$$\begin{aligned} R_{xx}(D_{ij}) &= \int_{-\pi}^{\pi} \cos(D_{ij}\sin\phi) \cdot PAS(\phi)\, d\phi \\ R_{xy}(D_{ij}) &= \int_{-\pi}^{\pi} \sin(D_{ij}\sin\phi) \cdot PAS(\phi)\, d\phi. \end{aligned} \tag{6.9}$$

The truncated Laplacian distribution is used to model the statistics of angle-of-arrival/departure (this, then, is taken as the PAS shape) [59, 63]

$$PAS(\phi) = \frac{1}{\sqrt{2}\sigma_{PAS}} e^{-|\sqrt{2}\phi/\sigma_{PAS}|} \quad -\pi \le \phi \le \pi \tag{6.10}$$

where σ_{PAS} is the angular spread of the PAS under consideration (i.e., σ_{PAS} equals either σ_{BS} or σ_{MS} of Table 6.1, depending on whether $\mathbf{R_{tx}}$ or $\mathbf{R_{rx}}$ is being calculated.).

From (6.7)-(6.10) it is clear that $\left[\rho_{ij}^{tx}\right]$ and $\left[\rho_{ij}^{rx}\right]$ have a Toeplitz structure. To summarize, frequency-selectivity ($\mathbf{H_{iid}}$) is obtained using the procedure in Section 6.2.2, while frequency-selectivity *and* path-correlation ($\mathbf{H_{corr}}$) are obtained using $\mathbf{H_{iid}}$ and spatial correlation matrices (Section 6.2.2).

Canceller-Equalizer Structures

The cross-dispersion canceller at the receiver is characterized by a cross-network of functions. Here, the g_{ij} are functions of frequency, and adaptively compensate for the channel functions h_{ij}. In this investigation, two types of cross-dispersion cancellers are considered: the *ideal canceller* and the *optimal non-dispersive canceller*.

The ideal canceller cancels all XSI in each stream at *all* frequencies. After cancellation, each stream contains dispersive versions of the intended signal and noise, but no interfering signals. Referring to Figs. 6.1 and 6.2, we see that this can be accomplished by requiring that

$$\mathbf{HG} = \mathbf{D} \tag{6.11}$$

where $\mathbf{H}$ is the channel matrix comprising of h_{ij}'s ($\mathbf{H}$ equals either $\mathbf{H_{iid}}$ or $\mathbf{H_{corr}}$, depending on whether frequency-selectivity, or frequency-selectivity-with-path-correlation is being investigated), $\mathbf{G}$ is the canceller matrix of g_{ij}'s, and $\mathbf{D}$ is a diagonal matrix (not necessarily the identity matrix).

The optimal non-dispersive canceller uses functions which are independent of frequency, and hence, attempts a best-effort *minimization* (but not entire removal) of the XSI in each stream based on a mean-square error criterion. For the MIMO $(2,2)$ channel, we define the optimal non-dispersive canceller by

$$g_{11} = 1; \qquad g_{12} = g_{opt}. \tag{6.12}$$

Since both the streams are statistically identical, it is necessary to analyze only one stream. In (6.12), we are specifying the upper stream (i.e. stream 1). We postpone a derivation on the value for g_{opt} until the link-level analysis considered in Section 6.2.3. Extending the above derivation to MIMO (n,n) channels is straightforward. This study does not consider MIMO (n,m) with $n \neq m$. It is obvious that the ideal canceller is more agressive than the non-dispersive canceller in mitigating XSI. Our aim is to see if the latter, which is simpler, can be effective in a dispersive channel.

At the receiver, the data stream from the canceller is fed to an MMSE equalizer. This equalizer maximizes the ratio of the sampled signal half-distance to the total root-mean-square (rms) distortion (thermal noise, XSI, and intersymbol interference).

6.2.3 Link-Level Analysis

Signal and Distortion at the Equalizer Output

For the purpose of link-level analysis, let P_0 be the average received power in an M-QAM signal in the absence of fading, and let N_0 be the total power spectral density of CCI and thermal noise at the input of the receiver. Then, the input SINR is defined here to be

$$SINR \triangleq P_0 T / N_0 \tag{6.13}$$

where T is the symbol duration and equals the reciprocal of the channel bandwidth, W. We use SINR as an input parameter in the link-level simulations, and (6.13) allows us to compute the corresponding P_0 to be used. The analysis below closely follows the one in [34].

From Figs. 6.1 and 6.2, for an M-QAM signal, it can be seen that a data pulse at the output of the canceller will have a Fourier transform of

$$S\left(f\right) = \sqrt{P_0}\left(T\sqrt{C\left(f\right)}\right)A\left(f\right) \tag{6.14}$$

where

$$A\left(f\right) = [H_{11}\left(f\right)G_{11}\left(f\right) + H_{21}\left(f\right)G_{12}\left(f\right)]. \tag{6.15}$$

Note that (6.15) applies to a MIMO $(2, 2)$ system. For a MIMO (n, n) system, we have

$$A\left(f\right) = [H_{11}\left(f\right)G_{11}\left(f\right) + H_{21}\left(f\right)G_{12}\left(f\right) + \ldots + H_{n1}\left(f\right)G_{1n}\left(f\right)]. \tag{6.16}$$

The noise-plus-CCI component at the output of the canceller will have a power spectral density

$$N\left(f\right) = N_0 B_n\left(f\right) \tag{6.17}$$

where

$$B_n\left(f\right) = [|G_{11}\left(f\right)|^2 + |G_{12}\left(f\right)|^2]. \tag{6.18}$$

Again, for a MIMO (n, n) system,

$$B_n(f) = [|G_{11}(f)|^2 + |G_{12}(f)|^2 + \ldots |G_{1n}(f)|^2]. \tag{6.19}$$

The XSI at the canceller output will have a power spectral density

$$\begin{aligned} X(f) &= P_0 T \cdot C(f) B_c(f) \\ &= N_0 \cdot SINR \cdot C(f) B_c(f) \end{aligned} \tag{6.20}$$

where

$$B_c(f) = |H_{12}(f) G_{11}(f) + H_{22}(f) G_{12}(f)|^2. \tag{6.21}$$

In this treatment, the XSI is regarded to be noise like, so that the composite of the XSI, CCI and thermal noise, hereafter referred to as *total-interference*, will have a power spectral density

$$\begin{aligned} N'(f) &= N(f) + X(f) \\ &= N_0 [B_n(f) + SINR \cdot C(f) B_c(f)]. \end{aligned} \tag{6.22}$$

The MMSE equalizer response can be shown to be [34]

$$\begin{aligned} G_{eq}(f) &= \frac{A^*(f)}{B_n(f) + SINR \cdot [B_c(f) + |A(f)|^2]}; \qquad |f| \leq \frac{1}{2T} \\ &= 0; \qquad elsewhere \end{aligned} \tag{6.23}$$

The data pulse following the equalizer will have a real, non-negative Fourier transform. Assuming optimal carrier timing and recovery, we can show that the squared half-distance between adjacent signal samples at the detector is [34, 65]

$$P_s = \left[\int S(f) G_{eq}(f) df \right]^2. \tag{6.24}$$

The mean-squared intersymbol interference (ISI) at the sample times can be shown to be

$$P_i = \left[\frac{1}{T} \int |S(f) G_{eq}(f)|^2 df - P_s \right] \tag{6.25}$$

and the mean-squared total-interference is given by

$$P_{n'} = \int N'(f) |G_{eq}(f)|^2 df. \tag{6.26}$$

Finally, the output SINR is given by

$$\gamma \triangleq P_s / \left(P_i + P_{n'}\right). \tag{6.27}$$

From the output SINR, the link-throughput can be obtained for two cases of interest [1, 2, 24]: Ideally Coded Signals and Uncoded Signals (to be explained shortly). Since all streams are statistically identical, $\gamma = \gamma_j$, and all streams have the same average throughput. The link throughput TP is therefore simply n times the average throughput per stream

$$TP = n \cdot T_j. \tag{6.28}$$

Having the analysis framework in place, we can now evaluate the system when an optimal non-dispersive canceller is incorporated. The non-dispersive canceller uses the g_{opt} which minimizes the mean XSI (over frequency). For MIMO $(2, 2)$, g_{opt} can be derived using (6.20) and (6.21) as

$$g_{opt} = -\frac{\overline{H_{22}^*\left(f\right) H_{12}\left(f\right)}}{\overline{\left|H_{22}\left(f\right)\right|^2}} \tag{6.29}$$

where the overbar denotes expectation over frequency. The derivation for (6.29) appears in the Appendix in Section 6.6. Extension to MIMO (n, n) is straightforward.

Link Throughput Bounds

The *instantaneous* per-user data throughput is the sum of the throughputs of the sub-streams. We determine the instantaneous throughput T_j of sub-stream j for two extreme cases:

Ideally Coded Signals: The instantaneous throughput is upper-bounded by the Shannon capacity

$$T_j = \log_2\left(1 + \gamma_j\right). \tag{6.30}$$

Uncoded Signals: Assuming no coding, and error detection in each block, the instantaneous throughput is

$$T_j(M_j) = (1 - BLER_j)\log_2(M_j) = (1 - BER_j)^L \log_2(M_j) \tag{6.31}$$

where $\log_2(M_j)$ is the number of bits per symbol in stream j, and BLER is the corresponding block error rate for L-bit blocks. In this study $L = 500$ bits is assumed, though the results are robust for values of L over a wide practical range [2].

We wish to simplify (6.31) to the form of (6.30) for convenience of calculation. Under the simplifying assumption of quasi-static block fading, it is possible to regard the channel as *AWGN conditioned on the instantaneous path gains*. For QAM modulation, we can then use the procedure in [1, 2, 38] to bring this to the form

$$T_j = \max\ T_j(M_j) \approx \log_2\left(1 + \frac{\gamma_j}{6.4}\right). \tag{6.32}$$

Thus the envelope curve, which closely approximates the exact curve for uncoded transmission, is 8 dB ($= 10\log_{10}(6.4)$) shifted from the curve for a perfectly-coded (Shannon) transmission. A variety of practical coding strategies can then be modeled by using shifts less than 8 dB [29].

6.3 Simulation Methodology

At the link-level, link throughputs are computed for SINR's ranging from $[-6 \ldots 30]$ dB in increments of 3 dB, and $W\tau$ ranges over the set $[0, \frac{1}{16}, \frac{1}{8}, \frac{1}{2}, 1, 2]$. A total of 1000 channel realizations are used for each $\{SINR,\ W\tau\}$ combination. Instantaneous output SINRs are computed from (6.27) leading to instantaneous throughputs (for a given channel fading condition) given by (6.30) or (6.32) (in conjunction with (6.28)). Averaging over the channel realizations, creates a link-level lookup-table of average throughput values for each $\{SINR,$ $W\tau\}$ combination.

Averaging the instantaneous throughputs over the ensemble of shadow fadings and path loss will result in the cell-wide mean throughputs. For the purpose of averaging, system-level simulations have been conducted, wherein the MS is distributed with uniform randomness at 1000 locations over a given cell/sector. Furthermore, the MS is made to experience 100 different shadow-fades for each location. This allows computation of SINRs for each {location, shadow-fading} combination (using (6.1)). SINR is parameterized over a range of $[-6 \ldots 30]$ dB which is practical for present-day cellular implementations[6].

Using the link-level lookup-table for the distribution of SINRs obtained by the system-level simulation results in stream throughputs of dispersive MIMO systems. Spline-interpolation is used to obtain link throughputs for system SINR values for which exact link simulations were

[6]See Item 16 in Table 3.1.

not conducted (e.g. SINR $= 7.3$ dB). The total MIMO throughput is given by the sum of the throughputs of the individual streams (6.28). The statistical performance of the throughputs was checked for robustness with respect to the number of realizations being conducted.

At the beginning of each block-fade interval, the receiver determines array weights via either adaptive search or channel estimation. The receiver then determines the constellation size (M) for each transmit antenna from the substream post-processing SINRs and communicates this information to the transmitter. Adaptive modulators at each transmit antenna then quickly select the corresponding optimal QAM constellation. This whole process (estimation-feedback-adaptation) is assumed to occur before the channel can change appreciably (within the block fade interval).

6.4 Numerical Results

The simulation platform has been used to produce extensive numerical results for the single-carrier frequency-dispersive MIMO channel, for Rayleigh fading (K-factor $= 0$), both i.i.d. and correlated path-gains, and carrier frequencies of 2 and 5 GHz[7]. We report throughput statistics of various MIMO systems over the many key design dimensions stated earlier.

Effect of Channel-Dispersion: As $W\tau$ is increased from 0 to 2, the cell-wide mean throughput decreases by about 15% for the ideal canceller as shown in Fig. 6.3. Throughput decrease is to be expected, since a higher degree of dispersion implies higher ISI. The percentage decline is relatively low, due to the fact that the ideal canceller removes the XSI perfectly (at all frequencies) and the MMSE equalizer compensates for the ISI to the best of its ability.

Two important observations are to be highlighted: (1) Most of the throughput loss going from $W\tau = 0$ to 2 happens fairly quickly, within $W\tau = 0.5$. This implies that even a small amount of dispersion can significantly reduce throughputs; i.e., OFDM or MIMO-OFDM systems must have enough tones to avoid ISI in order to be able to reach its full potential. (2) The 15% drop is consistent across most dimensions (except non-dispersive cancellation). However,

[7]Although, we have performed exhaustive experiments over all combinations of the dimensions under consideration, we present only a representative subset of the results, to keep the presentation useful and concise. A comprehensive set of result data appears in the Tables in Section 6.7

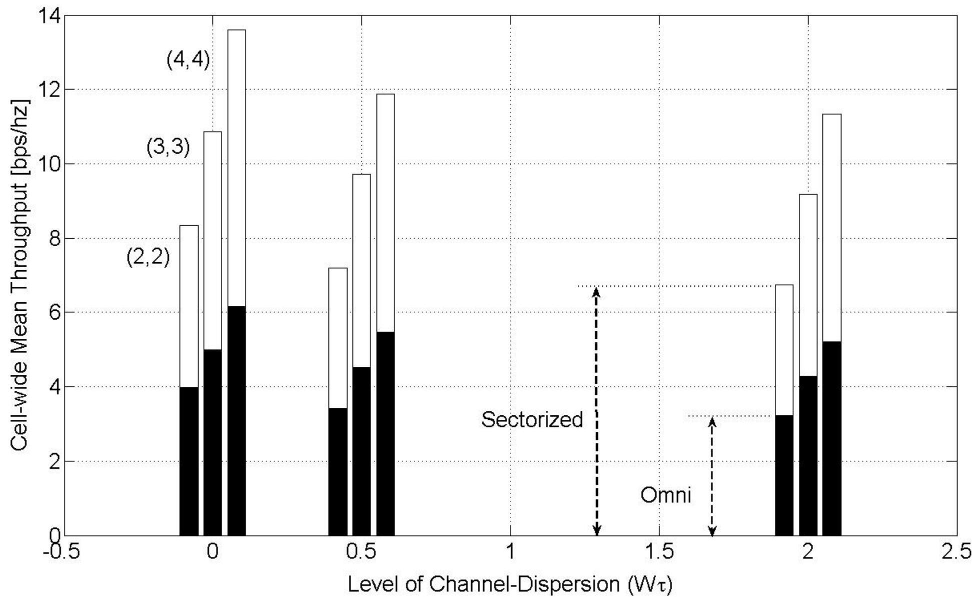

Figure 6.3: Effect of channel dispersion. The figure is for channels with i.i.d. path gains, with Co-channel interference (multi-cell case), with Shannon Coding, and employing the Ideal Canceller.

at low output SINR (e.g. uncoded transmission in the multi-cell case) the drop is closer to 20% and noise enhancement by the canceller begins to become significant.

Effect of Ideal vs. Non-Dispersive Cancellation: When the non-dispersive canceller is used, a sharp percent drop is noticed in cell-wide mean throughputs (36%) even at a very low degree of dispersion $W\tau = \frac{1}{8}$, as shown in Fig. 6.4. However, the drop in throughput going from $W\tau = \frac{1}{8}$ to $W\tau = 2$ is less severe at about 60% (for the range of $W\tau$ under consideration). At $W\tau = \frac{1}{8}$, the dispersion is relatively small, however there is residual XSI (at all frequencies). This implies that XSI from interfering streams is significant. That is, channel dispersion smears XSI in the time domain, which the non-dispersive canceller is unable to remove. We conclude that non-dispersive cancellation is not suitable for use even at low degrees of channel dispersion.

Effect of Array Size: Although MIMO systems can lead to throughputs which increase linearly in the number of antennas [4, 8], this is applicable for high SNR regimes only. When

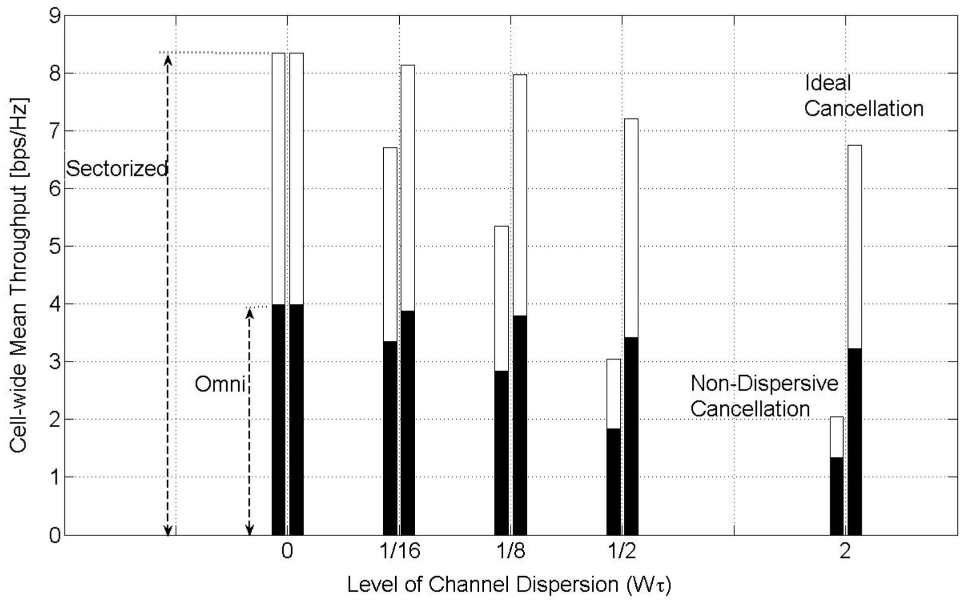

Figure 6.4: Effect of receiver responsiveness as a function of channel dispersion. The figure is for MIMO $(2, 2)$ channels with i.i.d. path gains, with Co-channel interference (multi-cell case), with Shannon Coding.

CCI comes into play, $SINR << SNR$, and the linear increase no longer holds. Accordingly, in Fig. 6.5, we see that the ratio of the throughputs is nearly $2 : 3 : 4$ for the single-cell case[8], whereas throughputs are comparable for the multi-cell case. For the CCI case, MIMO $(4, 4)$ will not have twice the throughput as MIMO $(2, 2)$, despite the creation of four parallel streams. This is because in the low SINR regime, the available antennas at the receiver are used to combat XSI at the cost of noise enhancement (which now becomes significant). Moreover, each transmit antenna now uses only $1/2$ the available power as compared to the MIMO $(2, 2)$ system.

Effect of Co-Channel Interference and Antenna Sectorization: It is clear that the throughput performances of the single-cell case (noise only, no interferers), and the multi-cell case (omni-antenna, six interferers) bracket those of the sectorized antenna case (two interferers). From the results shown in Fig. 6.5, we observe that the multi-cell throughput is about 30% that

[8]Note that SNRs were clipped to a maximum of 30 dB, even for the single-cell case. For a cell-boundary SNR of 20 dB, this is reasonably severe. Without this limitation, the throughputs would have been closer to the actual $2 : 3 : 4$ ratio.

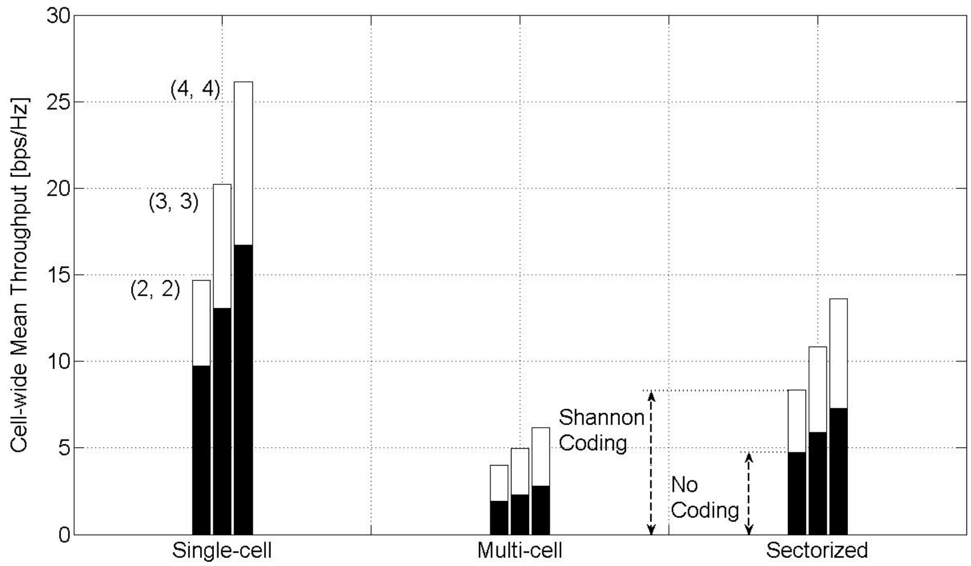

Figure 6.5: Effect of Co-channel interference and sectorization. The figure is for channels with i.i.d. path gains, $W\tau = 0$, and employing the Ideal Canceller. Note that the shaded and full portions of the bar refer to the uncoded and coded parts respectively. The abcissa scaling for this figure is also different.

of the single-cell case; and using sectorized antennas leads to a two-fold improvement in link throughput over omni-directional antennas. These results are consistent with those obtained for the flat-channel case for limited constellation sizes (or equivalently by limiting maximum achievable SINR) [24, 38]. The result continues to hold for dispersive channels over the entire range of $W\tau$ values that were considered. This follows from the facts that dispersion accounts for a small loss as compared to flat-channels, and that loss is nearly independent of SINR at 15% to 20%.

Effect of Coding: The throughput curve for uncoded transmission is about 8 dB shifted from that for perfectly-coded (Shannon) transmission. The reduction in throughput for transmitting uncoded signals relative to Shannon-coded signals is about 40% for the single-cell case, 45% for the sectorized antenna case, and 55% for the multi-cell case as seen in Fig 6.5.

Effect of Path-Correlation and Carrier Frequency: Correlations in path gains are created by generating transmit and receive correlation matrices. These matrices are obtained by assuming

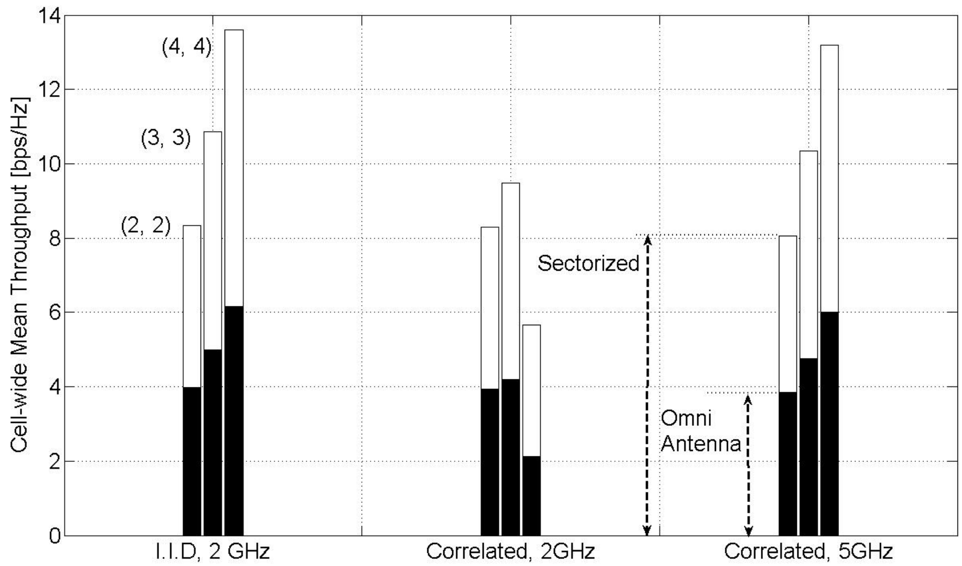

Figure 6.6: Effect of channel correlation and carrier frequency. The figure is for channels with $W\tau = 0$, with Co-channel interference (multi-cell case), with Shannon Coding, and employing the Ideal Canceller.

suitable physical lengths for the BS and the MS, and assuming PAS shapes and AS values for the AoD/AoA statistics, as in Table 6.1. The physical lengths of the BS and MS are assumed constant, regardless of whether $(2, 2)$, $(3, 3)$ or $(4, 4)$ configuration is used. This implies that as the number of antennas increases, antenna spacing becomes smaller, and path gains are thus more correlated. On the other hand, a higher carrier frequency results in a smaller wavelength, and hence, a smaller decorrelation distance. The overall effect of operating in a higher band, therefore, is reduced path correlation and higher transmit power.

From Fig. 6.6, we see that path-correlation has the effect of dramatically reducing the throughputs of MIMO $(4, 4)$, and that throughputs of MIMO $(3, 3)$ are affected to a lesser extent, while those of MIMO $(2, 2)$ remain essentially unchanged. Increasing the number of antennas does *not* result in automatic throughput increase since channel path-correlation can lead to a *reversal* in the observed throughput trends. Using a carrier frequency of 5 GHz has the effect of nearly restoring the throughputs of all MIMO configurations. By virtue of the base station's larger physical length the transmit correlation matrices are very nearly i.i.d. (identity matrix) at both carrier frequencies. Thus, the observed influences of MIMO array size and frequency band relate solely to the way they affect the receive correlation matrix.

6.5 Conclusion

The cell-wide mean throughputs of dispersive MIMO systems have been quantified along several system-level design dimensions. Following earlier work [38], it was decided to limit SINRs to a maximum 30 dB (equivalently using limited signal constellation sizes) that are prevalent in practical present day systems. From the results, we observe that the ideal canceller suffers very little loss in throughput even for severely distorted channels, while the non-dispersive canceller was deemed an impractical choice. The conclusion is that channel dispersion is a significant adversary; it smears XSI in the time domain, which the non-dispersive canceller is unable to mitigate. CCI, although also a source of throughput deterioration, it is less damaging as compared to XSI.

The earlier conclusion can be used to gain another perspective into the working of a MIMO-OFDM system. OFDM will successfully mitigate ISI. However, even small amounts of dispersion in any tone of such a system will greatly reduce its performance (via XSI). This implies that MIMO-OFDM systems must use a sufficient number of sub-carriers to maintain flat-fading in each tone.

Further, it is seen that channel path-correlation severely affects throughput performances of devices with higher number of antennas (in particular, the case of MIMO $(4, 4)$). Channel correlation is particularly the case at the user end, where device sizes are extremely limited. Increasing number of antennas does *not* necessarily lead to better throughputs, as a result of path-correlations. Use of a higher carrier frequency (5 GHz or greater) restores MIMO throughputs at the cost of higher base station transmit power. It is clear that the nature of interaction between the device size, number of antennas, path-correlation (as dictated by the particular terrain profile via its AoA/AoD statistics), and carrier frequency, must be taken into account by system designers and cellular operators.

6.6 Appendix: Derivation of g_{opt}

From (6.20) and (6.21), we have

$$\begin{aligned} X(f) &= P_0 T \cdot C(f) B_c(f) \\ &= P_0 T \cdot C(f) \left[|H_{12}(f) G_{11}(f) + H_{22}(f) G_{12}(f)|^2 \right]. \end{aligned} \tag{6.33}$$

Noting that $C(f)$ is constant over $\left[-\frac{1}{2T}, \frac{1}{2T}\right]$, which is the signal band, our aim is to minimize the average of $X(f)$ (or equivalently, minimize the average of $B_c(f)$) over that band. For our purposes, $G_{11}(f) = 1$, and $G_{12}(f) = g$, independent of frequency. Thus,

$$B_c(f) = |H_{12}(f) + H_{22}(f) g|^2. \tag{6.34}$$

Expanding this and taking the average over the frequency interval $\left[-\frac{1}{2T}, \frac{1}{2T}\right]$, we get

$$\overline{B_c(f)} = \overline{|H_{12}(f)|^2} + g^* \overline{H_{12}(f) H_{22}^*(f)} + g \overline{H_{22}(f) H_{12}^*(f)} + g g^* \overline{|H_{22}(f)|^2}. \tag{6.35}$$

At this point, we differentiate with respect to g^*, treating g as a constant. Thus,

$$\frac{\partial}{\partial g^*} \overline{B_c(f)} = \overline{H_{12}(f) H_{22}^*(f)} + g \overline{|H_{22}(f)|^2}. \tag{6.36}$$

Setting this to zero and solving, we obtain the desired g_{opt} in (6.29).

6.7 Tabular Results for Channel Dispersion and Path Correlation Study

Cell-wide mean throughputs (in units of bps/Hz) for the dispersive MIMO $(2, 2)$ channel with i.i.d. path gains. The throughputs are displayed as a function the dispersion level ($W\tau$).

	$W\tau$	0	$\frac{1}{16}$	$\frac{1}{8}$	$\frac{1}{2}$	1	2
Single-cell	Ideal Cancellation	14.66	14.33	14.06	12.83	12.31	12.01
	Non-Disp. Cancellation	14.66	10.67	7.88	3.95	2.94	2.51
Multi-cell	Ideal Cancellation	3.98	3.88	3.79	3.42	3.29	3.22
	Non-Disp. Cancellation	3.98	3.35	2.83	1.84	1.50	1.34
Sectorized	Ideal Cancellation	8.34	8.13	7.96	7.20	6.91	6.74
	Non-Disp. Cancellation	8.34	6.70	5.35	3.05	2.36	2.05

Table 6.2: Shannon coding.

	$W\tau$	0	$\frac{1}{16}$	$\frac{1}{8}$	$\frac{1}{2}$	1	2
Single-cell	Ideal Cancellation	9.72	9.43	9.16	7.97	7.46	7.17
	Non-Disp. Cancellation	9.72	6.07	3.86	1.26	0.77	0.60
Multi-cell	Ideal Cancellation	1.90	1.84	1.77	1.48	1.37	1.31
	Non-Disp. Cancellation	1.90	1.42	1.05	0.48	0.34	0.28
Sectorized	Ideal Cancellation	4.72	4.56	4.40	3.72	3.46	3.31
	Non-Disp. Cancellation	4.72	3.32	2.32	0.90	0.58	0.47

Table 6.3: No coding.

Cell-wide mean throughputs (in units of bps/Hz) for the dispersive MIMO $(2, 2)$ channel with correlated path gains, and 2 GHz carrier frequency. The throughputs are displayed as a function of the dispersion level ($W\tau$).

	$W\tau$	0	$\frac{1}{16}$	$\frac{1}{8}$	$\frac{1}{2}$	1	2
Single-cell	Ideal Cancellation	14.60	14.42	13.93	12.88	12.29	12.17
	Non-Disp. Cancellation	—	—	—	—	—	—
Multi-cell	Ideal Cancellation	3.94	3.90	3.74	3.44	3.31	3.27
	Non-Disp. Cancellation	—	—	—	—	—	—
Sectorized	Ideal Cancellation	8.29	8.19	7.87	7.22	6.91	6.84
	Non-Disp. Cancellation	—	—	—	—	—	—

Table 6.4: Shannon coding.

	$W\tau$	0	$\frac{1}{16}$	$\frac{1}{8}$	$\frac{1}{2}$	1	2
Single-cell	Ideal Cancellation	9.66	9.50	9.05	8.01	7.43	7.31
	Non-Disp. Cancellation	—	—	—	—	—	—
Multi-cell	Ideal Cancellation	1.88	1.85	1.74	1.49	1.38	1.34
	Non-Disp. Cancellation	—	—	—	—	—	—
Sectorized	Ideal Cancellation	4.67	4.59	4.34	3.75	3.46	3.38
	Non-Disp. Cancellation	—	—	—	—	—	—

Table 6.5: No coding.

Cell-wide mean throughputs (in units of bps/Hz) for the dispersive MIMO $(2, 2)$ channel with correlated path gains, and 5 GHz carrier frequency. The throughputs are displayed as a function of the dispersion level ($W\tau$).

	$W\tau$	0	$\frac{1}{16}$	$\frac{1}{8}$	$\frac{1}{2}$	1	2
Single-cell	Ideal Cancellation	14.64	14.45	13.93	12.86	12.33	12.24
	Non-Disp. Cancellation	—	—	—	—	—	—
Multi-cell	Ideal Cancellation	3.85	3.81	3.64	3.35	3.24	3.22
	Non-Disp. Cancellation	—	—	—	—	—	—
Sectorized	Ideal Cancellation	8.06	7.95	7.62	6.99	6.72	6.67
	Non-Disp. Cancellation	—	—	—	—	—	—

Table 6.6: Shannon coding.

	$W\tau$	0	$\frac{1}{16}$	$\frac{1}{8}$	$\frac{1}{2}$	1	2
Single-cell	Ideal Cancellation	9.69	9.52	9.05	7.99	7.47	7.37
	Non-Disp. Cancellation	—	—	—	—	—	—
Multi-cell	Ideal Cancellation	1.81	1.78	1.67	1.42	1.32	1.30
	Non-Disp. Cancellation	—	—	—	—	—	—
Sectorized	Ideal Cancellation	4.48	4.40	4.15	3.57	3.31	3.26
	Non-Disp. Cancellation	—	—	—	—	—	—

Table 6.7: No coding.

Cell-wide mean throughputs (in units of bps/Hz) for the dispersive MIMO $(3, 3)$ channel with i.i.d. path gains. The throughputs are displayed as a function of the dispersion level ($W\tau$).

	$W\tau$	0	$\frac{1}{16}$	$\frac{1}{8}$	$\frac{1}{2}$	1	2
Single-cell	Ideal Cancellation	20.22	20.48	19.69	18.18	17.47	17.14
	Non-Disp. Cancellation	—	—	—	—	—	—
Multi-cell	Ideal Cancellation	4.99	5.14	4.93	4.51	4.36	4.28
	Non-Disp. Cancellation	—	—	—	—	—	—
Sectorized	Ideal Cancellation	10.86	11.08	10.62	9.72	9.36	9.18
	Non-Disp. Cancellation	—	—	—	—	—	—

Table 6.8: Shannon coding.

	$W\tau$	0	$\frac{1}{16}$	$\frac{1}{8}$	$\frac{1}{2}$	1	2
Single-cell	Ideal Cancellation	13.05	13.24	12.52	11.03	10.35	10.03
	Non-Disp. Cancellation	—	—	—	—	—	—
Multi-cell	Ideal Cancellation	2.29	2.36	2.21	1.88	1.75	1.69
	Non-Disp. Cancellation	—	—	—	—	—	—
Sectorized	Ideal Cancellation	5.90	6.03	5.66	4.85	4.52	4.37
	Non-Disp. Cancellation	—	—	—	—	—	—

Table 6.9: No coding.

Cell-wide mean throughputs (in units of bps/Hz) for the dispersive MIMO $(3, 3)$ channel with correlated path gains, and 2 GHz carrier frequency. The throughputs are displayed as a function of the dispersion level ($W\tau$).

	$W\tau$	0	$\frac{1}{16}$	$\frac{1}{8}$	$\frac{1}{2}$	1	2
Single-cell	Ideal Cancellation	18.35	18.60	17.90	16.31	15.62	15.28
	Non-Disp. Cancellation	—	—	—	—	—	—
Multi-cell	Ideal Cancellation	4.20	4.34	4.15	3.74	3.60	3.53
	Non-Disp. Cancellation	—	—	—	—	—	—
Sectorized	Ideal Cancellation	9.49	9.71	9.30	8.40	8.05	7.88
	Non-Disp. Cancellation	—	—	—	—	—	—

Table 6.10: Shannon coding.

	$W\tau$	0	$\frac{1}{16}$	$\frac{1}{8}$	$\frac{1}{2}$	1	2
Single-cell	Ideal Cancellation	11.43	11.62	10.98	9.42	8.77	8.46
	Non-Disp. Cancellation	—	—	—	—	—	—
Multi-cell	Ideal Cancellation	1.88	1.94	1.81	1.50	1.39	1.33
	Non-Disp. Cancellation	—	—	—	—	—	—
Sectorized	Ideal Cancellation	4.97	5.10	4.77	3.97	3.67	3.53
	Non-Disp. Cancellation	—	—	—	—	—	—

Table 6.11: No coding.

Cell-wide mean throughputs (in units of bps/Hz) for the dispersive MIMO $(3, 3)$ channel with correlated path gains, and 5 GHz carrier frequency. The throughputs are displayed as a function of the dispersion level ($W\tau$).

	$W\tau$	0	$\frac{1}{16}$	$\frac{1}{8}$	$\frac{1}{2}$	1	2
Single-cell	Ideal Cancellation	20.05	20.21	19.59	17.83	17.52	17.34
	Non-Disp. Cancellation	—	—	—	—	—	—
Multi-cell	Ideal Cancellation	4.76	4.86	4.70	4.31	4.27	4.22
	Non-Disp. Cancellation	—	—	—	—	—	—
Sectorized	Ideal Cancellation	10.34	10.48	10.14	9.19	9.07	8.97
	Non-Disp. Cancellation	—	—	—	—	—	—

Table 6.12: Shannon coding.

	$W\tau$	0	$\frac{1}{16}$	$\frac{1}{8}$	$\frac{1}{2}$	1	2
Single-cell	Ideal Cancellation	12.90	13.00	12.40	10.72	10.40	10.20
	Non-Disp. Cancellation	—	—	—	—	—	—
Multi-cell	Ideal Cancellation	2.15	2.18	2.06	1.73	1.68	1.64
	Non-Disp. Cancellation	—	—	—	—	—	—
Sectorized	Ideal Cancellation	5.53	5.59	5.29	4.46	4.32	4.22
	Non-Disp. Cancellation	—	—	—	—	—	—

Table 6.13: No coding.

Cell-wide mean throughputs (in units of bps/Hz) for the dispersive MIMO $(4, 4)$ channel with i.i.d. path gains. The throughputs are displayed as a function of the dispersion level ($W\tau$).

	$W\tau$	0	$\frac{1}{16}$	$\frac{1}{8}$	$\frac{1}{2}$	1	2
Single-cell	Ideal Cancellation	26.13	25.74	24.92	22.92	21.91	21.83
	Non-Disp. Cancellation	—	—	—	—	—	—
Multi-cell	Ideal Cancellation	6.16	6.13	5.90	5.46	5.24	5.22
	Non-Disp. Cancellation	—	—	—	—	—	—
Sectorized	Ideal Cancellation	13.60	13.43	12.95	11.88	11.38	11.33
	Non-Disp. Cancellation	—	—	—	—	—	—

Table 6.14: Shannon coding.

	$W\tau$	0	$\frac{1}{16}$	$\frac{1}{8}$	$\frac{1}{2}$	1	2
Single-cell	Ideal Cancellation	16.70	16.34	15.54	13.58	12.62	12.53
	Non-Disp. Cancellation	—	—	—	—	—	—
Multi-cell	Ideal Cancellation	2.78	2.73	2.57	2.19	2.03	2.01
	Non-Disp. Cancellation	—	—	—	—	—	—
Sectorized	Ideal Cancellation	7.26	7.12	6.70	5.73	5.30	5.24
	Non-Disp. Cancellation	—	—	—	—	—	—

Table 6.15: No coding.

Cell-wide mean throughputs (in units of bps/Hz) for the dispersive MIMO $(4, 4)$ channel with correlated path gains, and 2 GHz carrier frequency. The throughputs are displayed as a function of the dispersion level ($W\tau$).

	$W\tau$	0	$\frac{1}{16}$	$\frac{1}{8}$	$\frac{1}{2}$	1	2
Single-cell	Ideal Cancellation	13.64	12.90	12.34	11.22	10.69	10.65
	Non-Disp. Cancellation	—	—	—	—	—	—
Multi-cell	Ideal Cancellation	2.12	1.98	1.91	1.77	1.72	1.72
	Non-Disp. Cancellation	—	—	—	—	—	—
Sectorized	Ideal Cancellation	5.67	5.31	5.10	4.67	4.49	4.48
	Non-Disp. Cancellation	—	—	—	—	—	—

Table 6.16: Shannon coding.

	$W\tau$	0	$\frac{1}{16}$	$\frac{1}{8}$	$\frac{1}{2}$	1	2
Single-cell	Ideal Cancellation	6.84	6.26	5.78	4.72	4.28	4.21
	Non-Disp. Cancellation	—	—	—	—	—	—
Multi-cell	Ideal Cancellation	0.82	0.74	0.68	0.56	0.52	0.51
	Non-Disp. Cancellation	—	—	—	—	—	—
Sectorized	Ideal Cancellation	2.40	2.18	2.00	1.63	1.49	1.46
	Non-Disp. Cancellation	—	—	—	—	—	—

Table 6.17: No coding.

Cell-wide mean throughputs (in units of bps/Hz) for the dispersive MIMO $(4, 4)$ channel with correlated path gains, and 5 GHz carrier frequency. The throughputs are displayed as a function of the dispersion level ($W\tau$).

	$W\tau$	0	$\frac{1}{16}$	$\frac{1}{8}$	$\frac{1}{2}$	1	2
Single-cell	Ideal Cancellation	26.38	25.52	24.90	22.89	22.24	21.80
	Non-Disp. Cancellation	—	—	—	—	—	—
Multi-cell	Ideal Cancellation	6.00	5.77	5.63	5.27	5.13	4.99
	Non-Disp. Cancellation	—	—	—	—	—	—
Sectorized	Ideal Cancellation	13.19	12.71	12.37	11.42	11.09	10.83
	Non-Disp. Cancellation	—	—	—	—	—	—

Table 6.18: Shannon coding.

	$W\tau$	0	$\frac{1}{16}$	$\frac{1}{8}$	$\frac{1}{2}$	1	2
Single-cell	Ideal Cancellation	16.87	16.11	15.51	13.57	12.91	12.51
	Non-Disp. Cancellation	—	—	—	—	—	—
Multi-cell	Ideal Cancellation	2.65	2.51	2.39	2.07	1.96	1.87
	Non-Disp. Cancellation	—	—	—	—	—	—
Sectorized	Ideal Cancellation	6.93	6.58	6.28	5.41	5.11	4.91
	Non-Disp. Cancellation	—	—	—	—	—	—

Table 6.19: No coding.

Chapter 7

Multi-Carrier Wideband MIMO (MIMO-OFDM) Systems

7.1 Introduction

In the past decade, multi-antenna links (multiple-input/multiple-out, or MIMO links in particular) have been the focus of much research in the area of wireless communications. As newer and richer applications and services continue to become available at increasingly affordable costs to the average consumer, systems designers are forced to push the frontiers of research in an effort to attain better throughputs to match ever-increasing customer demands. At the present time, MIMO links employing orthogonal frequency division multiplexing (MIMO-OFDM) have been proposed as the most sophisticated and practical solution. Researchers and system engineers continue to evaluate the attainable throughputs/capacities of MIMO-OFDM systems, using ever more accurate techniques (or more accurate channel models) as they become available. This study aims to advance the endeavor by removing a key assumption made by analysts up to the present, namely that each tone is perfectly flat. Removing this assumption will lead to more accurate throughput estimates.

Previous Research: Most investigations relating to MIMO capacity/throughputs have considered rather idealized channel behavior. Early research assumed the flat-fading (no channel dispersion) i.i.d. path gain model for MIMO channels [4–14, 39]. Later research developed more sophisticated channel models to incorporate path correlations and other effects (e.g., keyholes) [40, 53–58], while continuing use of the flat-fading model [59, 60]. Current research efforts propose more sophisticated modems that employ Orthogonal Frequency Division Multiplexing (OFDM) to "flatten" the dispersive channel [47, 50–52]. This strategy improves performance of the MIMO link. However, it encourages systems analysts (attempting to estimate throughputs of MIMO-OFDM systems) to continue using the flat channel assumption, thereby continuing to ignore the effect of channel dispersion via inter-symbol interference (ISI), and cross-stream interference (XSI).

Frequency-selective MIMO channels were previously analyzed (Chapter 6), and evaluated on a cell-wide mean throughput metric. In the study, the effect of channel dispersion (frequency selectivity) leading to ISI and XSI was quantified under a wide range of system-level parameters. The observations were that: (i) for an ideal canceller with MMSE equalizer, the loss in throughput by way of ISI is small, and that most of this performance loss occurs at very small levels of dispersion; (ii) channel dispersion is a significant adversary because it smears XSI in the time domain which is hard to mitigate without using a cross-dispersive canceller.

In MIMO-OFDM systems each tone may be considered to be a MIMO channel which will not be perfectly flat. OFDM will be able to minimize ISI by using an appropriate value for guard time and incorporating a cyclic prefix. Moreover, XSI can also be removed completely by careful system design[1]. Nevertheless, it is instructive to study the effects of ISI and XSI, since perfect removal of either ISI or XSI may be difficult for a variety of practical reasons including synchronization and imperfect channel estimation. By investigating the effects due to ISI and XSI for the two cases of optimal removal and no removal at all, we will be able to bracket the throughput performance of all MIMO-OFDM systems.

Contribution of this study: The effects of (i) channel dispersion (particularly due to XSI); and, (ii) signaling inefficiency as a result of guard time (indirectly, ISI) in MIMO-OFDM systems are quantified in this investigation. For simplicity, cosine roll-off pulse-shaping is not used in the guard time. Rather, the guard time is regarded as a time gap, during which no signal is transmitted. To a first order, the study evaluates the loss in throughput resulting from XSI and signaling inefficiency, within a given signal bandwidth, over several different values of the channel rms delay spread, and number of tones in the MIMO-OFDM system.

This study uses the cell-wide mean throughput per user as the primary metric. This metric

[1] In the dispersive MIMO systems considered in Chapter 6, the overall transmit-receive pulse shaping was an ideal sinc waveform in the time domain. This choice was based on the design that would result in nearly zero ISI at signal sampling instants [28, 65]. Channel fading distorts the signal, leading to XSI in MIMO systems which is not possible to cancel completely unless an ideal canceller is employed. This is because the sinc pulse extends indefinitely along time, and the XSI sample has terms from *all* symbols (i.e., ISI terms from other streams), which cannot all be cancelled with just one tap.

In MIMO-OFDM systems, rectangular signaling pulses (rather than sinc pulses) are employed, which extend only for a finite time interval. Consequently, ISI extends only for a finite duration, and it becomes possible to cancel XSI perfectly, by requiring that the XSI be zero only at the signal sample instants. This cancellation is implicit within the IFFT-FFT process. For $T_g \ll \tau_{rms}$, XSI cancellation with a non-dispersive canceller will require several taps, and XSI removal will be incomplete if just one tap is employed. When $T_g \gg \tau_{rms}$, ISI becomes extremely limited, and the XSI sample (comprising of ISI from other streams) may come from just the current symbol. In this latter case, XSI can be cancelled with a non-dispersive canceller having a single tap.

is obtained by averaging over all user locations (path loss), shadow fadings, and multipath. In a system with many users, this metric closely approximates the average performance any user can expect [1, 2, 24].

7.2 The Multi-Carrier Wideband MIMO (Dispersive MIMO-OFDM) Simulation Platform

We continue to use the simulation platform presented in Chapter 6 since the system-level platform, in particular, is identical. The link-level platform is only slightly different, and we discuss the differences below.

Link-level Description: Figures 7.1 and 7.2 depict an *equivalent* system diagram for *each tone* of an MIMO-OFDM system. The tones incorporate frequency-selective fading in their path gains. For simplicity, we have shown, and used for illustrative purposes a MIMO $(2, 2)$ channel, although the discussion can easily be extended to the general case of MIMO (n, m).

Each tone of the MIMO-OFDM system is a dispersive-MIMO channel. Furthermore, as in Chapter 6, each tone is characterized by a pair of co-dispersive $[h_{11}(f), h_{22}(f)]$ and cross-dispersive $[h_{12}(f), h_{21}(f)]$ channel frequency response functions which are assumed to obey the WSSUS model [61].

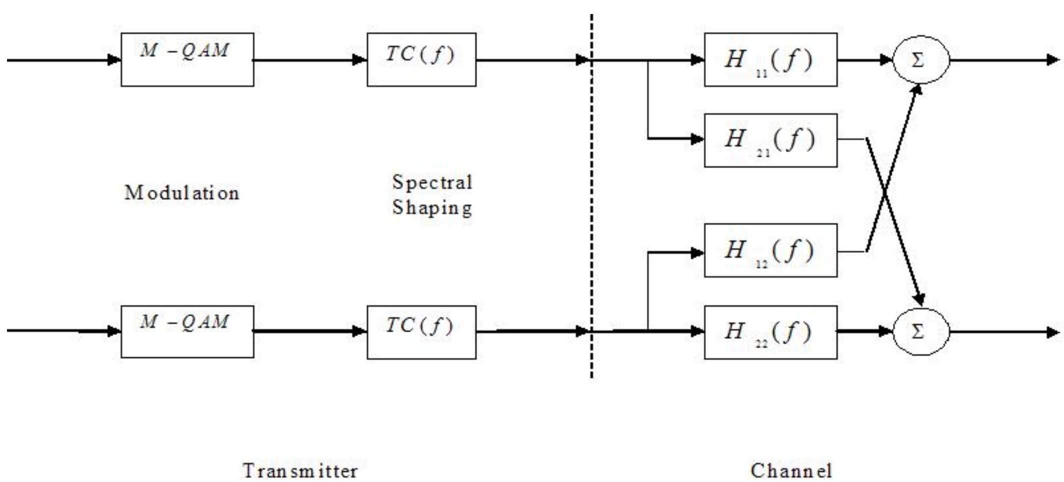

Figure 7.1: The *equivalent* system diagram for *each tone* of a MIMO-OFDM Transmitter.

The transmitter operates in the Spatial Multiplexing (SM) mode [4, 8–10] and uses M-ary Quadrature Amplitude Modulation (M-QAM) in its various transmit streams. The transmit

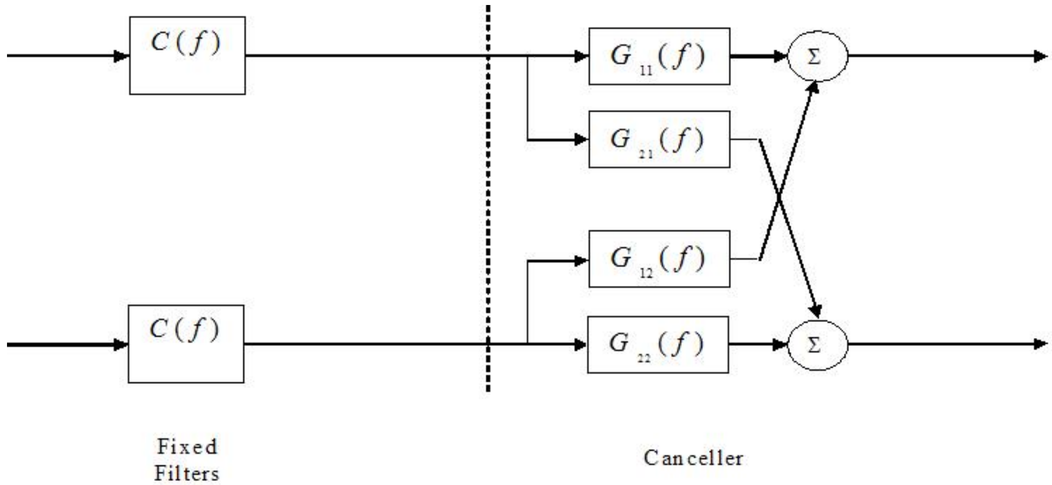

Figure 7.2: The *equivalent* system diagram for *each tone* of a MIMO-OFDM Receiver. The canceller is *non-dispersive*.

pulse is rectangular with duration T', of which an interval of T (having voltage of unit amplitude) is used for transmission, and an interval T_g is maintained for the guard spacing, i.e.,

$$T' = T + T_g. \tag{7.1}$$

The transmit and receive pulse-shaping filters $c(t)$ are matched to T. Hence, they are rectangular with unit amplitude in the time interval $[-\frac{T}{2}, \frac{T}{2}]$. These pulse-shaping filters are *implicit* in the IFFT and the FFT processes of the MIMO-OFDM system. Thus,

$$\begin{aligned} C(f) \quad &\stackrel{\mathcal{F}}{\longleftrightarrow} \quad c(t) \\ C(f) \quad &= \quad sinc(fT) \end{aligned} \tag{7.2}$$

where, we have omitted a scaling factor of T in $C(f)$ and used it directly in the transmitter configuration.

The IFFT-FFT circuits at the transmitter and the receiver respectively, can be considered to be a combination of the spectral shaping circuit at the transmit end, the fixed-filters $C(f)$, and a *non-dispersive* cross-stream canceller[2], which is comprised of a bridge network of functions $[G_{11}(f), G_{12}(f), G_{21}(f), G_{22}(f)]$.

[2]In this study, we use the single-tap solution. We use the math from Chapter 6 to compute the "impact of XSI". We follow this up with an investigation of the case of perfect removal of XSI (even with the single-tap solution, since $T_g \gg \tau_{rms}$). As explained earlier, by investigating the throughput performance curves for both cases, we bracket the throughput performance of all other scenarios.

The non-dispersive canceller does *not* cancel XSI at all frequencies, it does however *minimize* XSI in each stream based on a mean-square criterion. The optimal non-dispersive canceller is given by

$$G_{11}(f) = g_{11} = 1; \qquad G_{12}(f) = g_{12} = g_{opt} \tag{7.3}$$

and,

$$g_{opt} = -\frac{\overline{|C(f)|^4 H_{22}^*\left(f\right) H_{12}\left(f\right)}}{\overline{|C(f)|^4 |H_{22}\left(f\right)|^2}} \tag{7.4}$$

where the overbar denotes expectation over frequency. Since both streams are statistically identical, we are analyzing only the upper stream of the canceller. The derivation for (7.4) is explained in Section 7.3. Extension to MIMO (n, n) is straightforward.

Channel Dispersion Modeling: Each tone of the MIMO-OFDM channel considered in this study is frequency-selective, but slowly varying. The complex baseband channel impulse response between the jth transmit antenna of a given BS, and the ith receive antenna of a given MS is modeled by

$$h_{ij}(t) = \sum_{l=0}^{50} h_{ij}^{l} \delta\left(t - 0.02lT\right) \tag{7.5}$$

where T is the transmission period (excluding the guard interval), and h_{ij}^{l} is the amplitude of the l^{th} tap ($l = 0$ corresponds to the tap (or multipath) with zero delay).

Each tap is assumed to be comprised of several individual rays such that the h_{ij}^{l} are complex Gaussian with zero-mean and variance distributed according to an exponential delay profile,

$$h_{ij}^{l} \sim \mathbb{CN}\left(0, \sigma_l^2\right), \qquad \sigma_l^2 = \frac{1}{\tau_{rms}} \exp^{-\theta_l/\tau_{rms}}, \qquad \theta_l = 0.02lT. \tag{7.6}$$

The h_{ij}^{l} are normalized, so that

$$\sum_{l} |h_{ij}^{l}|^2 = 1 \tag{7.7}$$

where θ_l is the delay of the l^{th} multipath, and τ_{rms} is the rms delay spread of the tone. The impulse response is allowed to extend over one signal duration, thereby resulting in a channel having a memory of one symbol duration. Moreover, a factor of fifty (50) oversampling is employed, which results in taps that are spaced $0.02\ T$ apart.

In the frequency domain, the channel path from transmit antenna j to receive antenna i is characterized by the Discrete Fourier Transform (DFT) of the channel impulse response

$$H_{ij}\left(f\right) = \sum_{l=0}^{50} h_{ij}^{l} \exp^{-j2\pi f 0.02 l T}. \tag{7.8}$$

In our system

$$T_g = 3\, \tau_{rms}. \tag{7.9}$$

Moreover, $T > T_g > \tau_{rms}$, so that only multipaths with negligible power are discarded from consideration in (7.6).

7.3 Link-Level Analysis

Following a procedure similar to that employed in Chapter 6, we can derive the various relationships for the MIMO-OFDM transmitter-receiver, as described below.

For the purpose of link-level analysis, let P_0 be the average received power in an M-QAM signal in the absence of fading, and let N_0 be the total power spectral density of CCI and thermal noise at the input of the receiver. Then, the input $SINR$ is defined here to be

$$SINR \triangleq \frac{P_0\, T'}{N_0} \tag{7.10}$$

where T' equals the reciprocal of the tone bandwidth, $\frac{W}{N}$, i.e.,

$$T' = \frac{N}{W} \tag{7.11}$$

with W being the signal bandwidth, and N the number of tones in the system.

We use $SINR$ as an input parameter in the link-level simulations, and (7.10) allows us to compute the corresponding P_0 to be used. Our analysis below closely follows the one in [34]. From Figs. 7.1 and 7.2, for an M-QAM signal, we can see that a data pulse at the output of the canceller will have a Fourier transform of

$$S(f) = \sqrt{P_0}\, T\, C(f)\, A(f) \tag{7.12}$$

where

$$A(f) = H_{11}(f)\, C(f)\, g_{11} + H_{21}(f)\, C(f)\, g_{12}. \tag{7.13}$$

The noise-plus-CCI component at the output of the canceller will have a power spectral density

$$N(f) = N_0\, B_n(f) \tag{7.14}$$

where

$$B_n(f) = |C(f)\, g_{11}|^2 + |C(f)\, g_{12}|^2. \tag{7.15}$$

The XSI at the canceller output will have a power spectral density

$$\begin{aligned} X(f) &= P_0\, T\, |C(f)\, H_{12}(f)\, C(f)\, g_{11} + C(f)\, H_{22}(f)\, C(f)\, g_{12}|^2 \\ &= P_0\, T\, |C(f)|^4\, B_c(f) \\ &= N_0\, SINR\, \frac{T}{T'}\, |C(f)|^4\, B_c(f) \end{aligned} \tag{7.16}$$

where

$$B_c\,(f) = |H_{12}\,(f)\, g_{11} + H_{22}\,(f)\, g_{12}|^2. \tag{7.17}$$

In our treatment, we regard the XSI to be noise like so that the composite of the XSI, CCI and thermal noise, hereafter referred to as *total-interference*, will have a power spectral density

$$\begin{aligned} N'(f) &= N(f) + X(f) \\ &= N_0[B_n(f) + SINR\, \frac{T}{T'}\, |C(f)|^4\, B_c(f)]. \end{aligned} \tag{7.18}$$

Assuming optimal carrier timing and recovery, we can show that the squared half-distance between adjacent signal samples at the detector is [34, 65]

$$P_s = \left[\int |S\,(f)\,|\; df \right]^2. \tag{7.19}$$

We assume that the mean-squared intersymbol interference (ISI) at the sample times is very nearly zero as a result of the guard interval spacing, that is

$$P_i \approx 0. \tag{7.20}$$

The mean-squared total-interference is given by

$$P_{n'} = \int N'\,(f)\, df. \tag{7.21}$$

Finally, the output SINR is given by

$$\gamma \triangleq \frac{P_s}{P_{n'}}. \tag{7.22}$$

From the output SINR, we can obtain the link-throughput for two cases of interest [1,2,24]: Ideally Coded Signals and Uncoded Signals. Since all streams are statistically identical, $\gamma = \gamma_j$, and all streams have the same average throughput. The link throughput TP_{XSI} (assuming presence of XSI) is, therefore, simply n times the average throughput per stream

$$TP_{XSI} = n \cdot T_j. \tag{7.23}$$

Adjusting for guard interval spacing, the signaling inefficiency results in an actual throughput of

$$TP_{XSI,\,Tg} = \frac{T}{T'}\,TP_{XSI}. \tag{7.24}$$

For flat channels, $\tau_{rms} = 0$, so that T_g is also zero. For this case, the non-dispersive canceller is *exact*, and we have no XSI, i.e.,

$$TP = TP_{XSI} = TP_{XSI,\,T_g} \quad \text{when} \quad \tau_{rms} = 0. \tag{7.25}$$

In reality, for our design with $T_g \gg \tau_{rms}$, even for dispersive channels, the single-tap non-dispersive canceller can completely remove cross-stream interference, so that

$$X(f) = 0. \tag{7.26}$$

In this case, the throughput for each tone can be obtained directly from the narrowband case with a T_g overhead due to the guard interval

$$TP_{T_g\ only} = \frac{T}{T'}TP \tag{7.27}$$

where, TP represents the throughput for the flat channel.

With the analysis methodology established, we can use (7.16) to obtain the expression for g_{opt} (Equation (7.4)) using the same procedure as presented in Section 6.6.

7.4 Numerical Results and Conclusions

We follow a simulation methodology similar to the one described in Chapter 6. Results for the throughputs (in bps/Hz) achieved for various values of the channel rms delay spread, and the number of tones used are as tabulated in Section 7.5.

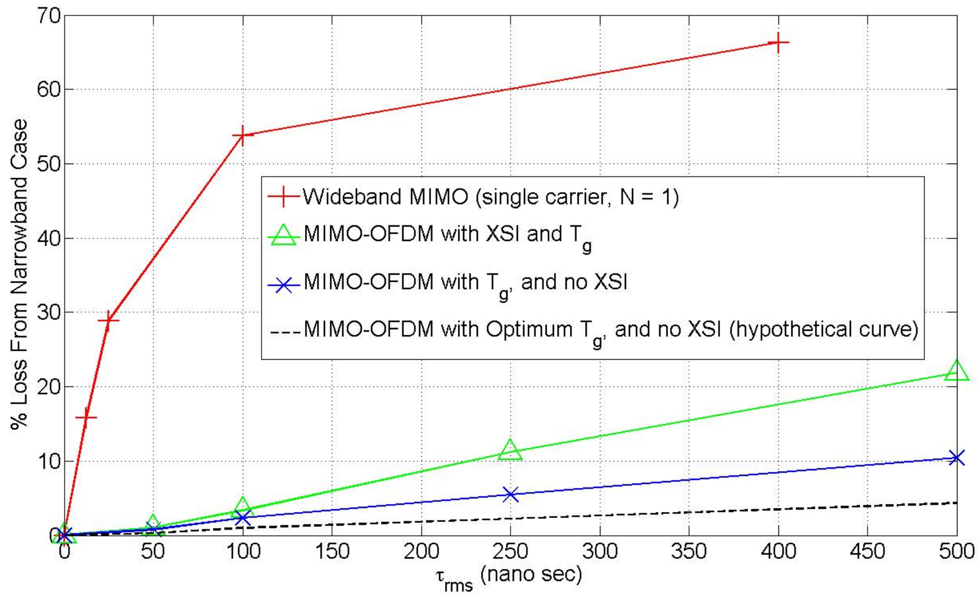

Figure 7.3: Throughputs in bps/Hz of the various schemes. For MIMO-OFDM signaling, the data displayed are for $N = 64$.

Figure 7.3 displays the effect of channel dispersion leading to ISI and XSI for four cases, namely: (i) when a wideband MIMO channel (single carrier, $N = 1$) is employed; (ii) when multi-carrier signaling (MIMO-OFDM) with suboptimal XSI and ISI removal is employed ($TP_{XSI,\ T_g}$); (iii) when multi-carrier signaling with optimal XSI but suboptimal ISI removal is employed ($TP_{T_g\ only}$); and, (iv) when multi-carrier signaling with optimal XSI and ISI removal is employed ($TP_{opt\ T_g}$). These curves were plotted by using data from the tables in Sections 6.7 and 7.5. For the multi-carrier case, the curves refer to the values for $N = 64$ tones.

From the plot, we observe that single-carrier signaling is a poor strategy to employ for frequency-selective channels. Moreover, when multi-carrier signaling is employed, throughput losses will lie between the performance curve for MIMO-OFDM with $\{XSI, T_g\}$ and that for the case of MIMO-OFDM with $\{T_g\}$. The case of MIMO-OFDM with $\{\text{optimum } T_g\}$ is that of a hyphothetical performance curve achievable by using an optimal guard spacing that attempts to optimize the tradeoff between throughput inefficiency and impact of ISI[3].

Figure 7.4 displays the amount of channel dispersion which can be tolerated by the MIMO-OFDM scheme for different number of tones (N) to achieve a signaling inefficiency less than

[3]See "Suggestions for Future Research" in Section 9.4

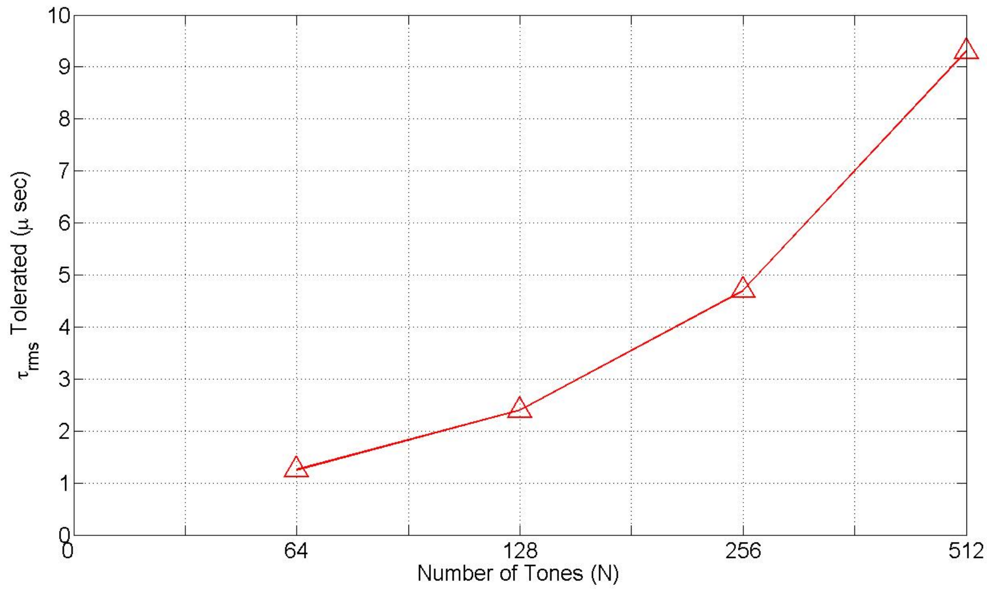

Figure 7.4: The amount of channel dispersion which can be tolerated by the MIMO-OFDM scheme for different number of tones (N) to achieve a signaling inefficiency less than 20%.

20%. From the figure, it is obvious that increasing the number of tones increases our ability to combat channel dispersion.

7.5 Tabular Results for the MIMO-OFDM Study

Table 7.1: THROUGHPUTS IN BPS/HZ ACHIEVED (WITH ONLY SIGNALING INEFFICIENCY PRESENT) FOR VARIOUS VALUES OF CHANNEL RMS DELAY SPREAD (NANOSEC), AND NUMBER OF TONES (N).

	$N = 64$	$N = 128$	$N = 256$	$N = 512$
0 ns	3.84	3.84	3.84	3.84
50 ns	3.81	3.82	3.83	3.84
100 ns	3.75	3.80	3.81	3.83
250 ns	3.63	3.73	3.77	3.81
500 ns	3.44	3.62	3.73	3.78
1000 ns	3.14	3.44	3.63	3.73
2500 ns	2.70	3.04	3.36	3.58
5000 ns	X	2.70	3.03	3.36
10000 ns	X	X	2.70	3.04

Table 7.2: PERCENTAGE LOSS RELATIVE TO THE FLAT-CHANNEL (WITH ONLY SIGNALING INEFFICIENCY PRESENT), FOR VARIOUS VALUES OF CHANNEL RMS DELAY SPREAD (NANOSEC), AND NUMBER OF TONES (N).

	$N = 64$	$N = 128$	$N = 256$	$N = 512$
0 ns	0.00%	0.00%	0.00%	0.00%
50 ns	0.78%	0.52%	0.26%	0.00%
100 ns	2.34%	1.04%	0.78%	0.26%
250 ns	5.47%	2.86%	1.56%	0.78%
500 ns	10.42%	5.73%	2.86%	1.30%
1000 ns	18.23%	10.42%	5.47%	2.86%
2500 ns	29.69%	20.83%	12.50%	6.77%
5000 ns	X	29.69%	21.09%	12.50%
10000 ns	X	X	29.69%	20.83%

Part III

Multi-User Diversity

Chapter 8

Evaluation of Multi-User Diversity Systems

8.1 Introduction

Since the publication of seminal papers [4, 8] a decade ago, multi-element antenna (MEA) systems have been an area of considerable interest to the wireless communications community. Commercial interest in multiple-input/multiple-output (MIMO) systems, which employ multiple antennas at both ends of the link, grew after the successful laboratory implementation of the well-known vertical Bell-Labs layered space-time architecture (VBLAST) [9]. VBLAST demonstrated the feasibility of the MIMO concept, delivering spectral efficiencies of 20–40 bps/Hz under indoor conditions. Later research demonstrated the different 'modes' of MIMO systems, notably, Diversity and Spatial Multiplexing. The diversity mode improves signal quality using the spatial resources [5–7]; the multiplexing mode, a chief reason for the industry's interest in MIMO systems, increases the data rate that can be pumped through a given bandwidth. By appropriate signal processing at the transmitter and/or the receiver, several de-coupled parallel single-input/single-output (SISO) channels can be created, which greatly enhances link capacity of the MIMO channel [1, 2, 4, 8, 10, 24, 38]. A tradeoff between these modes has been established [11], and linear codes that use a combination of both modes have been discovered [12]. Relevant definitions pertaining to MIMO/MEA[1] systems appear in the Appendix A.

Previous Research: In much of previous MEA/MIMO research, a *link-level* view, that of point-to-point communication, is taken. More recently, a *network-level* view of a cellular system has been adopted which permits a new form of diversity known as Multi-user Diversity (MuD) [19, 20, 66–68]. MuD can be viewed as a form of selection diversity (SD), in which the base station (BS) transmits to (or receives from) a mobile station (MS) with a good channel. Diversity is possible since all users are subject to independent fading, and in a system with sufficient number of users, a 'good' user exists with high probability. MuD is suitable for

[1]MEA links are assumed to have n transmitters and m receivers. They are denoted as MEA (n, m) or simply (n, m).

delay-elastic applications, i.e., those applications that can tolerate reasonable delays, such as data (but not voice). The implication of the network view was a paradigm shift in exploiting MEA/MIMO techniques: the multi-antenna link could now be used in multiplexing mode to extract maximal rate benefit, while diversity would come from the network itself [20, 69].

Most MuD performance studies (e.g., [3, 13, 14, 18, 20, 69]) focus only on a particular link between the transmitter and the receiver. Performance measures such as bit error rate (BER) or throughput (TP) are determined with signal-to-noise ratio (SNR) treated as a parameter, with external factors such as co-channel interference (CCI) ignored or indirectly treated using the signal-to-interference-plus-noise ratio (SINR) in place of the SNR. Some work on SISO/MEA (but not MuD) systems has been reported, however, that takes a broader system-level view (e.g., [1, 2, 24, 38]). This work determines the *distribution* of performance over a coverage area, e.g., the cumulative distributive function (CDF) of TP over the randomness of user location and shadow fading, which jointly specify the SNR value. Furthermore, in the case of multi-cell environments, it also means taking into account the CCI produced by co-channel users in other cells.

Contribution of this study: In this study, we extend the system-level study of SISO/MEA systems, to the multi-user scenario with scheduling. We quantify cell-wide mean throughputs of SISO- and MIMO-based cellular systems which employ multi-user diversity, and this is done over several useful system-level design dimensions: number of transmit/receive antennas; antenna-pattern (omni-directional or sectorized); degree of error-protection (Shannon coding, no coding or intermediate coding strategies); allowable constellation size; Rician κ-factor[2]; number of users and scheduling algorithm (Greedy, Proportional Fair or Equal Grade of Service) in single-cell (noise-limited) and multi-cell (CCI-limited) environments. In this connection, we note that the greedy and the equal grade-of-service scheduling algorithms define upper and lower bounds on throughput that any useful scheduler can offer; the proportional fair scheduler is considered owing to its popularity both in industry and in academic communities.

---

[2]Normally, K is used instead of κ, but, we use K here for the number of users sharing the channel.

We also provide a comparison between single-user systems having excess degrees of freedom (SU-EDoF) and multi-user diversity systems having no excess degrees of freedom (MuD-wo-EDoF). Both mechanisms attempt to improve received signal quality, as measured by the post-processing SINR. In SU-EDoF, a receiver does so by using excess receive antennas to obtain diversity and/or null one or more interfering co-channel streams on an optimal basis [27]. By contrast, MuD-wo-EDoF improves signal quality by scheduling the user with the best signal (and weakest interference), i.e., interference avoidance is an inherent feature. Since costs of RF chains, mobile size, device form factor and other practical considerations limit the number of antennas a receiver can have, multi-user diversity may be a more practical and cost-effective option. Studying the tradeoffs between SU-EDoF and MuD-wo-EDoF enriches our ability to make sound, well-founded engineering decisions, while designing practical systems that use these promising technologies.

Metric: For single-user scenarios, cell-wide average throughput per-user is typically used as a performance metric. For multi-user scenarios, wherein a channel is shared over many simultaneous users, a more appropriate metric is cell-wide average throughput *per-channel*. For the single-user case, 'channel' and 'user' are synonymous, and the metric continues to remain relevant[3]. We do not consider specific and precise metrics for fairness and stability. Even so, these considerations do enter our presentation, since they are prevalent in the literature. Essentially, when the throughput per-channel differences between the various scheduling algorithms are small, a sub-optimal scheduling algorithm may be used, trading a small throughput loss for greater 'fairness' or 'stability'.

8.2 The SISO/MEA Multi-User Diversity Simulation Platform

A system-level simulation platform has been developed for computing the throughputs of multiuser SISO/MEA cellular systems which employ network scheduling. The test-bed is sufficiently general to allow us to work with the several key system-level parameters noted earlier.

[3]The reader is cautioned against attempting conversion from the per-channel metric to an 'equivalent' per-user metric (e.g., by dividing the per-channel metric by the number of users). MuD leads to gains that are logarithmically proportional to the number of users. Since, the per-user metric normalizes this figure by the number of users, it will cast multi-user diversity in poor light. We take the view that such a conversion is inappropriate, since multi-user diversity applies only for *delay-elastic* applications. Users are willing to wait, and are scheduled only when a channel becomes available.

8.2.1 Network-Level Description: Base Station Viewpoint (MAC-layer)

Figure 8.1 shows a wireless system with a base station serving K downlink mobile stations. Each user MS tracks its individual channel from the BS, and sends a measure of the channel quality index (CQI) to the BS. The BS schedules any one user in a given time slot depending on the present CQI, past transmissions to all users, and fairness/latency requirements.

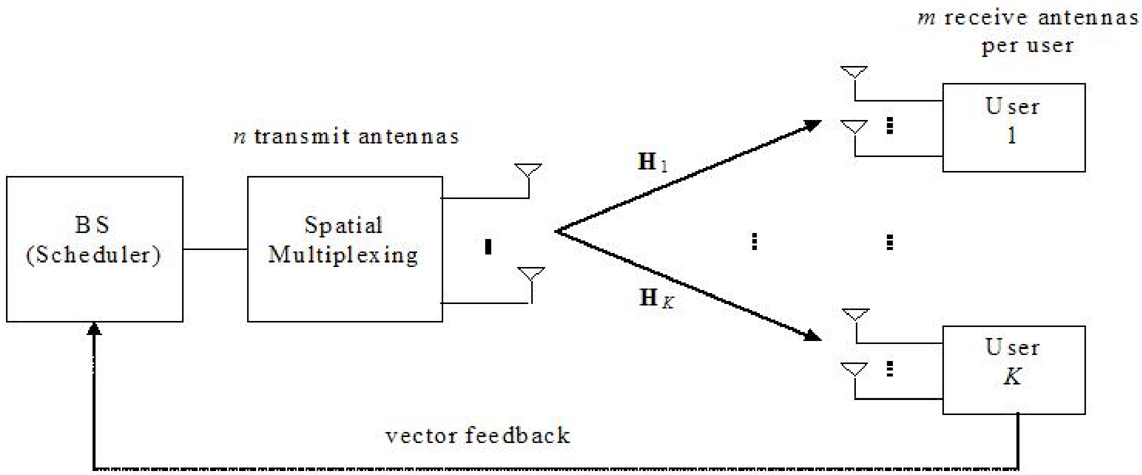

Figure 8.1: A multiuser scheduling system with n transmit antennas at the BS and m receive antennas at each MS. The scheduler can employ any user selection algorithm. In this study, the Greedy (MAX), Proportional Fair (PF) and the Equal Grade of Service (EGoS) schedulers are considered. (Figure taken from [3]).

In this study, substream-throughput is used as the (vector) CQI for that transmission interval[4]; Perfect and instantaneous feedback of the CQI from each MS to the BS is assumed. Users always have data to receive, and all transmissions are initiated at the start of the simulation (i.e., users cannot 'enter' or 'leave' a set of users being serviced by the BS). The three scheduling algorithms considered in this study are the Greedy (MAX), Proportional Fair (PF) and Equal Grade of Service (EGoS) algorithms.

Maximal Throughput Scheduling (MAX)

Schedules the user with maximum sum-CQI (SCQI) over all sub-streams. Thus,

$$k^*(t) = \arg\max_k \;\; SCQI(k,t) \qquad k = 1, 2, \cdots, K \tag{8.1}$$

[4]We note that, although a single scalar quantity such as the total link-capacity would suffice as CQI information for user scheduling, a vector CQI is needed for adaptive transmission reasons. See Section 8.3.

where $k^*(t)$ denotes the link selected at time t. MAX is optimum from a throughput standpoint in that no other algorithm can achieve more throughput. However, it ignores the past transmission history of all users, and hence, is unfair and biased in that aspect.

Equal Grade of Service Scheduling (EGoS)

Schedules that user who has been relatively starved throughput-wise over a time-window that extends to the indefinite past. Thus,

$$k^*(t) = \arg\min_k \sum_t TP(k,t) \qquad k = 1, 2, \cdots, K \tag{8.2}$$

EGoS can be considered to be the ultimate *throughput-fair* scheduler, since it allows each user to catch-up with other users, regardless of their channel conditions.

Proportional Fair Scheduling (PF)

All other schedulers will lead to performances that will be bracketed by the above two schedulers. We use the well-known PF scheduler [19, 67] as an example of one that attempts a better balance between throughput performance and fairness. Thus,

$$k^*(t) = \arg\max_k \frac{SCQI(k,t)}{\overline{TP}(k,t)} \qquad k = 1, 2, \cdots, K \tag{8.3}$$

where $\overline{TP}(k,t)$ is a measure of the mean throughput of link k over a window extending from t back to the indefinite past[5]. $\overline{TP}(k,t)$ is updated using an exponentially weighted IIR filter as

$$\overline{TP}(k,t+1) = \beta * \overline{TP}(k,t) + \delta(k^*,k) * SCQI(k,t) \tag{8.4}$$

where, δ is the Kronecker delta (sifting) operator, and β is the decay rate (or forgetting factor). We use $\beta = 0.98$ in the simulations, corresponding to an effective averaging window of 50 transmissions. This is a reasonable number permitting an accurate evaluation of the mean.

We note that Round-Robin (RR) is another plausible scheduler. RR is a fair scheduler from a service-time perspective. However, it is known that for users with i.i.d. fades, the benefit of mulituser diversity is lost when RR is employed [69]. On the other hand, it is also known that

[5] Our averaging formula for $\overline{TP}(k,t)$ is slightly different from the formula introduced in [19, 67].

Table 8.1: PARAMETER VALUES USED IN THE SYSTEM SIMULATIONS.

Cell Geometry	Hexagonal Array with side $R = 1000$ m
Carrier Frequency	$f_c = 2$ GHz
System Bandwidth	$W = 5$ MHz
Path Loss Exponent	$\Gamma = 3.7$
Shadow Fading	Lognormal, with Standard Deviation $\sigma = 8$ dB
Multipath Fading	Rician, with κ-factor = 0 (Rayleigh), 10, or a function of T-R distance (see Table 8.2)
Antenna Pattern	Omnidirectional or Uniform over 120°
Thermal Noise Density	$N_0 = -174$ dBm/Hz
Mobile Station's Noise Figure	$N_F = 8$ dB
Transmit Power	$P_T = 5$ W
Median Cell-Boundary SNR	$\rho = 20$ dB

Table 8.2: VARIATION OF RICIAN κ-FACTOR AS A FUNCTION OF BS-MS SEPARATION DISTANCE (PERCENTAGES SPECIFY THE DISTANCES RELATIVE TO THE CELL RADIUS).

Distance %	0-5	5-15	15-25	25-35	35-45	45-55	55-65	65-75	75-85	85-100
Rician κ	10	9	8	7	6	5	4	3	2	0

PF best balances between the conflicting tradeoffs thereby offering service-time fairness to all users (in the asymptotic sense), while optimizing user performance at the same time [19, 70].

8.2.2 Link-level Description: Mobile Station Viewpoint (PHY-layer)

While the simulation platform developed in this study is quite general with respect to system and channel parameters, most numerical results were obtained using the parameters detailed in Table 8.1. The various assumptions invoked in developing the platform are outlined here.

Channel Model

We consider three cases for Rician κ-factor, namely, $\kappa = 0$ (Rayleigh fading, i.e., only the scatter component); $\kappa = 10$ (dominant specular component); and κ a function of distance. The κ-factor typically decreases as the MS moves farther away from the BS, and the variation of κ with distance assumed here for the third case is given in Table 8.2.

The complex baseband channel gain between the jth transmit antenna of a given base station and the ith receive antenna of a given user-terminal is modeled by

$$h_{ij} = \sqrt{A\left(\frac{d_0}{d}\right)^{\Gamma} s}\left[\sqrt{\frac{\kappa}{\kappa+1}}e^{j\phi} + \sqrt{\frac{1}{\kappa+1}}z_{ij}\right] \tag{8.5}$$

where,

- d is the link length, Γ is the path loss exponent, and A is the median of the path gain at reference distance d_0 ($d_0 = 100$ m in the simulations).
- $s = 10^{S/10}$ is a log-normal shadow fading variable, where S is a zero-mean Gaussian random variable with standard deviation σ dB.
- κ is the Rician κ-factor for the given base-to-mobile path.
- $\phi = 2\pi d/\lambda$ is the phase shift of a line-of-sight (LOS) plane wave from the transmitter to the receiver. We assume that for a given transmit-receive pair, all LOS paths have the same length.
- z_{ij} represents the phasor sum of scattering components for the (i, j) path which are assumed to be zero-mean, unit-variance, i.i.d. complex Gaussian random variables.

We assume a base station height of $h = 30$ m above ground. For receivers located close to the ground, the direct path has a length $d = [r^2 + h^2]^{1/2}$, where r is the distance along the ground from the receiver to the base station. This implies that all Transmitter-Receiver (T-R) distances are 30 m or greater. A loss exponent of 2.0 (free space loss) is used for distances close to the base station ($30 - 100$ m), and 3.7 is used for distances beyond 100 m. Shadow fading is also applied regardless of the T-R distance. This has been shown to be an empirically reasonable model [25]. For antenna sectoring, perfect beams are assumed instead of shaped antenna patterns.

Simplifying System Assumptions

We invoke assumptions often made in conjunction with MEA systems [4, 8]: (i) narrowband signaling, (ii) quasi-static (block) fading, (iii) long burst interval, and (iv) independently faded complex Gaussian path gains. This permits a mathematical representation for the SISO/MEA cellular system[6] as follows

$$\mathbf{Y} = \mathbf{H}\mathbf{X} + \mathbf{Z} \tag{8.6}$$

where $\mathbf{X} \in \mathbb{C}^{7n}, \mathbf{Y} \in \mathbb{C}^{m}$, are transmit (serving and interfering) and receive signal vectors, $\mathbf{H} \in \mathbb{C}^{m \times 7n}$ is the channel gain matrix, and $\mathbf{Z} \in \mathbb{C}^{m}$ is a thermal noise vector, that is Gaussian distributed with zero-mean and one-sided power spectral density (PSD) N_0. Since the noise processes corrupting the different receive antennas are independent, $\mathbf{Z}$ has an autocorrelation matrix $N_0\mathbf{I}$, with $\mathbf{I}$ being the identity matrix.

Only one tier of interferers around the serving BS is assumed. This assumption is made to simplify the simulations and is slightly optimistic. However, the rapid decay of signal power with distance makes this assumption reasonable. Moreover, we offset it with the pessimistic assumption that all co-channel interferers are transmitting all the time. (In the single-cell case co-channel interferers are not present, and $\mathbf{H} \in \mathbb{C}^{m \times n}$).

An adaptive transmission algorithm is assumed that perfectly adapts the transmission on each transmit antenna (via the constellation size) according to the instantaneous radio channel and interference conditions. It is possible for different transmit antennas to choose different bit rates (constellation sizes), although all transmissions operate at the same symbol rate. The procedure to compute the optimum size of the transmit constellations appears in the Section 8.3.

Since cell-site (macro) diversity has been shown to have minimal impact on mean throughput calculations [1, 2], it is not used in the simulations, i.e., for simplicity, we assume that users communicate with the base station that is the nearest, and not necessarily the strongest. Finally, perfect channel estimation, T-R synchronization, and instantaneous feedback are also assumed. These simplifications focus the problem on the essential issues we wish to investigate.

---

[6]Following explanation offered in the Introduction, configurations employing Transmit Diversity are not considered. Hence, configurations that have more transmit than receive antennas ($n > m$) are excluded from this study.

Array Processing

Depending on the availability of channel state information (CSI) at the transmitter, it is possible to design transmit-adaptation (e.g. eigen-beamforming) and receive-adaptation (e.g., minimum mean-square error) array processing strategies. Since we assume CQI feedback, but not CSI feedback to the transmitter, only the receive-adaptation scheme is discussed here. The minimum mean-square error (MMSE) scheme uses uniform power allocation among the m transmit antennas. To analyze MMSE reception, the analyst takes into account the path gains from all BSs, both serving and interfering, within the channel gain matrix ($\mathbf{H} \in \mathbb{C}^{m\times 7n}$). Received data streams are separated by computing a linear combination of the received signals using a set of weights that achieves the minimum mean-square error between the output estimate and the true signal sample. Thus, we have that

$$\hat{\mathbf{X}} = \mathbf{W}^H \mathbf{Y}. \tag{8.7}$$

The performance index for a given weight matrix is

$$\zeta(\mathbf{W}^H) \triangleq E\left[\sum_{j=1}^{n} |\epsilon_j|^2\right] = E\left[\sum_{j=1}^{n} |x_j - \hat{x}_j|^2\right] \tag{8.8}$$

where x_j is the jth transmitted signal. The expectation in (8.8) is taken with respect to the noise and the statistics of the data sequences. The weight matrix $\mathbf{W}$ that yields the minimum mean-square error is [2]

$$\mathbf{W} = \mathbf{A}^{-\mathbf{1}}\mathbf{H}, \tag{8.9a}$$

$$\mathbf{A} = \mathbf{H}\mathbf{H}^H + \frac{\sigma^2}{P/n}\mathbf{I}_{m\times m}. \tag{8.9b}$$

The post-processing SINR on the jth decoded stream can be shown to be [2, 24]

$$\gamma_j = (\mathbf{H})_j^H \mathbf{R}_j^{-1} (\mathbf{H})_j, \;\; j = 1, 2, \ldots, n \tag{8.10}$$

where

$$\mathbf{R}_j = \sum_{l=1,\, l\neq j}^{7n} (\mathbf{H})_l (\mathbf{H})_l^H + \frac{\sigma^2}{P/n}\mathbf{I}_{m\times m} \tag{8.11}$$

and $(\mathbf{H})_j$ is the jth column of $\mathbf{H}$. For the noise-only (single-cell) case, the summation will have n terms, instead of $7n$.

Link Throughput Bounds

The *instantaneous* per-user data throughput is the sum of the instantaneous throughputs of the sub-streams. The throughput T_j of sub-stream j is determined for the following two extreme cases.

Ideally Coded Signals: The throughput is upper-bounded by the Shannon capacity

$$T_j = \log_2 (1 + \gamma_j) . \tag{8.12}$$

Uncoded Signals: Assuming error detection in each block, the throughput is

$$T_j(M_j) = (1 - BLER_j) \log_2(M_j) = (1 - BER_j)^L \log_2(M_j) \tag{8.13}$$

where $\log_2(M_j)$ is the number of bits per symbol in stream j, and BLER is the corresponding block error rate for L-bit blocks. In this study $L = 500$ bits is assumed, though the results are robust for values of L over a wide practical range [2].

We wish to simplify (8.13) to the form of (8.12) for convenience of calculation. Under the simplifying assumption that the channel undergoes quasi-static block fading, it is possible to regard the channel as *AWGN conditioned on the instantaneous path gains*. For QAM modulation, we can then use the procedure in [1, 2, 38] to obtain the form

$$T_j = \max\ T_j(M_j) \approx \log_2 \left(1 + \frac{\gamma_j}{6.4}\right) . \tag{8.14}$$

Thus, the curve for uncoded transmission is 8 dB ($= 10 \log_{10}(6.4)$) shifted from the curve for perfectly-coded (Shannon) transmission. A variety of practical coding strategies can then be modeled by using other shifts less than 8 dB [29].

8.3 Simulation Methodology

The intention in this study is to compute throughput statistics of several SISO/MIMO configurations in a multi-user scenario (employing network diversity scheduling) for various design options. Highlights of the steps involved are as follows:

(1) Distribute K MSs in a cell (uniform random uncorrelated locations) and generate channel matrices $\mathbf{H_1}, \cdots, \mathbf{H_K}$ as given by (8.5).

(2) For each user k, compute the post-processing SINR for each substream j, assuming MMSE reception ((8.10)-(8.11)).

(3) For each user k, compute the throughput for each substream j ((8.12), (8.14)). This is the vector CQI for user k.

(4) For each user k, compute $SCQI = \sum_{substreams} CQI$.

(5) Schedule user $k^*(t)$ (Equations (8.1), (8.2), (8.3)), and update his cumulative throughput $(\sum_t TP(k^*, t))$.

(6) Update the averages ((8.4)) of all users.

(7) Compute the average cell-wide multi-user throughput over 500 locations (each with log-normal shadow fading) and 1000 multipath fades per location.

This computation leads to *instantaneous* throughputs, for given values of MS location (path loss), shadow fading, and instantaneous channel fades from serving and interfering BSs. Averaging over all these, results in the cell-wide mean throughput per channel. For the purpose of averaging throughput over a cell, we conduct 500 trials in a simulation. In any given trial, K users are distributed at random locations uniformly over the cell/sector. A given trial assigns a location, shadow-fade combination to each user, and user locations are uncorrelated. In each trial, users experience 1000 different multipath fades[7]. Thus, there are $500,000$ quasi-static-block-fade transmission intervals in all. In this study, we consider both limited and unlimited constellation sizes. For the limited constellation case, modulation constellation sizes up to 16-QAM (leading to a symbol rate of up to 4 bits/symbol) are considered. This maximum is practical for present-day cellular implementations[8].

At the beginning of each block-fade interval, pilot signals are transmitted to estimate the receiver array weights. The receiver then determines the constellation size (M) from the substream post-processing SINRs, and communicates this information to the transmitter. Based on CQI, past transmission history, delay/latency constraints and the particular scheduling algorithm in use, a particular user is selected for transmission. Adaptive modulations at each

[7]Since Rayleigh fading has significant density at the tail, 1000 realizations are needed for statistical stability.

[8]The state-of-art is 16-QAM for mobile wireless systems and 64-QAM for fixed wireless systems.

transmit antenna then quickly select the corresponding optimal QAM constellation. The channel remains known throughout, since estimation-feedback-adaptation occurs within the block fade interval. By assumption, we exclude all overheads (pilot signaling, channel estimation at receiver, feedback and signal-adaptation) from the throughput computation procedure.

8.4 Numerical Results

Figures 8.2–8.5 show the cell-wide average throughputs that are offered by MMSE systems for the many dimensions we considered. We show only a representative listing, instead of presenting throughputs over all dimensions, to keep the presentation useful and concise[9]. Our initial presentation refers to the case of a Rician κ-factor of $\kappa = 0$ and omni-directional antennas. Any deviations considered from this baseline case appearing in subsequent paragraphs will be carefully highlighted.

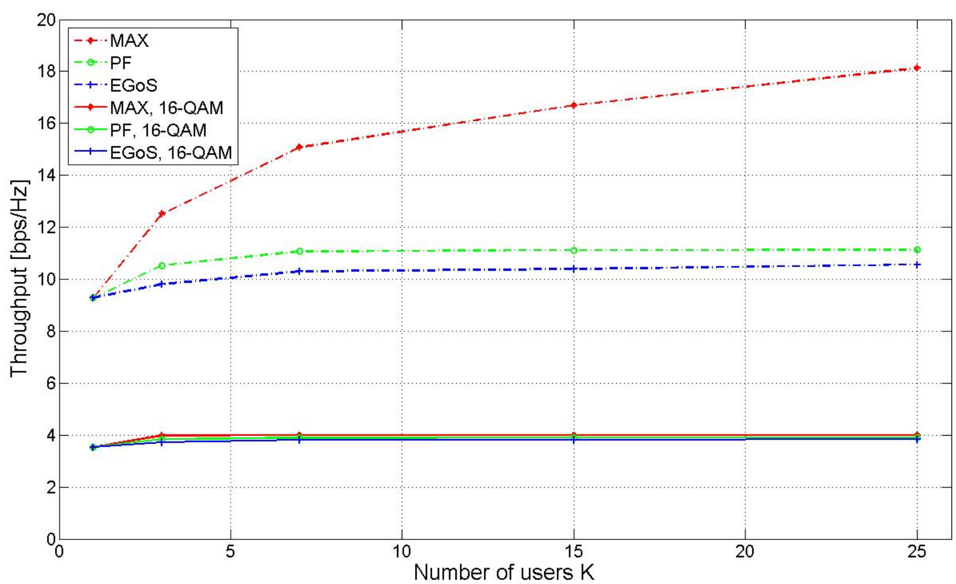

Figure 8.2: Mean throughput as a function of number of users for the $(1,1)$ system, single-cell environment, $\kappa = 0$, and omni-directional antennas. Throughputs are plotted for all three scheduling algorithms, for both unlimited constellation (with ideal coding) and limited constellation size (16-QAM).

[9]A comprehensive set of result data appears in the Tables in Section 8.7

Effect of Number of Users and Scheduling Algorithm: It is known that at the link-level, multi-user diversity with network scheduling leads to gains that grow as $O(\log K)$. Referring to Figs. 8.2–8.5, we see that this is also the case for system-level simulations for unlimited constellation sizes (although the scalar multipliers, and lower order terms, are different for different scheduling algorithms).

It is clear that MAX leads to higher gains with increasing K, while EGoS leads to limited gains. In some cases (the multicell scenarios), EGoS leads to throughput *loss* rather than gain. This is readily explained by the fact that EGoS is a "poor man's" scheduling algorithm. It penalizes users with better channels to allow users with poor channels to catch up. This leads to a situation in which users with weak channels determine the overall scheduler performance.

The PF scheduler, in contrast to the EGoS scheduler, always leads to gains with increasing number of users. It is also evident from the figures 8.2–8.5 that PF with $\beta = 0.98$ leads to curves parallel to those for EGoS in the mid-to-high region of K. Different values of β can lead to a range of 'tunable' PF schedulers, although, $0.90 \leq \beta < 1.00$ is a practical range[10].

As explained earlier, MAX leads to very good gains as compared to EGoS and PF. However, it is a biased/greedy algorithm, which may not serve well for environments having quality of service (QoS) requirements. EGoS attempts throughput fairness, while PF attempts to strike a balance between cell-wide throughput and fairness. However, as will be seen shortly, EGoS can also be useful under practical circumstances.

Effect of Co-Channel Interference: In the single-cell scenario, multi-user diversity improves the signal (channel) quality, while in the multi-cell case, it has room to perform an additional function: that of interference avoidance [19]. This means that better gains can be expected with increasing K for the multi-cell case. This is indeed so, as evidenced by a comparison between Fig's. 8.2 and 8.3 or 8.4 and 8.5. Notice that the ratio of throughputs for $K = 25$ and $K = 1$ is greater for the multi-cell case.

SINRs in the single-cell case (20 dB to 60 dB) are much higher than those in the multi-cell case (-5 dB to 25 dB), leading to correspondingly lower throughputs for the latter. MAX and

---

[10]With $0.90 \leq \beta < 1.00$, the effective averaging window is 10 transmissions or greater, which is sufficient for averaging purposes. For $\beta < 0.90$, exponential averaging will have an extremely short memory.

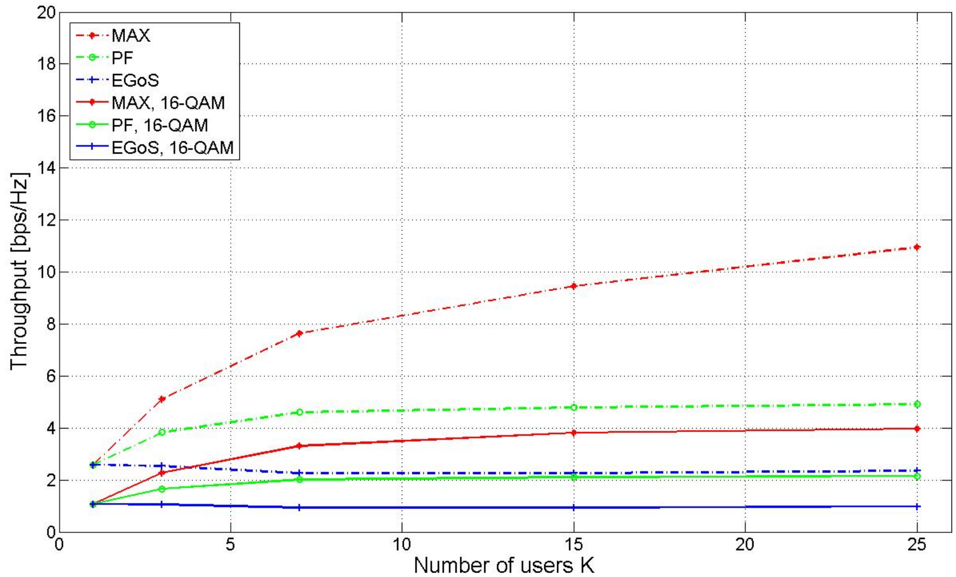

Figure 8.3: Mean throughput as a function of number of users for the $(1, 1)$ system, multi-cell environment, $\kappa = 0$, and omni-directional antennas. Throughputs are plotted for all three scheduling algorithms, for both unlimited constellation (with ideal coding) and limited constellation size (16-QAM).

EGoS curves display more or less similar trends for the single and multi-cell cases, except that PF yields better gains (the PF curve moves away from EGoS, closer to the MAX curve) for the multi-cell case.

Effect of Degrees of Freedom: In a $(1, 1)$ system, multi-user diversity improves the operating SINR. In a $(3, 3)$ system, multi-user diversity improves both the operating SINR, as well as the available degrees of freedom of the system. In other words, the entire channel subspace structure (the number, as well as values of the eigen-space) is improved [20].

Note that neither the SISO (1, 1), nor the MIMO (3, 3) system have excess degrees of freedom. It is clear that, although we see a substantial increase in mean throughput for the MIMO (3, 3) system as compared to the SISO (1, 1) system, we cannot expect the increase to be three-fold, despite the creation of three parallel de-coupled streams at the receiver. This is because the available degrees of freedom (receive antennas) are used to combat cross-stream interference (XSI), even at the cost of noise enhancement. Also, each transmit antenna in the (3, 3) system now uses only $1/3$ the total transmit power as compared to the SISO system.

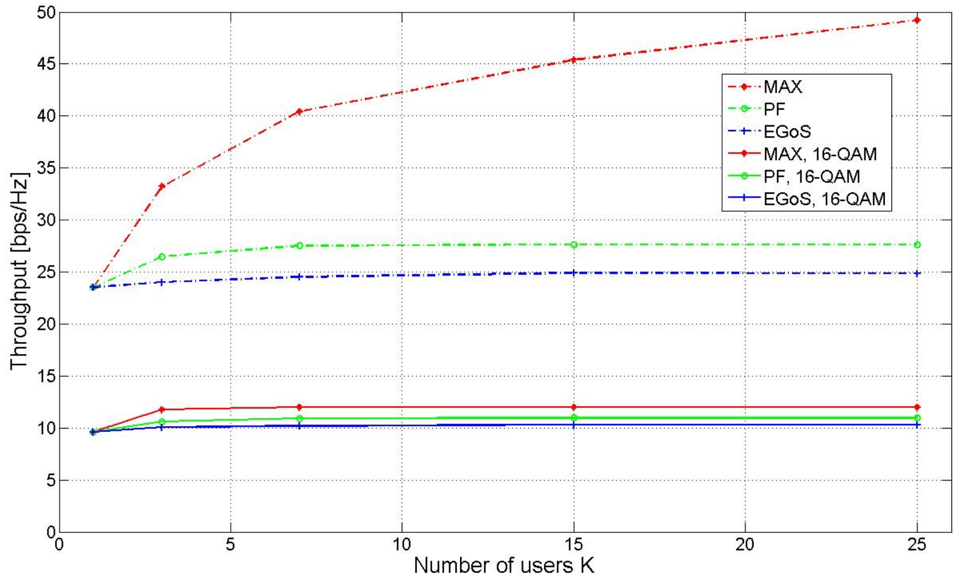

Figure 8.4: Mean throughput as a function of number of users for the $(3, 3)$ system, single-cell environment, $\kappa = 0$, and omni-directional antennas. Throughputs are plotted for all three scheduling algorithms, for both unlimited constellation (with ideal coding) and limited constellation size (16-QAM). (Note the change in the vertical scale relative to Figures 8.2 and 8.3).

Similar trends are seen for both single and multi-cell cases. Note the change in scale of the y-axis for the $(3, 3)$ configuration in Figs. 8.4 and 8.5 as compared to the $(1, 1)$ configuration shown in Figs. 8.2 and 8.3.

Effect of Antenna Sectorization: Antenna sectorization is an interference suppression technique. Co-channel interference is reduced by using antenna beam patterns and frequency coloring [15, 16]. In contrast, multi-user diversity is an interference avoidance technique, which also improves channel subspace structure (by avoiding ill-conditioned channels). Since antenna sectorization cannot improve channel structure, it is clear that multi-user diversity is the superior technique, particularly for a system with many users. Antenna sectorization and multi-user diversity can be used in conjunction, since their goals are not necessarily conflicting. It stands to reason that as the number of users increases, the combined gain will have diminishing benefit with multi-user diversity playing an increasingly major role.

Using sectorized antennas and a reuse factor of 1 leads to about a two-fold improvement in link throughput over the results for omni-directional antennas for the single-user case ($K = 1$).

This is consistent with results from conventional systems (using three-sector antennas enables cellular system planners to bring down the reuse factor from 12 to 7, which amounts to a similar throughput increase [16, Ch. 3]). As the number of users is increased, the benefit due to antenna sectorization gradually decreases for all three schedulers, as was expected. As a percentage, sectorization leads to far more improvement in EGoS performance as compared to MAX and PF (compare Figs. 8.6 and 8.7 with Fig 8.5).

Effect of Rician κ-Factor: It is known that, in the presence of a strong specular component ($\kappa \sim 10$) the mean throughput of SISO $(1,1)$ systems increases, whereas that of MIMO $(3,3)$ systems decreases [1, 4, 13, 38]. Adding users and scheduling algorithms results in the following changes: Mean throughput for the $(1,1)$ system increases slightly ($\sim 3\%$) for the MAX scheduler, decreases slightly ($\sim 5\%$) for PF, and decreases moderately ($\sim 9\%$) for EGoS, over all K. Similar trends hold for the single and multi-cell cases.

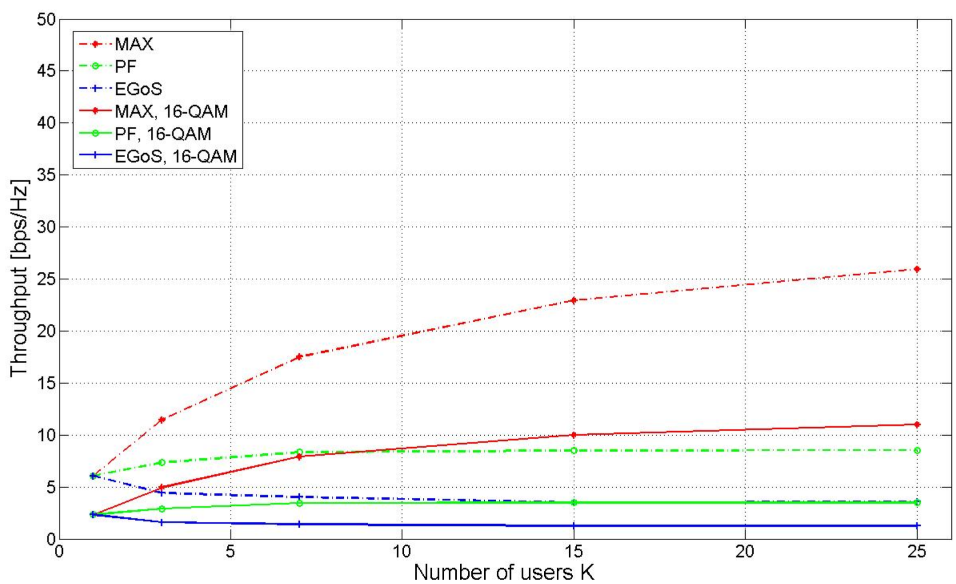

Figure 8.5: Mean throughput as a function of number of users for the $(3,3)$ system, multi-cell environment, $\kappa = 0$, and omni-directional antennas. Throughputs are plotted for all three scheduling algorithms, for both unlimited constellation (with ideal coding) and limited constellation size (16-QAM). (Note the change in the vertical scale relative to Figures 8.2 and 8.3).

For the MIMO $(3,3)$ system, going from $\kappa = 0$ to $\kappa = 10$ leads to a substantial decrease in capacity [1, 4, 13, 38]. However, as the number of users is increased, the losses are reduced.

This can be explained by the inherent property of multi-user diversity to choose the relatively best channel. Loss reduction with increasing number of system users is the highest in MAX, followed in order by the PF and EGoS schedulers.

Assuming Rician fading with κ-factor a function of distance (Table 8.2) leads to values that are bracketed by $\kappa = 0$ and $\kappa = 10$, with mean throughput values closer to those obtained using $\kappa = 10$.

Effect of Coding: For SISO $(1, 1)$ and MIMO $(3, 3)$ systems with $K = 1$, the reduction in throughput for uncoded signals relative to Shannon coded signals is about 20% for the single-cell case, and about 40 to 50% for the multi-cell case [38]. As the number of users is increased, we experience a decrease in the throughput loss for uncoded transmission. Throughput loss is about 15% for the MAX scheduler, 22% for PF and 25% for EGoS for the single-cell case at $K = 25$. For the multi-cell case, the losses are about 25%, 45% and 50%, respectively. Thus, there is an improvement for the MAX scheduler, but no improvement for the PF and EGoS schedulers in the multi-cell case. Similar trends are observed for the MIMO $(3, 3)$ system.

This can be explained as follows: Loss due to uncoded transmission depends on the operating SINR. For the single-cell case, the operating SINR is high, hence the throughput loss is comparatively low, and comparable percentage losses are recorded by all three schedulers. On the other hand, operating SINRs are significantly lower for the multi-cell case, hence throughput losses are higher. Multi-user diversity has the inherent property of seeking users with good SINRs; however, this applies to the MAX scheduler more than to the PF and EGoS schedulers. Depending on past transmission history, PF and EGoS schedulers may not be able to choose the best user. Hence, they lead to correspondingly less improvement. For sectorization, SINRs, and hence losses observed, will be bracketed by the single-cell and multi-cell cases.

Effect of Limited Constellation Sizes: Whereas unlimited constellation size provides insight to the potentially achievable throughputs the system can offer, it is also necessary to look into throughputs that practical systems can actually realize. Figures 8.2–8.5 give some illustrative results. Limiting the transmit alphabet size to 16-QAM amounts to capping throughput at $4n$ bps/Hz. The effect is to reduce the potential benefit from increasing number of users in the system, particular choice of scheduling algorithm, and antenna sectorization.

Compared to the case of unlimited constellation sizes, there is a substantial throughput loss for both $(1,1)$ and $(3,3)$ systems. Throughput saturation (due to constellation size capping) is almost immediate ($K = 3$) for the single-cell case. For the multi-cell case, throughput leveling occurs at $K = 7$ for PF and EGoS, and the differences between the throughputs offered by the scheduling algorithms are substantially reduced.

Since throughput per-cell differences between the various schedulers are negligible for the single-cell case, and significantly reduced even for the multi-cell case, it becomes reasonable to view these findings through the prism of other metrics. In this context, we note the following: EGoS can be more suitable than MAX and PF for the single-cell case since it is the ultimate throughput-fair scheduler; MAX may be unsuitable since it is biased, while PF may be unsuitable since it is *not* stable[11] [71]. For the multi-cell case, PF may be a more suitable scheduler than MAX, depending on QoS requirements. This observation has important implications for current state-of-the-art systems that can support signal constellations up to 16-QAM.

8.5 Multi-User Diversity Systems with No Excess Degrees of Freedom vs. Single-user Systems with Excess Degrees of Freedom

A brief comparison is now provided between single-user systems employing excess degrees of freedom (SU-EDoF), and multi-user diversity systems having no excess degrees of freedom (MuD-wo-EDoF). Both mechanisms attempt to improve received signal quality, as measured by the post-processing SINR, and use of one technique does not preclude using the other (i.e., it is possible to combine multi-user diversity with excess degrees of freedom (MuD-EDoF)).

In SU-EDoF, a receiver uses excess antennas ($n > m$) achieving diversity to combat fading, or to suppress one or more co-channel interference streams, or a combination of both [27]. SU-EDoF is a *radio-layer* technique, and can be used for all application types (delay-elastic, as in data applications, or delay-intolerant as in voice applications). In contrast, multi-user diversity schedules the user with the best signal quality, i.e., interference avoidance is inherently

[11] A stable algorithm always results in bounded queue lengths under any conceivable traffic scenario.

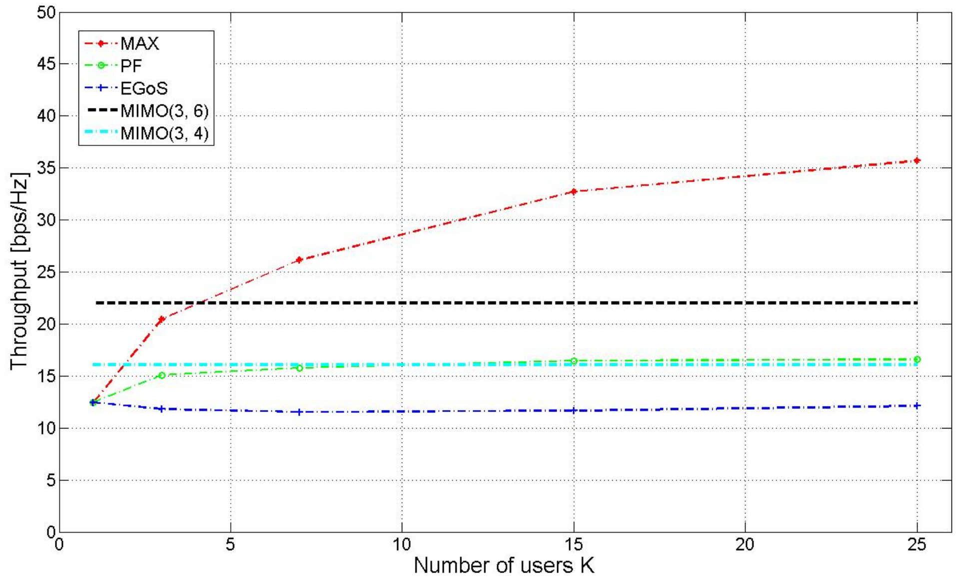

Figure 8.6: Mean throughput as a function of number of users for the $(3, 3)$ system, with unlimited constellation sizes and ideal coding, multi-cell environment, $\kappa = 0$, and sectorized antennas. Throughputs for all three scheduling algorithms are plotted. The upper horizontal line is for the single-user MIMO $(3, 6)$ system (no multi-user diversity), while the lower horizontal line is for the single-user MIMO $(3, 4)$ system

.

achieved. However, multi-user diversity (both MuD-EDoF and MuD-wo-EDoF) is applicable only to delay-elastic applications, wherein the scheduler selects one user for transmission. Viewed from this perspective, multi-user diversity may be considered as a *cross-layer technique* in which the radio (PHY)-layer continually educates the medium access control (MAC)-layer. Since multi-user diversity is able to improve the channel subspace structure (by avoiding ill-conditioned channels), a capability which SU-EDoF does not have, it can be the superior technique, particularly in a system having many users.

We now explain how MuD-wo-EDoF may be used in lieu of SU-EDoF, thereby leading to a reduction in the number of receive antennas, while offering comparable or greater throughput[12]. We have seen previously that EGoS leads to small gains for the single-cell scenario and moderate loss for the multi-cell scenario as a function of number of users K. Hence, EGoS cannot be used as a scheduler in MuD-wo-EDoF to compete against SU-EDoF. Similarly, we

[12]Since there is a reduction in the number of receive antennas, there is considerable impact, since it affects all mobiles.

have seen that the PF scheduler has curves that are nearly parallel to those of EGoS with higher multi-user diversity gains. This implies that the PF scheduler can be used with MuD-wo-EDoF to compete against SU-EDoF wherein the excess degrees of freedom in SU-EDoF are few (e.g. one). When excess degrees of freedom in SU-EDoF are many, e.g. MIMO $(3, 6)$, the MAX scheduler should be used.

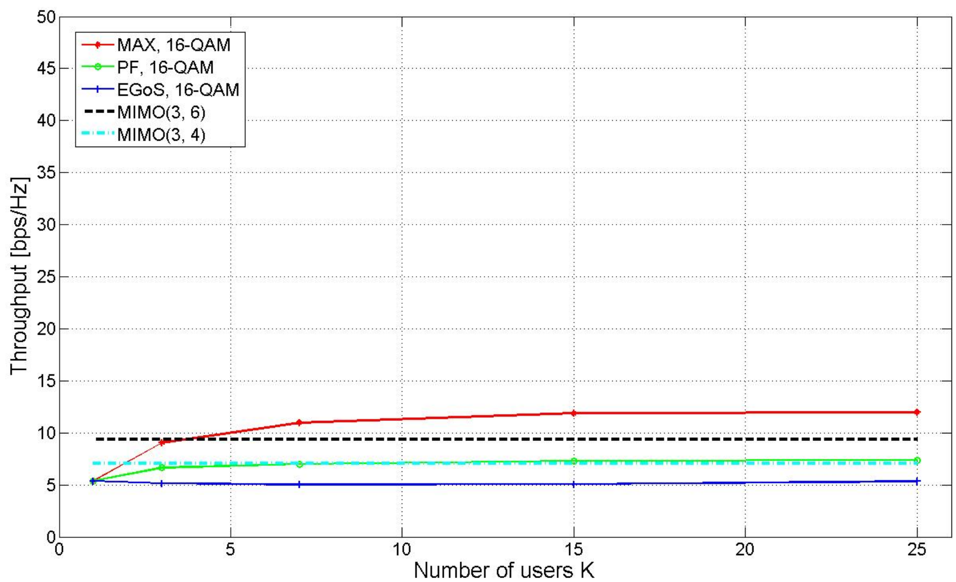

Figure 8.7: Mean throughput as a function of number of users for the $(3, 3)$ system, with limited constellation size (16-QAM), multi-cell environment, $\kappa = 0$, and sectorized antennas. Throughputs for all three scheduling algorithms are plotted. The upper horizontal line is for the single-user MIMO $(3, 6)$ system (no multi-user diversity), while the lower horizontal line is for the single-user MIMO $(3, 4)$ system.

Figure 8.6 illustrates a representative example, where the upper horizontal line indicates the performance of the single-user MIMO $(3, 6)$ system, and the lower horizontal line indicates the performance of the single-user MIMO $(3, 4)$ system. These systems are able to suppress up to 3 and 1 interfering streams, respectively. We see that a MuD-wo-EDoF system incorporating the MAX scheduler, with 2 or more users can offer equal or better performance than the single-user MIMO $(3, 4)$ system, while 4 or more users are needed to achieve performance equal to or better than that for single-user MIMO $(3, 6)$. With a MuD-wo-EDoF system incorporating a PF scheduler, 10 or more users are needed to compete with a single-user MIMO $(3, 4)$ system. A PF-based MuD-wo-EDoF system cannot compete with a single-user MIMO $(3, 6)$ system, no matter how large K is.

The above comparisons hold even for the case of limited constellation sizes, as seen in Fig. 8.7. In this case, however, the differences, in terms of design choices and their consequences, are markedly reduced.

8.6 Conclusion

The throughput performance of SISO and MIMO-based cellular systems have been evaluated which employ multi-user diversity over several useful system-level design dimensions. By evaluating the performance of two extreme schedulers (MAX, EGoS), we have been able to obtain a perspective on the performances realized by a variety of useful schedulers. The PF scheduler was also considered as a representative and widely popular example. The chief observation is that, although the various dimensions are important considerations for SISO and MEA systems, the potential benefits need to be weighed in the context of limited signal constellations that are prevalent in present day practical systems. Since per-channel throughput differences were negligible for the single-cell case, and dramatically reduced for the multi-cell case, other metrics (fairness and stability) were employed to get another perspective on the findings. There, EGoS was deemed a reasonable choice for the single-cell case, and PF was deemed reasonable in multi-cell scenarios when delay tolerance was allowed.

We also compared single-user MIMO systems that use excess degrees of freedom (SU-EDoF) and those that use multi-user diversity without excess degrees of freedom (MuD-wo-EDoF). Here, among scheduler choices, it is clear that EGoS is not a viable candidate; that PF has limitations in the number of excess receive antennas it can compete against in SU-EDoF based systems; and, that MAX is the best option in terms of cell-wide throughput.

In general, for applications that are delay-tolerant, a MuD-wo-EDoF system with a large number of users can deliver substantially higher throughputs than SU-EDoF links. This is especially the case when using SU-EDoF with only one extra antenna, but applies even to the case of up to three. Finally, the amount of improvement using MuD-wo-EDoF instead of SU-EDoF decreases with increasing limits on constellation size.

8.7 Tabular Results for Multi-User Diversity Study

Per-link cell-wide average throughputs (in units of bps/Hz) of multi-user MIMO $(1, 1)$ links employing MMSE receivers, for Rayleigh fading ($K = 0$), in a single-cell environment. The simulation results are for the various schedulers (MAX, PF, EGoS), and number of users.

	MAX	PF	EGoS
3	12.5243	10.5347	9.8107
7	15.0832	11.0638	10.3017
15	16.7017	11.1100	10.3867
25	18.1247	11.1330	10.5554

Table 8.3: Infinite-QAM with Shannon coding.

	MAX	PF	EGoS
3	9.8561	7.8995	7.2082
7	12.4063	8.4163	7.6747
15	14.0240	8.4614	7.7629
25	15.4467	8.4838	7.9218

Table 8.4: Infinite-QAM with no coding.

	MAX	PF	EGoS
3	3.9808	3.8481	3.7272
7	4.0000	3.8944	3.8155
15	4.0000	3.9050	3.8138
25	4.0000	3.9048	3.8465

Table 8.5: 16-QAM with no coding.

Per-link cell-wide average throughputs (in units of bps/Hz) of multi-user MIMO $(1, 1)$ links employing MMSE receivers, for Rayleigh fading ($K = 0$), in a multi-cell environment. The simulation results are for the various schedulers (MAX, PF, EGoS), and number of users.

	MAX	PF	EGoS
3	5.1120	3.8264	2.5370
7	7.6358	4.6025	2.2699
15	9.4550	4.7908	2.2608
25	10.9410	4.9077	2.3533

	MAX	PF	EGoS
3	8.8171	7.1841	5.9869
7	10.9068	7.7816	6.3262
15	12.9696	8.2279	6.7114
25	14.1837	8.3298	7.0611

Table 8.6: Infinite-QAM with Shannon coding. (Left - Omni antenna, Right - Sectorized antenna)

	MAX	PF	EGoS
3	3.0205	2.0914	1.2520
7	5.1294	2.6454	1.0835
15	6.8269	2.7795	1.1006
25	8.2805	2.8653	1.1666

	MAX	PF	EGoS
3	6.2409	4.7615	3.7628
7	8.2491	5.2790	4.0404
15	10.2957	5.6992	4.4040
25	11.5072	5.7886	4.6958

Table 8.7: Infinite-QAM with no coding. (Left - Omni antenna, Right - Sectorized antenna)

	MAX	PF	EGoS
3	2.2736	1.6584	1.0488
7	3.3035	2.0039	0.9284
15	3.8142	2.1038	0.9300
25	3.9661	2.1563	0.9790

	MAX	PF	EGoS
3	3.5962	3.0906	2.6308
7	3.9499	3.3386	2.7933
15	3.9992	3.4415	2.8989
25	4.0000	3.4795	3.0393

Table 8.8: 16-QAM with no coding. (Left - Omni antenna, Right - Sectorized antenna)

Per-link cell-wide average throughputs (in units of bps/Hz) of multi-user MIMO $(1, 1)$ links employing MMSE receivers, for Rician fading ($K = 10$), in a single-cell environment. The simulation results are for the various schedulers (MAX, PF, EGoS), and number of users.

	MAX	PF	EGoS
3	12.9220	10.4118	9.6339
7	15.3850	10.3747	9.7537
15	16.9475	10.4698	9.6173
25	18.3777	10.4685	9.6967

Table 8.9: Infinite-QAM with Shannon coding.

	MAX	PF	EGoS
3	10.2501	7.7821	7.0336
7	12.7078	7.7439	7.1413
15	14.2697	7.8346	7.0178
25	15.6997	7.8335	7.0886

Table 8.10: Infinite-QAM with no coding.

	MAX	PF	EGoS
3	3.9924	3.8259	3.7150
7	4.0000	3.8301	3.7532
15	4.0000	3.8498	3.7229
25	4.0000	3.8485	3.7440

Table 8.11: 16-QAM with no coding.

Per-link cell-wide average throughputs (in units of bps/Hz) of multi-user MIMO $(1, 1)$ links employing MMSE receivers, for Rician fading ($K = 10$), in a multi-cell environment. The simulation results are for the various schedulers (MAX, PF, EGoS), and number of users.

	MAX	PF	EGoS
3	5.3986	3.8253	2.2804
7	7.5707	4.3937	2.1905
15	9.9118	4.4738	2.0857
25	11.2199	4.5505	2.0425

	MAX	PF	EGoS
3	9.2286	7.2445	6.0652
7	11.2131	7.6136	6.1948
15	13.2223	7.9393	6.4402
25	14.3977	8.0044	6.7198

Table 8.12: Infinite-QAM with Shannon coding. (Left - Omni antenna, Right - Sectorized antenna)

	MAX	PF	EGoS
3	3.2562	2.0862	1.0786
7	5.0496	2.4928	1.0260
15	7.2716	2.5433	0.9918
25	8.5556	2.5942	0.9728

	MAX	PF	EGoS
3	6.6193	4.8087	3.8159
7	8.5502	5.1235	3.9181
15	10.5475	5.4304	4.1607
25	11.7209	5.4841	4.3865

Table 8.13: Infinite-QAM with no coding. (Left - Omni antenna, Right - Sectorized antenna)

	MAX	PF	EGoS
3	2.3800	1.6580	0.9246
7	3.3611	1.9039	0.8872
15	3.8751	1.9560	0.8426
25	3.9804	1.9884	0.8309

	MAX	PF	EGoS
3	3.7224	3.1354	2.6780
7	3.9722	3.2956	2.7548
15	3.9998	3.3718	2.8154
25	4.0000	3.4021	2.9387

Table 8.14: 16-QAM with no coding. (Left - Omni antenna, Right - Sectorized antenna)

Per-link cell-wide average throughputs (in units of bps/Hz) of multi-user MIMO $(1, 1)$ links employing MMSE receivers, for Rician fading (K is a function of the distance from the base station), in a single-cell environment. The simulation results are for the various schedulers (MAX, PF, EGoS), and number of users.

	MAX	PF	EGoS
3	12.8936	10.5914	9.9214
7	15.3664	10.7662	10.0074
15	17.0448	10.7781	10.0851
25	18.3703	10.8015	10.1281

Table 8.15: Infinite-QAM with Shannon coding.

	MAX	PF	EGoS
3	10.2227	7.9560	7.3085
7	12.6893	8.1222	7.3874
15	14.3669	8.1328	7.4632
25	15.6923	8.1570	7.5046

Table 8.16: Infinite-QAM with no coding.

	MAX	PF	EGoS
3	3.9911	3.8523	3.7613
7	4.0000	3.8843	3.7903
15	4.0000	3.8933	3.8079
25	4.0000	3.8879	3.8054

Table 8.17: 16-QAM with no coding.

Per-link cell-wide average throughputs (in units of bps/Hz) of multi-user MIMO $(1, 1)$ links employing MMSE receivers, for Rician fading (K is a function of the distance from the base station), in a multi-cell environment. The simulation results are for the various schedulers (MAX, PF, EGoS), and number of users.

	MAX	PF	EGoS
3	5.2277	3.7997	2.4478
7	7.8159	4.4168	2.2565
15	9.9693	4.6262	2.2535
25	10.9626	4.6875	2.1971

	MAX	PF	EGoS
3	8.8995	7.0850	5.8702
7	11.4118	7.8444	6.3168
15	13.2617	8.1325	6.7224
25	14.4375	8.1558	6.8418

Table 8.18: Infinite-QAM with Shannon coding. (Left - Omni antenna, Right - Sectorized antenna)

	MAX	PF	EGoS
3	3.1212	2.0633	1.1741
7	5.2911	2.4945	1.0701
15	7.3309	2.6424	1.0829
25	8.3012	2.6903	1.0596

	MAX	PF	EGoS
3	6.3147	4.6730	3.6671
7	8.7471	5.3453	4.0479
15	10.5867	5.6038	4.3938
25	11.7607	5.6266	4.5053

Table 8.19: Infinite-QAM with no coding. (Left - Omni antenna, Right - Sectorized antenna)

	MAX	PF	EGoS
3	2.2788	1.6245	1.0046
7	3.3928	1.9336	0.9180
15	3.8630	2.0369	0.9215
25	3.9680	2.0654	0.9041

	MAX	PF	EGoS
3	3.6458	3.0893	2.6087
7	3.9768	3.3392	2.7654
15	3.9997	3.4374	2.9381
25	4.0000	3.4381	2.9673

Table 8.20: 16-QAM with no coding. (Left - Omni antenna, Right - Sectorized antenna)

Per-link cell-wide average throughputs (in units of bps/Hz) of multi-user MIMO $(3, 3)$ links employing MMSE receivers, for Rayleigh fading ($K = 0$), in a single-cell environment. The simulation results are for the various schedulers (MAX, PF, EGoS), and number of users.

	MAX	PF	EGoS
3	33.2376	26.4754	24.0030
7	40.4361	27.5199	24.5161
15	45.3951	27.6345	24.8889
25	49.2249	27.6551	24.8752

Table 8.21: Infinite-QAM with Shannon coding.

	MAX	PF	EGoS
3	25.2800	18.8153	16.4881
7	32.4152	19.7647	16.9876
15	37.3641	19.8723	17.3020
25	41.1920	19.8945	17.3133

Table 8.22: Infinite-QAM with no coding.

	MAX	PF	EGoS
3	11.7667	10.6058	10.0901
7	11.9923	10.9310	10.1771
15	11.9999	10.9562	10.3230
25	12.0000	10.9457	10.3223

Table 8.23: 16-QAM with no coding.

Per-link cell-wide average throughputs (in units of bps/Hz) of multi-user MIMO $(3, 3)$ links employing MMSE receivers, for Rayleigh fading ($K = 0$), in a multi-cell environment. The simulation results are for the various schedulers (MAX, PF, EGoS), and number of users.

	MAX	PF	EGoS
3	11.4456	7.3378	4.4285
7	17.5008	8.3252	4.0084
15	22.9287	8.4930	3.5150
25	25.9472	8.5190	3.5626

	MAX	PF	EGoS
3	20.4776	15.0755	11.8178
7	26.1538	15.7717	11.5199
15	32.7410	16.4743	11.6655
25	35.6843	16.5784	12.1074

Table 8.24: Infinite-QAM with Shannon coding. (Left - Omni antenna, Right - Sectorized antenna)

	MAX	PF	EGoS
3	5.9718	3.4629	1.7337
7	10.6377	4.0948	1.5640
15	15.3774	4.2589	1.3602
25	18.1546	4.2287	1.3779

	MAX	PF	EGoS
3	13.2436	8.8809	6.3766
7	18.3761	9.4041	6.1574
15	24.7630	9.9902	6.3236
25	27.6767	10.0552	6.6377

Table 8.25: Infinite-QAM with no coding. (Left - Omni antenna, Right - Sectorized antenna)

	MAX	PF	EGoS
3	4.9491	2.9202	1.5889
7	7.8968	3.4429	1.4251
15	10.0034	3.4745	1.2352
25	11.0137	3.5000	1.2561

	MAX	PF	EGoS
3	9.0486	6.6345	5.1274
7	10.9739	7.0069	5.0153
15	11.8759	7.2843	5.0776
25	11.9739	7.3742	5.3168

Table 8.26: 16-QAM with no coding. (Left - Omni antenna, Right - Sectorized antenna)

Per-link cell-wide average throughputs (in units of bps/Hz) of multi-user MIMO $(3,3)$ links employing MMSE receivers, for Rician fading ($K = 10$), in a single-cell environment. The simulation results are for the various schedulers (MAX, PF, EGoS), and number of users.

	MAX	PF	EGoS
3	24.2226	18.7358	15.6947
7	30.9211	19.8147	16.1285
15	36.8879	20.2787	16.4411
25	40.3784	20.0080	16.3982

Table 8.27: Infinite-QAM with Shannon coding.

	MAX	PF	EGoS
3	16.5940	11.8145	9.2538
7	22.9828	12.6943	9.5574
15	28.8752	13.1029	9.8396
25	32.3527	12.8500	9.8193

Table 8.28: Infinite-QAM with no coding.

	MAX	PF	EGoS
3	10.3208	8.2666	7.0106
7	11.7137	8.7036	7.2279
15	11.9861	8.8983	7.3697
25	11.9995	8.8168	7.3309

Table 8.29: 16-QAM with no coding.

Per-link cell-wide average throughputs (in units of bps/Hz) of multi-user MIMO $(3, 3)$ links employing MMSE receivers, for Rician fading ($K = 10$), in a multi-cell environment. The simulation results are for the various schedulers (MAX, PF, EGoS), and number of users.

	MAX	PF	EGoS
3	6.8274	4.4702	2.6725
7	10.7782	4.7109	2.3069
15	14.5875	4.8792	2.2444
25	18.0470	5.0205	2.3299

	MAX	PF	EGoS
3	13.5019	9.5053	6.9659
7	18.7151	10.1982	6.7030
15	23.5926	10.6337	6.9390
25	27.6641	10.7596	7.0129

Table 8.30: Infinite-QAM with Shannon coding. (Left - Omni antenna, Right - Sectorized antenna)

	MAX	PF	EGoS
3	2.9105	1.7358	0.8148
7	5.3148	1.8874	0.6767
15	8.0774	1.9481	0.6618
25	10.9049	2.0567	0.6956

	MAX	PF	EGoS
3	7.3526	4.6708	2.9800
7	11.5475	5.1567	2.8485
15	15.8933	5.4424	2.9865
25	19.7717	5.5528	3.0398

Table 8.31: Infinite-QAM with no coding. (Left - Omni antenna, Right - Sectorized antenna)

	MAX	PF	EGoS
3	2.5691	1.5799	0.7740
7	4.5961	1.6924	0.6509
15	6.6700	1.7366	0.6361
25	8.4035	1.8169	0.6647

	MAX	PF	EGoS
3	5.9533	3.9474	2.6802
7	8.5942	4.3125	2.5665
15	10.5661	4.5407	2.6893
25	11.5086	4.5792	2.7227

Table 8.32: 16-QAM with no coding. (Left - Omni antenna, Right - Sectorized antenna)

Per-link cell-wide average throughputs (in units of bps/Hz) of multi-user MIMO $(3, 3)$ links employing MMSE receivers, for Rician fading (K is a function of the distance from the base station), in a single-cell environment. The simulation results are for the various schedulers (MAX, PF, EGoS), and number of users.

	MAX	PF	EGoS
3	27.2871	22.0372	19.8042
7	33.2002	22.8830	20.2107
15	38.5042	23.1242	20.7734
25	41.8953	23.3096	20.8774

Table 8.33: Infinite-QAM with Shannon coding.

	MAX	PF	EGoS
3	19.4477	14.5761	12.5762
7	25.2111	15.3476	12.9393
15	30.4825	15.6629	13.4746
25	33.8662	15.8107	13.5851

Table 8.34: Infinite-QAM with no coding.

	MAX	PF	EGoS
3	11.2560	9.7568	8.9746
7	11.9265	10.0676	9.1662
15	11.9982	10.1793	9.3420
25	11.9999	10.2161	9.3379

Table 8.35: 16-QAM with no coding.

Per-link cell-wide average throughputs (in units of bps/Hz) of multi-user MIMO $(3, 3)$ links employing MMSE receivers, for Rician fading (K is a function of the distance from the base station), in a multi-cell environment. The simulation results are for the various schedulers (MAX, PF, EGoS), and number of users.

	MAX	PF	EGoS
3	7.9396	5.1855	3.3101
7	11.7547	5.8029	3.0043
15	15.8739	5.9556	2.8481
25	19.3364	6.0851	2.8224

	MAX	PF	EGoS
3	15.7105	11.5185	9.0196
7	21.0054	12.6135	8.9403
15	25.9357	12.9156	9.0139
25	29.4335	13.1906	9.3453

Table 8.36: Infinite-QAM with Shannon coding. (Left - Omni antenna, Right - Sectorized antenna)

	MAX	PF	EGoS
3	3.4932	2.0784	1.0939
7	5.8934	2.3889	0.9705
15	9.0472	2.4935	0.9180
25	11.9842	2.5902	0.9226

	MAX	PF	EGoS
3	9.0321	6.0012	4.2350
7	13.4750	6.8159	4.2541
15	18.0764	7.0379	4.3057
25	21.4819	7.2509	4.5383

Table 8.37: Infinite-QAM with no coding. (Left - Omni antenna, Right - Sectorized antenna)

	MAX	PF	EGoS
3	3.1098	1.8792	1.0390
7	5.1103	2.1724	0.9318
15	7.3601	2.2433	0.8807
25	9.0737	2.3131	0.8796

	MAX	PF	EGoS
3	7.2284	5.0528	3.7644
7	9.8450	5.6443	3.7516
15	11.3632	5.7746	3.7889
25	11.8098	5.9044	3.9653

Table 8.38: 16-QAM with no coding. (Left - Omni antenna, Right - Sectorized antenna)

Chapter 9

Concluding Remarks and Suggestions for Future Research

9.1 Narrowband MIMO Channels

I. Evaluation of Co-Channel Interference Limited SISO/MEA Systems:

(1) SINRs typically range from -5 dB to 25 dB. This is not the high SINR regime. The available degrees of freedom are used to combat cross-stream interference (XSI), even at the cost of noise enhancement. Consequently, cell-wide mean throughputs do *not* scale linearly in the number of degrees of freedom. A MIMO (n, n) link will not have n times the throughput of a SISO $(1, 1)$ link.

(2) Transmit-adaptation systems are better equipped to combat channel fading and XSI; Receive-adaptation systems (with excess degrees of freedom) are better CCI suppressors. In other words, Transmit-adaptation systems make better use of degrees of freedom, while Receive-adaptation systems make better use of *excess* degrees of freedom.

(3) Excess Degrees of Freedom (EDoF) can *potentially* lead to significant improvement in the throughputs of Receive-adaptation systems, and moderate improvement in Transmit-adaptation systems.

(4) Higher Reuse Factors do *not* lead to an increase in throughput per bandwidth per cell.

(5) Although Antenna Sectorization (with a reuse factor of 1) improves per-link throughputs, it does *not* improve the throughputs realized per sector.

(6) Uncoded streams lead to 40–50% reduction in throughput as compared to perfectly (Shannon) coded streams. Throughputs of practical (and useful) coding schemes will be bracketed by the above two extreme cases.

(7) A strong specular component (Rician K-factor of 10 or greater) significantly reduces throughputs pf MIMO Receive-adaptation systems, but not so much MIMO Transmit-adaptation systems. This follows from conclusion (I.2) above. For single transmitter

systems, there is a slight increase in throughput.

(8) Limited Constellation Sizes dramatically alter the performance of MEA systems, wherein the benefit from excess degrees of freedom (EDoF), antenna sectorization, and frequency reuse, can be meager. This situation is prononced in practical systems that possess little (if any) EDoF.

II. Evaluation of Practical MIMO/MEA Systems with Resource Overheads:

(1) In the context of a limited number of constellation sizes and for the case of differential SINR-offsets the $(1, 2)$ MMSE is the configuration of choice for both metrics considered (cell-wide mean throughput per link, and 30th percentile of the link throughput). The other four configurations (i.e., SISO $(1, 1)$, Div $(2, 1)$, Div $(2, 2)$, and SM $(2, 2)$) are comparable in performance with each other. The main reasons why $(1, 2)$ MMSE scores best are: (i) relatively low channel estimation penalty, (ii) absence of cross-stream interference at receive antennas, and (iii) an excess receive antenna to suppress CCI.

(2) For the case of uniform offsets (6 dB), the throughput results change by small amounts. However, the main conclusions do not change from those for differential offsets. This reinforces findings of this study and shows them to be robust to assumptions that have been used herein.

(3) The MMSE receiver assumed here for $(2, 2)$ SM is one example of the many receivers that can decouple the SM streams; ZF, SIC, OSIC, and OSIC-MMSE receivers are some others. Since changing the particular receiver amounts to changing the SINR offset, against which our conclusions are found to be insensitive, $(1, 2)$ MMSE is the preferred configuration regardless of the particular receiver chosen by $(2, 2)$ SM to de-couple its streams.

III. Investigating the Validity of the Noise Model for Co-Channel Intererence for MIMO/MEA Links:

(1) For Transmit-adaptation systems, the noise model for CCI is accurate regardless of whether or not excess degrees of freedom are available. This is because such systems are not very effective at interference suppression. See also (I.2) above.

(2) For Receive-adaptation systems, the noise model is accurate when excess degrees of freedom are few or none. When several excess degrees of freedom are available, the inaccuracy from the noise model can be substantial. This is because the latter systems are very effective at interference suppression. See also (I.2) and (I.3) above.

(3) The systems considered thus far were spatial multiplexing systems. Transmit diversity systems, send dependent bit-streams over the transmit antennas, i.e., they use only one degree of freedom. Moreover, they do not suppress CCI. We conjecture that the noise model will also serve with reasonable accuracy in such systems.

(4) Following (III.1)–(III.3) above, we claim that in most *practical* cases of interest, detailed channel modeling of the co-channel interferers is of limited value to the analyst. Figure 4.2 summarizes the findings of this study.

(5) Finally, the noise model for CCI simplifies the analysis of co-channel interference limited MEA/MIMO based cellular systems. As such, it is the foundation upon which the analytical treatment (Problem 4) is built.

IV. Analysis of Co-Channel Interference Limited MIMO-Based Cellular Systems:

(1) Use of the Zero-Forcing assumption for the MMSE receiver, the noise model for CCI, and the single-cell analysis by Catreux, have served as a starting point for the analysis of CCI-limited MIMO cellular systems.

(2) Using the log-normality result for the sum of log-normal variates, the independence of the SIR over the exact angle between the $0°$ azimuth and the BS-MS alignment, and a double curve-fitting technique, we were able to perform an accurate analysis.

(3) Following (III.2), the analysis was limited to the case of MEA systems with no excess degrees of freedom. Accuracy of the analysis was demonstrated for MIMO configurations over several system-level design options.

(4) The approach used here does not lead to an explicit single formula which covers all system design parameters. However, throughputs for any particular design option can be computed using the same overall framework. Cases involving different choices for

reuse factor, sectorization, path loss exponent, and level of shadowing can be dealt with by obtaining $\mu(r)$ and $\sigma^2(r)$ for each case via rapid simulations. The analysis can also be generalized to the cases of correlated path gains in the gain matrix $\mathbf{H}$.

(5) The method described in this study is straightforward and produces numerical solutions that are accurate, far less time-consuming than extensive simulations, and more useful for gaining an intuitive understanding of the impact that the different parameters have on overall system performance.

9.2 Wideband (Single-Carrier and Multi-Carrier) MIMO Channels

V. Evaluation of Single-Carrier Wideband MIMO Systems with Channel Dispersion and Path-Correlation Impairment:

(1) As in the narrowband MIMO case, cell-wide mean throughputs do *not* scale linearly in the number of degrees of freedom.

(2) For the ideal canceller, frequency selectivity in the channel (leading to ISI only, since XSI is completely cancelled) results in only a small loss in throughput. However, most of this performance loss occurs at very small levels of dispersion.

(3) The non-dispersive canceller is impractical for use in real systems. Channel dispersion is a significant adversary since it smears XSI in the time domain, which subsequently the non-dispersive canceller is unable to mitigate. The MMSE equalizer keeps ISI low (see V.2). CCI, although also a detractor, is less damaging as compared to XSI.

(4) Path correlation has a serious impact on performance; in some cases, increasing the number of antennas can lead to a *decrease* in observed throughput.

(5) The effect of path-correlation, as observable from the transmit and receive correlation matrices, is more serious at the user end. This is to be expected since MS device sizes are extremely limited.

(6) Use of a higher frequency carrier results in smaller path-correlations, which leads to better performance; however, higher transmit power must be used to combat the faster

path-loss.

(7) Overall, the interplay between: path-correlation; number of antennas; the physical sizes of the transmit and receive arrays; and carrier frequency, must be carefully considered.

VI. Multi-Carrier Wideband MIMO (MIMO-OFDM) Systems:

Each tone in a MIMO-OFDM system is a MIMO system. Assuming each tone to be perfectly flat, is an idealization that begs for further investigation. This study quantifies the effects of channel dispersion (by way of XSI) and guard time (to mitigate ISI), in the throughputs of MIMO-OFDM systems. Moreover, this quantification is made for several values of number of tones, and over several values of channel rms delay spread. Important findings of this study are:

(1) Cross-stream interference (XSI) can be fully cancelled in a narrowband MIMO system and in a MIMO-OFDM system (for reasons explained in their respective chapters). However XSI is always present in a wideband MIMO system (one which has frequency-selective fading) unless an *ideal canceller* is explicitly employed (see V.2).

(2) Single-carrier signaling is a poor strategy to employ for frequency-selective channels. Figure 7.4 displays the amount of channel dispersion which can be tolerated by the MIMO-OFDM scheme for different number of tones (N) to achieve a signaling inefficiency less than 20%. From the figure, it is obvious that increasing the number of tones increases our ability to combat channel dispersion.

9.3 Multi-User (Base Station Scheduled) MIMO Channels

VII. Evaluation of Multi-User Diversity Systems:

Multi-user diversity (i) improves signal (channel) quality in the single-cell case, (ii) additionally peforms interference avoidance in the multi-cell case, and (iii) also improves available degrees of freedom of the system in the MIMO case. In other words, the entire channel subspace structure (the number, as well as values of the eigen-space) is improved [20]. From this study, the important findings are listed below:

(1) As designed, MAX, PF, and EGoS were intended to offer throughput performance (gain) per channel according to $TP_{MAX} > TP_{PF} > TP_{EGoS}$. On the other hand, the fairness performance was intended to be in the reverse order. For the multi-cell case, EGoS leads to throughput *loss* rather than gain. Users with better channels are penalized in order to allow users with poor channels to attain comparable throughput performance, thereby determining the overall scheduler performance.

(2) Simulation experiments confirm that with increasing number of users K, multi-user gains in the multi-cell scenario are better than that for the single-cell case (see known results VII.(i) and VII.(ii) above).

(3) Again, as in the single-user MIMO case, throughput does *not* scale linearly in the number of degrees of freedom. Even using the MAX scheduler does not place the system in the high SINR regime and XSI continues to deteriorate system performance.

(4) Antenna sectorization suppresses interference, while multi-user diversity avoids interference. Since sectorization cannot improve channel structure, MuD is the superior technique (particularly for a system with many users). Both techniques can be used in conjunction with each other. It stands to reason that as the number of users increases, the combined gain will have diminishing benefit with multi-user diversity playing an increasingly major role. This is also confirmed by the simulation results obtained.

(5) The loss in throughput arising from a high Rician κ-factor can be improved by MuD, with increasing number of users. (See known results VII.(i) and VII.(ii) above).

(6) Under the constraint of limited constellation sizes, per-channel throughput differences were negligible for the single-cell case, and dramatically reduced for the multi-cell case. Hence, other metrics (fairness and stability) were employed to obtain another perspective on the findings. Consequently, based upon the other metrics, EGoS becomes a reasonable choice for the single-cell case, and PF becomes a reasonable choise in multi-cell scenarios when delay tolerance is allowed.

(7) SU-EDoF vs. MuD-wo-EDoF: EGoS leads to small gains for the single-cell scenario, and moderate loss for the multi-cell scenario, as a function of number of users. PF

offers limited network diversity gain. Thus, EGoS is not a viable candidate; PF has limitations in the number of excess receive antennas it can compete against in SU-EDoF based systems; and, MAX is the best option in terms of cell-wide throughput.

(8) For applications that are delay-tolerant, a MuD-wo-EDoF system with a large number of users can deliver substantially higher throughputs than SU-EDoF links. This is especially true when using SU-EDoF with only one extra antenna, but applies even to the case of up to three. Finally, the amount of improvement using MuD-wo-EDoF instead of SU-EDoF decreases with increasing limits on constellation size.

9.4 Suggestions for Future Research

(1) *More Accurate Modeling of CCI for MEA Systems:* In-depth detailed investigation of the noise model and other possible models for co-channel interference for MEA systems, both in the narrowband and wideband context.

(2) *Analysis of CCI-Limited MuD Systems:* Extending the analysis of single-user CCI-limited systems to the multi-user case, with any generic scheduler, should be the next step taken in conducting an investigation that continues the work of this thesis. The research efforts reported in [3, 18, 69] provide relevant and extremely useful information.

(3) *Optimum Guard Spacing in OFDM Systems:* Increasing the guard time reduces ISI, but also reduces (signaling) efficiency. Decreasing the guard time increases ISI, but also increases efficiency. We conjecture the existence of an optimal guard spacing which reduces ISI, while increasing efficiency. Finding this guard spacing is a worthwhile topic to be investigated.

Appendix A

Definitions of Terms

(1) A link-level perspective implies that performance measures such as bit error rate (BER) or throughput (TP) are determined with signal-to-noise ratio (SNR) treated as a parameter, and external factors such as CCI ignored or indirectly treated using the signal-to-interference-plus-noise ratio (SINR) in place as SNR.

(2) A system-level perspective implies the distribution of performance over a coverage area, e.g., the cumulative distribution function (CDF) of TP over the randomness of user location and shadow fading, which jointly specify the SNR value, as well as taking into account the CCI produced by co-channel users in other cells.

(3) Array processor: the unit at the receiver, which attempts to separate the received streams in the face of cross-stream interference (XSI) and co-channel interference (CCI) as optimally as possible.

(4) Degrees of Freedom: the number of decomposable parallel SISO channels that can be created after array processing. It equals the rank of the channel gain matrix $\mathbf{H}$, and is upper-bounded by $\min(n, m)$.

(5) Excess Degrees of Freedom: the number of receive elements that exceed the number of transmit elements, i.e., $m - n$. When the receive array has at least as many antenna elements as the transmit array, all of the transmitted streams can be accomodated at the receiver after array processing.

Appendix B

Simulation Platform Validation

In this thesis, a platform very similar to the standardized 3GPP2 platform has been employed to obtain mean throughput performance of various MIMO systems. System parameter values as given in Tables 2.1, 3.1, 3.2, 3.3, 6.1, 8.1, 8.2 are in close agreement with those that have been observed by other investigations wherein actual measurements were obtained. Additional points to establish validation of the simulation platform are presented below:

(1) The mean throughput performance values obtained in this study closely match mean throughput values reported previously by Catreux [1, 2, 24] for all cases wherein system configurations were similar.

(2) It is known that, in practice, the mean throughput values obtained for the multi-cell case are about 60% lower than the corresponding mean throughputs obtained for the single-cell case (from private communication with Dr. Larry J. Greenstein). The throughput performance values reported in this study conform with those expectations.

(3) For the case of sectorized antennas with a reuse factor of 1, different frequencies are employed for each sector (frequency coloring). It is known that the mean throughputs for the sectorized case will have a two-fold improvement over the results for the case of omni-directional antennas [16, Ch. 3]). This is indeed also the case for the data values provided in the tables presented throughout Chapters 2–8.

(4) As a result of the many measurement-based studies performed by Bell-Labs/Alcatel-Lucent Technologies, it is known that the ratio of mean throughputs of the Div (2, 1) system to the SISO (1, 1) system is about 1.06. This is indeed the case with the simulations (see Table 3.4), adding to our confidence that the throughput performance results reported using the simulation platform closely follow the throughput trends that have been observed in practice.

References

[1] S. Catreux, P. Driessen, and L. Greenstein, “Attainable throughput of an interference-limited multiple-input multiple-output (MIMO) cellular system,” *IEEE Trans. Commun.*, vol. 49, no. 8, pp. 1307–1311, August 2001.

[2] S. Catreux, “Techniques d’ antennes multi-entrees multi-sorties dans un systeme de type cellulaire,” Ph.D. dissertation, INSA, Paris, France, April 2000.

[3] C. Chen and L. Wang, “A unified capacity analysis for wireless systems with joint multiuser scheduling and antenna diversity in nakagami fading channels,” *IEEE Trans. Commun.*, vol. 54, no. 3, pp. 469–478, March 2006.

[4] I. Telatar, “Capacity of multi-antenna gaussian channels,” *Euro. Trans. Telecommun.*, vol. 10, no. 6, pp. 585–595, November 1999.

[5] S. Alamouti, “A simple transmit diversity technique for wireless communications,” *IEEE J. Sel. Areas Commun.*, vol. 16, no. 8, pp. 1451–1458, October 1998.

[6] V. Tarokh, H. Jafarkhani, and A. Calderbank, “Space-time block codes from orthogonal designs,” *IEEE Trans. Inf. Theory*, vol. 45, no. 5, pp. 1456–1467, July 1999.

[7] V. Tarokh, N. Seshadri, and A. Calderbank, “Space-time block codes for high data rate wireless communication: Performance, criterion and code construction,” *IEEE Trans. Inf. Theory*, vol. 44, no. 2, pp. 744–765, March 1998.

[8] G. Foschini and M. Gans, “On limits of wireless communications in a fading environment when using multiple antennas,” *IEEE Wireless Personal Communications*, vol. 6, no. 3, pp. 311–335, March 1998.

[9] P. Wolniansky, G. Foschini, G. Golden, and R. Valenzuela, “V-BLAST: an architecture for achieving very high data rates over the rich-scattering wireless channel,” *in Proc. Int. Symp. Signals, Systems, and Electronics (ISSSE ’98),* Pisa, Italy, pp. 295–300, October 1998.

[10] G. Foschini, “Layered space-time architecture for wireless communication in a fading environment when using multiple antennas,” *Bell-Labs Tech. J. (BLTJ)*, vol. 1, no. 2, pp. 41–59, 1996.

[11] L. Zheng and D. Tse, “Diversity and multiplexing: a fundamental tradeoff in multiple-antenna channels,” *IEEE Trans. Inf. Theory*, vol. 49, no. 5, pp. 1073–1096, May 2003.

[12] B. Hassibi and B. Hochwald, “High rate codes that are linear in space and time,” *IEEE Trans. Inf. Theory*, vol. 48, no. 7, pp. 1804–1824, July 2002.

[13] A. Paulraj, R. Nabar, and D. Gore, *Introduction to Space-Time Wireless Communications*. Cambridge University Press, 2003.

[14] D. Tse and P. Vishwanath, *Fundamentals of Wireless Communication*. Cambridge University Press, 2005.

[15] G. Stuber, *Principles of Mobile Communications*. Kluwer Academic Publishers, 2001.

[16] T. Rappaport, *Wireless Communications — principles and practice*. Prentice Hall, 2002.

[17] W. Jakes, *Microwave Mobile Communications*. Wiley, 1974.

[18] C. Chen and L. Wang, "Enhancing coverage and capacity for multiuser MIMO systems by utilizing scheduling," *IEEE Trans. Wireless Commun.*, vol. 5, no. 5, pp. 1148–1157, May 2006.

[19] P. Viswanath, D. Tse, and R. Laroia, "Opportunistic beamforming using dumb antennas," *IEEE Trans. Inf. Theory*, vol. 48, no. 6, pp. 1277–1294, June 2002.

[20] R. Heath, M. Airy, and A. Paulraj, "Multiuser diversity for MIMO wireless systems with linear receivers," *IEEE Proc. Asilomar Conf. Signals, Systems and Computers*, vol. 2, pp. 1194–1199, November 2001.

[21] M. Karakayali, G. Foschini, and R. Valenzuela, "Network coordination for spectrally efficient communications in cellular systems," *IEEE Wireless Commun. Mag.*, vol. 13, no. 4, pp. 56–61, August 2006.

[22] M. Karakayali, G. Foschini, R. Valenzuela, and R. Yates, "On the maximum common rate achievable in a coordinated network," *IEEE Proc. ICC*, vol. 9, pp. 4333–4338, June 2006.

[23] S. Venkatesan, A. Lozano, and R. Valenzuela, "Network MIMO: overcoming intercell interference in indoor wireless systems," *IEEE Proc. Asilomar Conf. Signals, Systems and Computers*, in review.

[24] S. Catreux, P. Driessen, and L. Greenstein, "Data throughputs using multiple-input-multiple-output (MIMO) techniques in a noise-limited cellular environment," *IEEE Trans. Wireless Commun.*, vol. 1, no. 2, pp. 226–235, April 2002.

[25] V. Erceg, L. Greenstein, S. Tjandra, S. Parkoff, A. Gupta, B. Kulic, A. Julius, and R. Bianchi, "An empirically based path loss model for wireless channels in suburban environments," *IEEE J. Sel. Areas Commun.*, vol. 17, no. 7, pp. 1205–1211, July 1999.

[26] A. Goldsmith and S. Chua, "Variable-rate M-QAM for fading channels," *IEEE Trans. Commun.*, vol. 45, no. 10, pp. 1218–1230, October 1997.

[27] J. Winters, "Optimum combining in digital mobile radio with cochannel interference," *IEEE J. Sel. Areas Commun.*, vol. 2, no. 4, pp. 528–539, July 1984.

[28] J. Proakis, *Digital Communications*, 4th ed. McGraw-Hill Series in Electrical and Computer Engineering, 2002.

[29] R. Pupala, Y. Yuan, Q. Bi, and L. Greenstein, "Downlink system throughput statistics for various MEA configurations," *IEEE Trans. Veh. Techol.*, in review.

[30] R. Pupala, L. Greenstein, and D. Daut, "Quantifying the system-level effects of channel dispersion and path correlations in MIMO-based cellular systems," *IEEE Trans. Wireless Commun.*, to be submitted.

[31] Q. Bi, S. Vitebsky, Y. Yang, and Y. Yuan, "Broadcast-multicast in 1x EV-DO revision a systems and its application to enhanced mobile services," *Bell-Labs Tech. J. (BLTJ)*, vol. 11, no. 4, pp. 237–252, December 2006.

[32] B. Saltzberg, "Intersymbol interference error bounds with application to ideal bandlimited signaling," *IEEE Trans. Inf. Theory*, vol. 14, no. 4, pp. 563–568, July 1968.

[33] G. Foschini and J. Salz, "Digital communications over fading radio channels," *Bell-System Tech. Journal*, vol. 62, no. 2 Part 1, pp. 429–456, February 1983.

[34] L. Greenstein, "Analysis/simulation study of cross-polarization cancellation in dual-polarization digital radio," *AT&T Bell-Labs Tech. J. (AT&T-BLTJ)*, vol. 64, no. 10, pp. 2261–2280, December 1985.

[35] L. Fenton, "The sum of log-normal probability distributions in scatter transmission systems," *IEEE Trans. Commun.*, vol. 8, no. 1, pp. 57–67, March 1960.

[36] S. Schwartz and Y. Yeh, "On the distribution function and moments of power sums with log-normal components," *Bell-System Tech. Journal*, vol. 61, pp. 1441–1462, September 1982.

[37] R. Pupala, L. Greenstein, and D. Daut, "Throughput analysis of interference-limited MIMO-based cellular systems," *IEEE Trans. Commun. Lett.*, to be submitted.

[38] ——, "Downlink throughput statistics in interference-limited cellular systems with multi-element antennas," *IEEE Trans. Commun.*, in review.

[39] S. Catreux, L. Greenstein, and V. Erceg, "Some results and insights on the performance gains of MIMO systems," *IEEE J. Sel. Areas Commun.*, vol. 21, no. 5, pp. 839–847, June 2003.

[40] P. Soma, D. Baum, V. Erceg, R. Krishnamoorthy, and A. Paulraj, "Analysis and modeling of multiple-input-multiple-output radio channel based on outdoor measurements conducted at 2.5 GHz for fixed BWA applications," *IEEE Proc. ICC*, vol. 1, pp. 272–276, April 2002.

[41] Y. Li, J. Winters, and N. Solenberger, "MIMO-OFDM for wireless communications: signal detection with enhanced channel estimation," *IEEE Trans. Commun.*, vol. 50, no. 9, pp. 1471–1477, September 2002.

[42] Y. Li, "Simplified channel estimation for OFDM systems with multiple transmit antennas," *IEEE Trans. Wireless Commun.*, vol. 1, no. 1, pp. 67–75, January 2002.

[43] H. Bolcskei and A. Paulraj, "Space-frequency coded broadband OFDM systems," *IEEE Proc. WCNC*, vol. 1, pp. 1–6, September 2000.

[44] A. Molisch, M. Win, and J. Winters, "Space-time-frequency (STF) coding for MIMO-OFDM systems," *IEEE Trans. Commun. Lett.*, vol. 6, no. 9, pp. 370–372, September 2002.

[45] H. Bolcskei, M. Borgmann, and A. Paulraj, "Space-frequency coded MIMO-OFDM with variable multiplexing-diversity tradeoff," *IEEE Proc. ICC*, vol. 4, pp. 2837–2841, May 2003.

[46] J. Wang and K. Yao, "Capacity scaling in OFDM based spatial multiplexing systems," *IEEE Proc. VTC*, vol. 1, pp. 28–32, September 2002.

[47] H. Bolcskei, D. Gesbert, and A. Paulraj, "On the capacity of OFDM-based spatial multiplexing systems," *IEEE Trans. Commun.*, vol. 50, no. 2, pp. 225–234, February 2002.

[48] M. Borgmann and H. Bolcskei, "On the capacity of noncoherent wideband MIMO-OFDM systems," *Int. Symp. Inf. Theory*, pp. 651–655, September 2005.

[49] S. Visuri and H. Bolcskei, "Multiple-access strategies for frequency-selective MIMO channels," *IEEE Trans. Inf. Theory*, vol. 52, no. 9, pp. 3980–3993, September 2006.

[50] H. Bolcskei, "MIMO-OFDM wireless systems: basics, perspectives, and challenges," *IEEE Wireless Commun. Mag.*, vol. 13, no. 4, pp. 31–37, August 2006.

[51] G. Stuber, J. Barry, S. McLaughlin, Y. Li, M. Ingram, and T. Pratt, "Broadband MIMO-OFDM wireless communications," *Proceedings of the IEEE*, vol. 92, no. 2, pp. 271–294, February 2004.

[52] H. Yang, "A road to future broadband wireless access: MIMO-OFDM-based air interface," *IEEE Commun. Mag.*, vol. 43, no. 1, pp. 53–60, January 2005.

[53] P. Almers and et al, "Survey of channel and radio propagation models for wireless MIMO systems," *EURASIP Journal on Wireless Commun. and Netw.*, vol. 2007, no. 1, pp. 56 (1–19), January 2007.

[54] V. Erceg, P. Soma, D. Baum, and S. Catreux, "Multiple-input multiple-output fixed wireless radio channel measurements and modeling using dual-polarized antennas at 2.5 GHz," *IEEE Trans. Wireless Commun.*, vol. 3, no. 6, pp. 2288–2298, November 2004.

[55] C. Oestges, V. Erceg, and A. Paulraj, "A physical scattering model for MIMO macrocellular broadband wireless channels," *IEEE J. Sel. Areas Commun.*, vol. 21, no. 5, pp. 721–729, June 2003.

[56] H. El-Sallabi, D. Baum, P. Zetterberg, P. Kyosti, T. Rautiainen, and C. Schneider, "Wideband spatial channel model for MIMO systems at 5 GHz in indoor and outdoor environments," *IEEE Proc. VTC*, vol. 6, pp. 2916–2921, May 2006.

[57] A. Molisch, "A generic model for MIMO wireless propagation channels in macro- and microcells," *IEEE Trans. Signal Process.*, vol. 52, no. 1, pp. 61–71, January 2004.

[58] J. Kermoal, L. Schumacher, K. Pedersen, P. Mogensen, and F. Frederiksen, "A stochastic MIMO radio channel model with experimental validation," *IEEE J. Sel. Areas Commun.*, vol. 20, no. 6, pp. 1211–1226, August 2002.

[59] L. Schumacher, K. Pedersen, and P. Mogensen, "From antenna spacings to theoretical capacities - guidelines for simulating MIMO systems," *Proc. IEEE Symp. PIMRC*, vol. 2, pp. 587–592, September 2002.

[60] D. Gesbert, H. Bolcskei, D. Gore, and A. Paulraj, "Outdoor MIMO wireless channels: models and performance prediction," *IEEE Trans. Commun.*, vol. 50, no. 12, pp. 1926–1934, December 2002.

[61] P. Bello, "Characterization of randomly time-variant linear channels," *IEEE Trans. Commun.*, vol. 11, no. 4, pp. 360–393, December 1963.

[62] W. Wong and L. Greenstein, "Multipath fading models and adaptive equalizers in microwave digital radio," *IEEE Trans. Commun.*, vol. 32, no. 8, pp. 928–934, August 1984.

[63] V. Erceg and et al, "IEEE P802.11 wireless LANs TGn channel models," *doc: IEEE 802.11-03/940r4*, pp. 1–45, May 2004.

[64] Q. Li, K. Yu, M. Ho, J. Lung, D. Cheung, and C. Prettie, "On the tap angular spread and kronecker structure of the WLAN channel," *doc: IEEE 802.11-03/584r0*, July 2003.

[65] R. Lucky, J. Salz, and E. Weldon, *Principles of Data Communication*. McGraw-Hill, 1968.

[66] R. Knopp and P. Humblet, "Information capacity and power control in single cell multiuser communications," *IEEE Proc. ICC*, vol. 1, pp. 331–335, June 1995.

[67] A. Jalali, R. Padovani, and R. Pankaj, "Data throughput of CDMA-HDR a high efficiency-high data rate personal communication wireless system," *IEEE Proc. VTC*, vol. 3, pp. 1854–1858, Spring 2000.

[68] M. Airy, R. Heath, and S. Shakkottai, "Multiuser diversity for the multiple antenna broadcast channel with linear receivers: asymptotic analysis," *IEEE Proc. Asilomar Conf. Signals, Systems and Computers*, vol. 1, pp. 886–890, November 2004.

[69] C. Chen and L. Wang, "Performance analysis of scheduling in multiuser MIMO systems with zero-forcing receivers," *IEEE J. Sel. Areas Commun.*, vol. 25, no. 7, pp. 1435–1445, July 2007.

[70] J. Holtzman, "Asymptotic analysis of proportional fair algorithm," *Proc. IEEE Symp. PIMRC*, vol. 2, pp. F33–F37, October 2001.

[71] M. Andrews, "Instability of the proportional fair scheduling algorithm for HDR," *IEEE Trans. Wireless Commun.*, vol. 3, no. 5, pp. 1422–1426, September 2004.

Curriculum Vitae

Rahul N. Pupala

EDUCATION

2008 Ph.D. (Electrical & Computer Engineering), Rutgers – The State University of New Jersey, US.

2003 M.S. (Computer Science), Rutgers – The State University of New Jersey, US.

1994 B.E. (Computer Engineering), Victoria Jubilee Technical Institute (VJTI), Bombay University, India.

EMPLOYMENT/CAREER

2004 – 2006 Graduate Research/Teaching Assistant, WINLAB and the Electrical & Computer Engineering Dept., Rutgers - The State University of New Jersey.

1999 – 2003 Graduate Research/Teaching Assistant, Computer Science Dept., Rutgers - The State University of New Jersey.

1994 – 1999 Various positions in Computer Science, Finance (applications), Logistics, and I.T. consulting industries; both in India and in US.

PUBLICATIONS

2008 R. Pupala, L. Greenstein, D. Daut, "Tone-Spacing in MIMO-OFDM Based Cellular Systems" *to be submitted IEEE Trans. Wireless Commun.*.

2008 R. Pupala, L Greenstein, D. Daut, "Quantifying the System-Level Effects of Channel Dispersion and Path Correlationsin MIMO-Based Cellular Systems," *to be submitted IEEE Trans. Wireless Commun.*.

2008 R. Pupala, L. Greenstein, D. Daut, "Throughput Analysis of Interference-Limited MIMO-Based Cellular Systems" *IEEE Trans. Wireless Commun. Lett., in review*.

2007 R. Pupala, L. Greenstein, D. Daut, "System-Level Impact of Multi-User Diversity in SISO and MIMO-Based Cellular Systems," *IEEE Trans. Veh. Technol., in review*.

2007 R. Pupala, L Greenstein, D. Daut, "Downlink Throughput Statistics in Interference-Limited Cellular Systems with Multi-Element Antennas," *IEEE Trans. Commun., in review*.

2007 R. Pupala, Y. Yuan, Q. Bi, L. Greenstein, "Downlink System Throughput Statistics for Various MEA Configurations," *IEEE Trans. Veh. Technol., in review*.